University of Alberta
Department of Civil Engineering

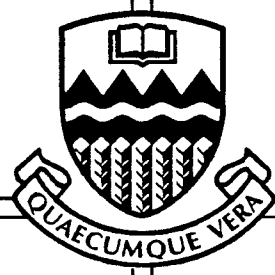


Structural Engineering Report No. 207

# ANALYTICAL INVESTIGATION OF THE COMPRESSIVE BEHAVIOR AND STRENGTH OF STEEL GUSSET PLATE CONNECTIONS

by

Michael C.H. Yam

and

J.J. Roger Cheng

December 1994

**Structural Engineering Report No. 207**

# ANALYTICAL INVESTIGATION OF THE COMPRESSIVE BEHAVIOR AND STRENGTH OF STEEL GUSSET PLATE CONNECTIONS

by

Michael C. H. Yam

and

J. J. Roger Cheng

Department of Civil Engineering

University of Alberta

Edmonton, Alberta, Canada T6G 2G7

December 1994

## ABSTRACT

Gusset plate connections are commonly used in bridge trusses and braced steel frames to transfer forces from one structural member to another. Due to the complexity of these connections, it is extremely difficult to evaluate the strength of gusset plate connections. Hence, a research program was initiated to investigate the compressive behavior and ultimate strength of gusset plate connections by testing full-scale diagonal bracing connections. A total of twenty-one tests were conducted on nineteen specimens. The results of the experimental investigations were reported in Yam and Cheng (1993).

To further examine the compressive behavior and strength of the gusset plate connections, analytical investigations by the finite element method, using the program ANSYS, were conducted. The analytical results are summarized in this report. The plastic bifurcation buckling loads of the test specimens by ANSYS are in good agreement with the test results. The elastic stress predicted by ANSYS at the gusset plate area underneath the splicing member agrees well with the experimental stress evaluated from the rosette readings. For the eccentrically loaded specimens, the load deflection analysis by ANSYS also compares well with the experimental ultimate loads. Based on the available test data and the finite element analysis, a modified Thornton method is proposed to estimate the inelastic buckling strength of the gusset plate specimens. A rigid plastic collapse analysis was conducted on the eccentrically loaded specimens and the results are in good agreement with the test results. The beam-column equation is also recommended for the design of eccentrically loaded specimens.

## ACKNOWLEDGEMENTS

The author wishes to express his deep appreciation and gratitude to Dr. J.J. Roger Cheng for his supervision and guidance throughout the course of this study. The helpful advice and suggestions given by Drs. G. L. Kulak, J. A. Packer, D. W. Murray, D. H-K Chan and D. J. Steigmann are greatly acknowledged. Financial support was provided by the Natural Sciences and Engineering Research Council of Canada to Dr. Cheng under grant No. A4727.

The assistance of the technical staff of the I. F. Morrison Structural Laboratory at the University of Alberta is acknowledged.

The author deeply appreciates the encouragement, support and patience of his wife, Monica, throughout the course of this study.

## TABLE OF CONTENTS


**Chapter** **Page**

1. INTRODUCTION ..... 1

1.1 General ..... 1

1.2 Brief Review of Test Program and Results ..... 1

1.2.1 Test Specimens and Test Setups ..... 1

1.2.2 Test Results ..... 2

2. ANALYSIS OF TEST SPECIMENS ..... 9

2.1 General ..... 9

2.2 Finite Element Analysis - Plastic Bifurcation Buckling ..... 9

2.3 Finite Element Model ..... 11

2.4 Finite Element Analysis Results ..... 13

2.4.1 General ..... 13

2.4.2 GP and SP Type Specimens ..... 14

2.4.2.1 In-Plane Stress Distribution ..... 14

2.4.2.2 Principal Stress Vector and In-Plane Deformation Plots ..... 17

2.4.3 AP Type Specimens ..... 18

2.4.3.1 In-Plane Stress Distribution ..... 18

2.4.3.2 Principal Stress Vector and In-Plane Deformation Plots ..... 18

2.4.4 MP Type Specimens ..... 19

2.4.4.1 In-Plane Stress Distribution ..... 19

2.4.4.2 Principal Stress Vector and In-Plane Deformation Plots ..... 20

2.4.5 Buckling Shapes of GP, SP, AP and MP Test Specimens ..... 20

2.4.6 EP Type Specimens ..... 21

2.4.6.1 Load Deflection Behavior ..... 21

2.4.6.2 In-Plane Stress Distribution ..... 21

2.4.6.3 Principal Stress Vector and Out-of-Plane Deformation Plots..... 23

2.5 Discussion and Comparison of Analytical Results..... 24

2.5.1 General..... 24

2.5.2 Effects of Gusset Plate Thickness and Size..... 24

2.5.3 Effects of Angle of Diagonal Brace Member (45° and 30°)..... 25

2.5.4 Effects of Beam and Column Moments ..... 26

2.5.5 Effects of Loading Eccentricity..... 27

2.6 Rigid-Plastic Analysis of Specimens EP1 and EP2..... 28

3. PROPOSED DESIGN GUIDELINES AND METHODS..... 85

3.1 General..... 85

3.2 Elastic Parametric Studies of Gusset Plate Connections..... 85

3.2.1 General..... ...85

3.2.2 Parametric Studies..... 86

3.2.2.1 General..... 86

3.2.2.2 Effects of Splice Plate Thickness..... 87

3.2.2.3 Effects of Splice Plate Length..... 88

3.2.2.4 Effects of Rotational Restraint at Conjunction of Bracing and Gusset Plate..... 89

3.2.2.5 General Design Guidelines..... 90

3.3 Modified Thornton Method..... 91

3.3.1 General..... 91

3.3.2 Proposed Design Method..... 93

3.4 Eccentrically Loaded Gusset Plates..... 95

3.4.1 General..... 95

3.4.2 General Design Guidelines..... 97

4. SUMMARY AND RECOMMENDATIONS ..... 111

4.1 Summary ..... 111

4.2 Design Recommendations ..... 111

4.2.1 Conentrically Loaded Gusset Plate Connections ..... 111

4.2.2 Eccentrically Loaded Gusset Plate Connections ..... 112

4.3 Recommendations for Future Research ..... 113

REFERENCES ..... 116

APPENDIX ..... 118

## LIST OF TABLES


| Tables | | Page |
|---|---|---|
| 1.1 | Specimen Descriptions and Test Results | 3 |
| 2.1 | Analytical Plastic Bifurcation Buckling Loads of Test Specimens | 32 |
| 2.2 | Rigid-Plastic Collapse Load for Specimens EP1 and EP2 | 32 |
| 3.1 | Buckling Loads of Test Specimens from Hu and Cheng (1987) | 98 |
| 3.2 | Critial Splice Plate Thickness for 850 x 550 and 850 x 700 Specimens | 98 |
| 3.3a | Effects of Splice Plate Length on Buckling Loads for Specimens with a Plate Size of 850 x 550 | 99 |
| 3.3b | Effects of Splice Plate Length on Buckling Loads for Specimens with a Plate Size of 850 x 700 | 99 |
| 3.4 | Effects of Rotational Restraint at the Conjunction of Bracing Member and the Gusset Plate | 100 |
| 3.5 | Comparsion of Test Loads with Analytical and Design Loads | 101 |
| 3.6 | Comparsion of Elastic Buckling Loads with Whitmore Loads of Test Specimens | 102 |
| 3.7 | Design Loads for Test Specimens from Hu and Cheng (1987) | 103 |
| 3.8 | Design Loads for EP Type Specimens | 104 |

## LIST OF FIGURES


| Figure | | Page |
|---|---|---|
| 1.1 | Schematic of Test Specimens | 4 |
| 1.2a | Splice Members and Splicing Arrangement for GP, SP, MP and AP Type Specimens | 5 |
| 1.2b | Splice Member Arrangement for EP Type Specimens | 6 |
| 1.3 | Schematic of Test Setup for Scheme I | 7 |
| 1.4 | Schematic of Test Setup for Scheme II | 8 |
| 2.1 | Flow Diagram for Plastic Bifurcation Buckling Analysis | 33 |
| 2.2 | Finite Element Model for GP and SP Type Specimens | 34 |
| 2.3a | Finite Element Model for AP and MP Type Specimens | 35 |
| 2.3b | Finite Element Model for EP Type Specimens | 36 |
| 2.4 | A Plot of Test to Predicted(ANSYS) Ratios for Various Specimens | 37 |
| 2.5a | In-Plane Stress Contour for Specimen GP1 at P = 1370 kN | 38 |
| 2.5b | In-Plane Stress Contour for Specimen GP1 at P = 1500 kN | 39 |
| 2.5c | In-Plane Stress Contour for Specimen GP1 at P = 1700 kN | 40 |
| 2.5d | In-Plane Stress Contour for Specimen GP1 at P = 1950 kN | 41 |
| 2.5e | In-Plane Stress Contour for Specimen GP1 at P = 2336 kN | 42 |
| 2.6 | In-Plane Stress Contour for Specimen GP1 at P = 1220 kN | 43 |
| 2.7a | Principal Stress Vector Plot for Specimen GP1 at P = 1370 kN | 44 |
| 2.7b | Principal Stress Vector Plot for Specimen GP1 at P =2336 kN | 45 |
| 2.8a | In-Plane Deformation Mode for Specimen GP1 at P = 1370 kN | 46 |
| 2.8b | In-Plane Deformation Mode for Specimen GP1 at P = 2336 kN | 47 |
| 2.9 | In-Plane Stress Contour for Specimen AP1 at P = 1380 kN | 48 |
| 2.10 | Principal Stress Vector Plot for Specimen AP1 at P = 1380 kN | 49 |
| 2.11 | In-Plane Deformation Mode for Specimen AP1 at P = 1380 kN | 50 |
| 2.12a | In-Plane Stress Contour for Specimen MP1 at P = 300 kN | 51 |
| 2.12b | In-Plane Stress Contour for Specimen MP1 at P = 1500 kN | 52 |
| 2.13a | Principal Stress Vector Plot for Specimen MP1 at P = 300 kN | 53 |
| 2.13b | Principal Stress Vector Plot for Specimen MP1 at P = 1500 kN | 54 |
| 2.14a | In-Plane Deformation Mode for Specimen MP1 at P = 300 kN | 55 |
| 2.14b | In-Plane Deformation Mode for Specimen MP1 at P = 1500 kN | 56 |
| 2.15a,b | Typical Buckling Shapes for Specimens GP1 and AP1 | 57 |
| 2.15c,d | Typical Buckling Shapes for Specimens MP1 and SP1 | 58 |
| 2.16 | Analytical Load Deflection Curve for Specimen EP1 | 59 |
| 2.17 | Analytical Load Deflection Curve for Specimen EP2 | 60 |

**Figure** **Page**

2.18 Analytical Load Deflection Curve for Specimen EP3 ..... 61
2.19 In-Plane Stress Distribution of Splice Plate Top Surface for Specimen EP1 at Ultimate..... 62
2.20 In-Plane Stress Distribution of Splice Plate Bottom Surface for Specimen EP1 at Ultimate..... 62
2.21 In-Plane Stress Distribution at Centerline Along Length of Splice Plate for Specimen EP1 ..... 63
2.22 In-Plane Stress Distribution of Gusset Plate Top Surface for Specimen EP1 at Ultimate..... 64
2.23 In-Plane Stress Distribution of Gusset Plate Bottom Surface for Specimen EP1 at Ultimate..... 64
2.24a In-Plane Stress Distribution of Splice Plate Top Surface for Specimen EP3 at Ultimate..... 65
2.24b In-Plane Stress Distribution of Splice Plate Bottom Surface for Specimen EP3 at Ultimate..... 65
2.25a In-Plane Stress Distribution of Gusset Plate Top Surface for Specimen EP3 at Ultimate..... 66
2.25b In-Plane Stress Distribution of Gusset Plate Bottom Surface for Specimen EP3 at Ultimate..... 66
2.26 Principal Stress Vector Plot of Gusset Plate Top Surface for Specimen EP1 at Ultimate..... 67
2.27 Principal Stress Vector Plot of Gusset Plate Bottom Surface for Specimen EP1 at Ultimate..... 67
2.28 Out-of-Plane Deformation for Specimen EP1..... 68
2.29 Out-of-Plane Deformation for Specimen EP2..... 68
2.30 Out-of-Plane Deformation for Specimen EP3..... 69
2.31 Analytical Out-of-Plane Deflection at Centerline of Splice Plate for Specimen EP1 ..... 70
2.32 Analytical Out-of-Plane Deflection at Centerline of Splice Plate for Specimen EP2 ..... 71
2.33 Load vs. Gusset Plate Specimen Thickness..... 72
2.34a In-Plane Stress Contour for Specimen MP3 at P = 630 kN..... 73
2.34b In-Plane Stress Contour for Specimen MP3A at P = 630 kN..... 74
2.34c In-Plane Stress Contour for Specimen MP3B at P = 630 kN..... 75
2.35a Principal Stress Vector Plot for Specimen MP3 at P = 630 kN..... 76

**Figure** **Page**

2.35b Principal Stress Vector Plot for Specimen MP3A at P = 630 kN ..... 77
2.35c Principal Stress Vector Plot for Specimen MP3B at P = 630 kN ..... 78
2.36a In-Plane Deformation Mode for Specimen MP3 at P = 630 kN ..... 79
2.36b In-Plane Deformation Mode for Specimen MP3A at P = 630 kN ..... 80
2.36c In-Plane Deformation Mode for Specimen MP3B at P = 630 kN ..... 81
2.37 Rigid-Plastic Collapse Mechanism for Specimens EP1 and EP2 ..... 82
2.38 Rigid-Plastic Unloading Line for Specimen EP1 ..... 83
2.39 Rigid-Plastic Unloading Line for Specimen EP2 ..... 84
3.1 Finite Element Model and Typical Specimen Size and Shape from Cheng et al. (1994) ..... 105
3.2 Triangular Area of Gusset Plates ..... 106
3.3 Effects of Splice Plate Thickness on the Elastic Buckling Loads of Gusset Plates ..... 107
3.4 Various Splice Plate Lengths for Gusset Plate Specimens ..... 108
3.5 Effects of Rotational Restraint on the Elastic Buckling Loads of Gusset Plates Specimens ..... 109
3.6 Modified Thornton Method ..... 110
4.1 Dimensions Required in the Design Method ..... 115

## LIST OF SYMBOLS

$b_w$ = Whitmore effective width

e = loading eccentricity

I = moment of inertia

k = effective length factor for the unit column strip

$l_b$ = distance between the first row and the last row of bolts in a connection

L = length of column strip in modified Thornton method

$L_{1,2,3}$ = length of column strips in Thornton method

Mb = applied beam moment

Mc = applied column moment

$M_p$ = plastic moment capacity of a section in beam-column formula

$M_{pc}$ = reduced plastic moment capacity in beam-column formula

$M_{pcG}$ = reduced plastic moment capacity of gusset plate

$M_{pG}$ = plastic moment capacity of gusset plate

$M_{pcS}$ = reduced plastic moment capacity of splice plate

$M_{pS}$ = plastic moment capacity of splice plate

P = ultimate load of test specimens

$P_a$ = applied axial load in beam-column formula

$P_{ANSYS}$ = plastic bifurcation buckling load of specimens by ANSYS

$P_{BC}$ = analytical load based on beam-column equation with total eccentric moment

$P_{cr}$ = compressive strength of gusset plate connections

$P_E$ = elastic buckling load of specimens by ANSYS

$P_{MBC}$ = analytical load based on beam-column equation with half of the eccentric moment

$P_{RBC}$ = analytical load based on rigid-plastic analysis

$P_t$ = Thornton load

$P_{TE}$ = Thornton elastic buckling load

$P_{t30}$ = Same as $P_t$, used for clarity

$P_{t45}$ = Thornton load with the effective width based on a $45^o$ angle

$P_w$ = Whitmore load

$P_y$ = yield load of the section

$P_{yG}$ = yield load of the gusset plate section

$P_{yS}$ = yield load of the splice plate section

r = radius of gyration

s = gauge of bolts

Sc = critcal splice plate thickness

| | | |
|---|---|---|
| SL | = | length of splice plate member |
| [D] | = | displacement vector |
| {R} | = | load vector |
| [K] | = | conventional stiffness matrix |
| $[K_\sigma]$ | = | stress stiffness matrix |
| $\Delta$ | = | out-of-plane displacement of eccentrically loaded specimens |
| $\lambda$ | = | arbitrary scalar multiplier |
| $\sigma_{cr}$ | = | critcal stress of a column |

# 1. INTRODUCTION

## 1.1 General

The compressive strength of gusset plate connections was investigated experimentally by the authors and published in a separate report (Yam and Cheng 1993). The objective of this current report is to present an analytical investigation of the compressive behavior and strength of gusset plate connections. The results from both the experiments and the analyses will be used to develop a preliminary design recommendations for the gusset plate connections.

In order to facilitate the discussion of the analytical results, the test results from the experimental program will be briefly described in the next section. This will be followed by the chapter on analytical results and concluded by the summary and the recommendations in the last chapter.

## 1.2 Brief Review of Test Program and Results

### 1.2.1. Test Specimens and Test Setups

The specimen sizes and designations are shown in Table 1.1. The test parameters included the gusset plate sizes, thicknesses, brace angle, out-of-plane restraint at the gusset-to-splice conjunction, beam and column moments and the out-of-plane loading eccentricity. The schematic of the specimens and the arrangement of the splice members are shown in Figs. 1.1 and 1.2 respectively. The test setups for the experimental program are shown in Figs. 1.3 and 1.4. Test setup shown in Fig. 1.4 was used to conduct the tests on the specimens with brace angle or beam and column as the test parameter. The remaining specimens were tested by the test frame shown in Fig. 1.3.

### 1.2.2 Test Results

The ultimate loads for all the specimens are shown in Table 1.1. The test results can be summarized as follows:

1) For specimens tested without the out-of-plane restraint boundary condition, the failure mode was sway buckling of the gusset plate connections. However, if an out-of-plane restraint boundary condition was imposed, a local buckling failure mode was observed.
2) In general, significant yielding was observed in the gusset plate specimens prior to their reaching the ultimate loads, except for the slender specimens (850 x 700 mm).
3) The ultimate loads of the specimens are almost linearly proportional to the gusset plate thickness.
4) Significant in-plane bending was observed for the specimens with a $30^{\circ}$ brace angle. The ultimate loads of the $30^{\circ}$ brace specimens were slightly lower than for the corresponding $45^{\circ}$ brace specimens.
5) The presence of beam and column moments did not affect the ultimate loads of the gusset plate specimens. However, the in-plane stiffness of the specimens was reduced by the moments, and yielding was observed at a load level significantly lower than the corresponding yield load estimated by the Whitmore effective width method.
6) The ultimate loads of the compact specimens (500x400 mm) were significantly higher than the corresponding yield load levels estimated by the Whitmore effective width method.
7) The Thornton method ($30^{\circ}$) produced conservative estimates of the ultimate loads of the specimens.
8) The eccentrically loaded specimens failed by extensive yielding at the splice member. The ultimate strength of the specimens was improved significantly when a tee-section splice member was used instead of a plate type splice member.

Table 1.1. Specimen Descriptions and Test Results

| Specimen Designation | Plate Size (mm x mm) | Plate Thickness (mm) | Loading Eccentricity (mm) | Beam Moment Mb (kN·m) | Column Moment Mc (kN·m) | Brace Angle | Ultimate Load P (kN) |
|---|---|---|---|---|---|---|---|
| GP1 | 500 x 400 | 13.3 | - | - | - | 45° | 1956 |
| GP2 | 500 x 400 | 9.8 | - | - | - | 45° | 1356 |
| GP3 | 500 x 400 | 6.5 | - | - | - | 45° | 742 |
| GP1R | 500 x 400 | 13.3 | - | - | - | 45° | 2057 |
| GP2R | 500 x 400 | 9.8 | - | - | - | 45° | 1487 |
| GP3R | 500 x 400 | 6.5 | - | - | - | 45° | 790 |
| SP1 | 850 x 700 | 13.3 | - | - | - | 45° | 1606 |
| SP2 | 850 x 700 | 9.8 | - | - | - | 45° | 1010 |
| AP1 | 500 x 400 | 13.3 | - | - | - | 30° | 1720 |
| AP2 | 500 x 400 | 9.8 | - | - | - | 30° | 1210 |
| AP3 | 500 x 400 | 6.5 | - | - | - | 30° | 728 |
| MP1 | 500 x 400 | 13.3 | - | 250 | 125 | 45° | 1933 |
| MP2 | 500 x 400 | 9.8 | - | 250 | 125 | 45° | 1316 |
| MP3 | 500 x 400 | 6.5 | - | 250 | 125 | 45° | 721 |
| MP3A | 500 x 400 | 6.5 | - | 375 | 187.5 | 45° | 819 |
| MP3B | 500 x 400 | 6.5 | - | 0 | 0 | 45° | 821 |
| EP1 | 500 x 400 | 13.3 | 11.4 | - | - | 45° | 310 |
| EP2 | 500 x 400 | 13.3 | 13.2 | - | - | 45° | 334 |
| EP3 | 500 x 400 | 13.3 | 53.0 | - | - | 45° | 890 |

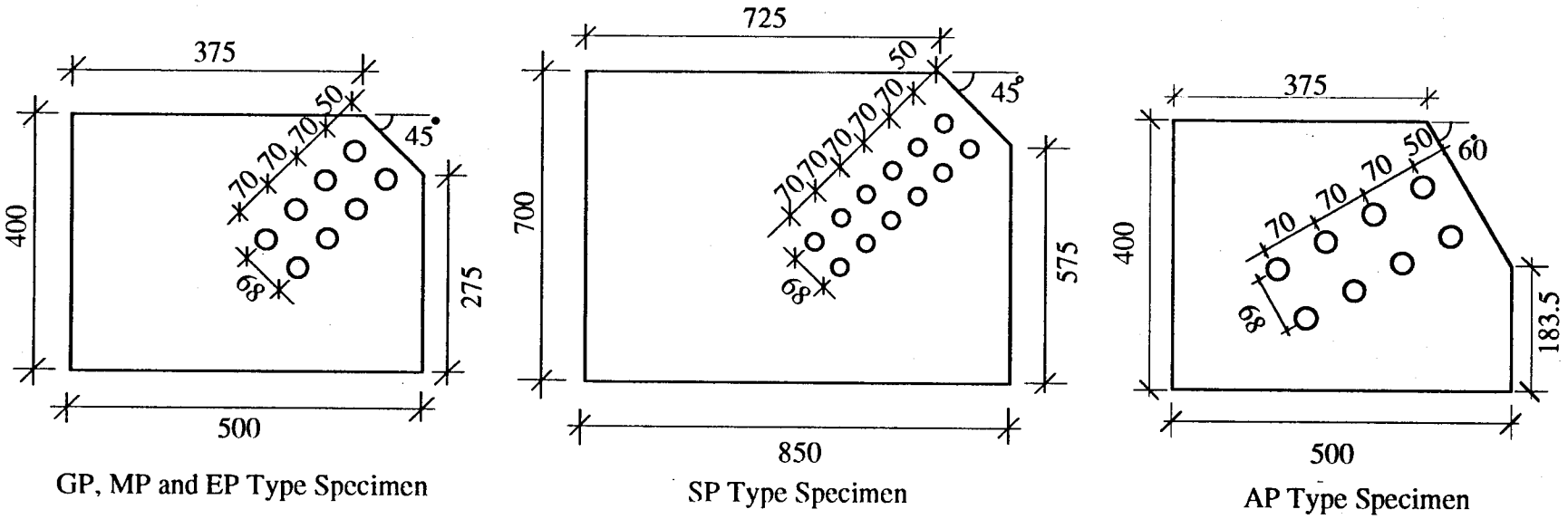


Fig. 1.1 Schematic of Test Specimens

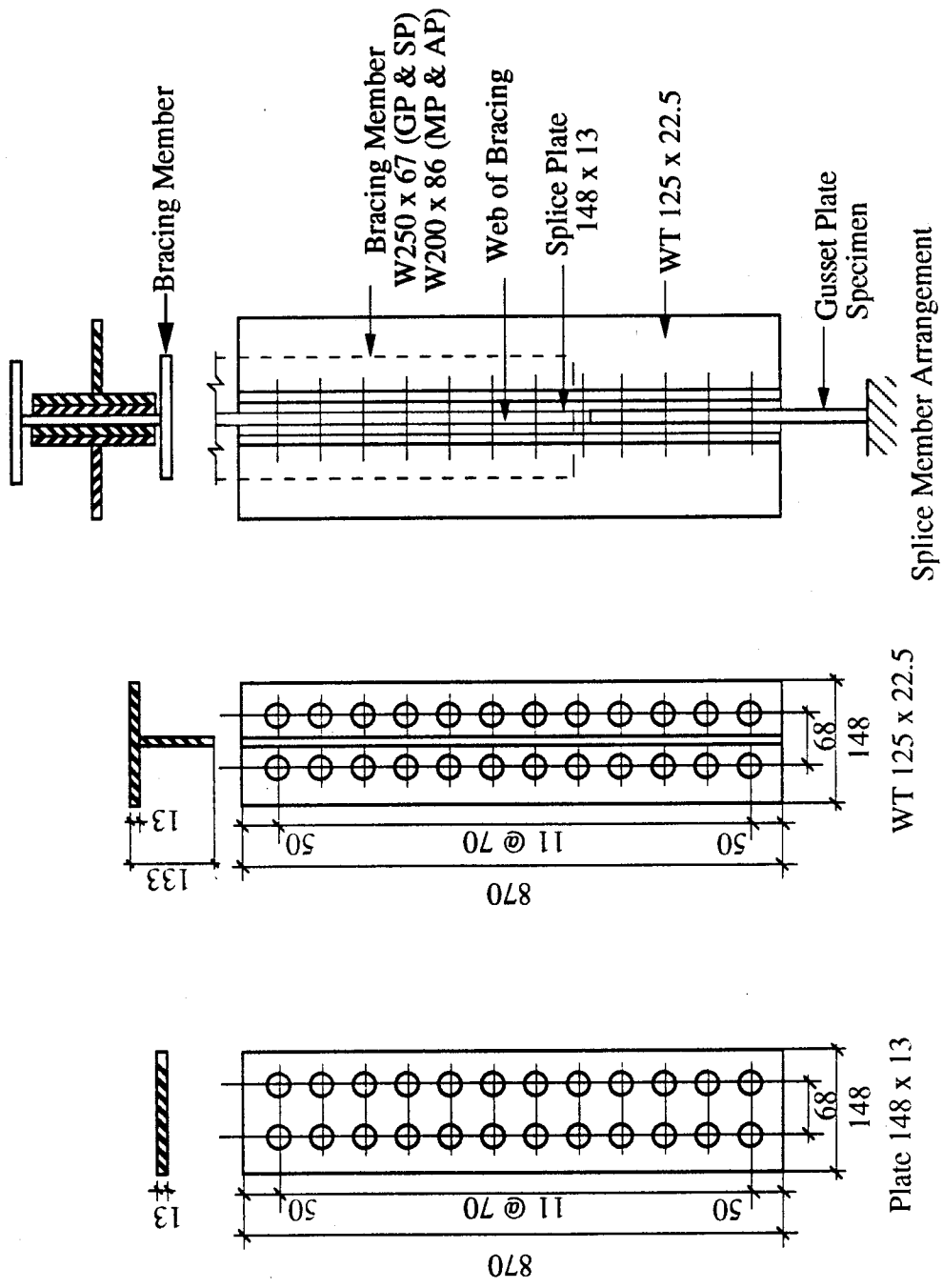


Fig. 1.2a Splice Members and Splicing Arrangement For GP, SP, MP and AP Type Specimens

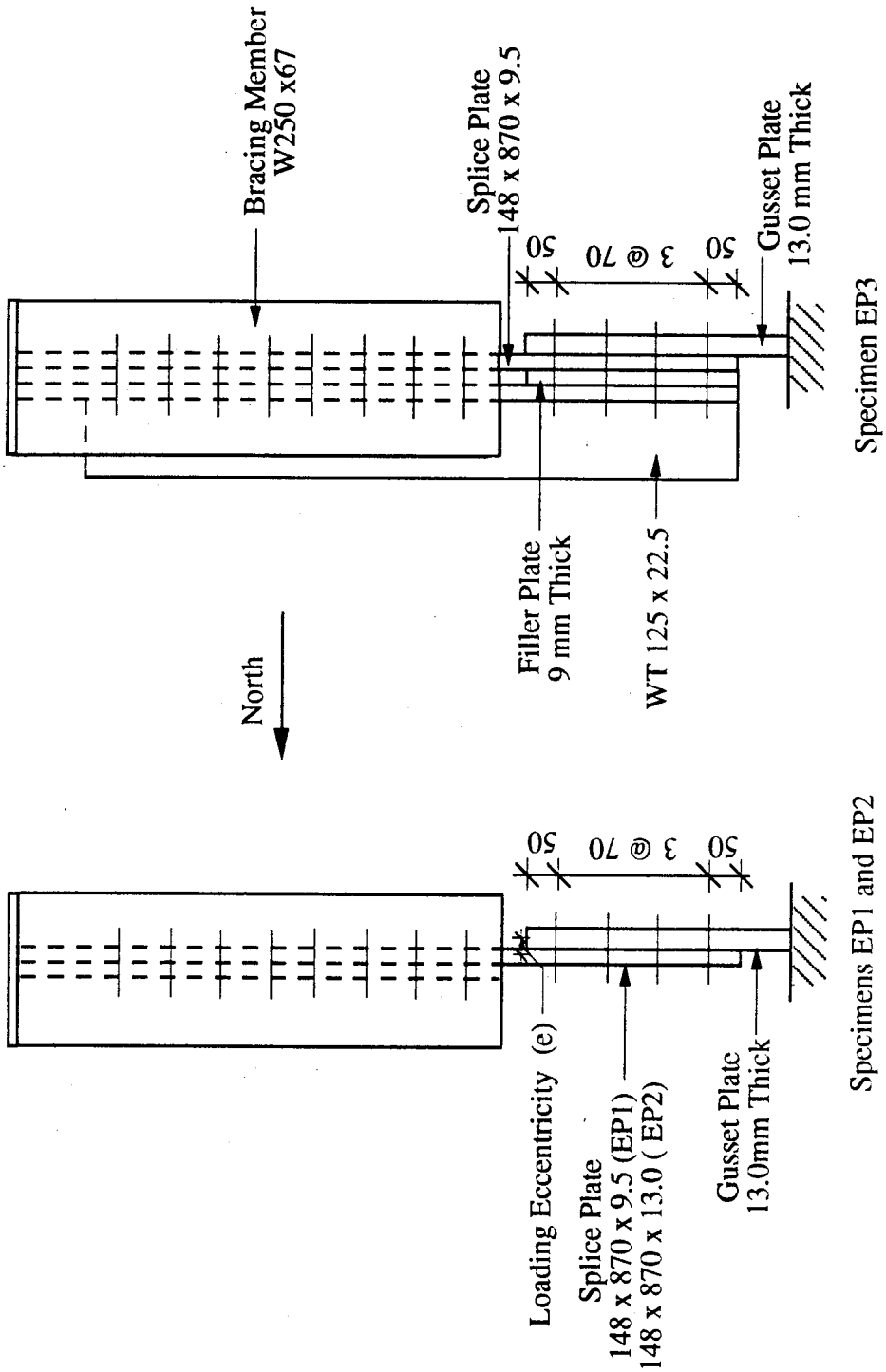


Fig. 1.2b Splice Member Arrangement for EP Type Specimens

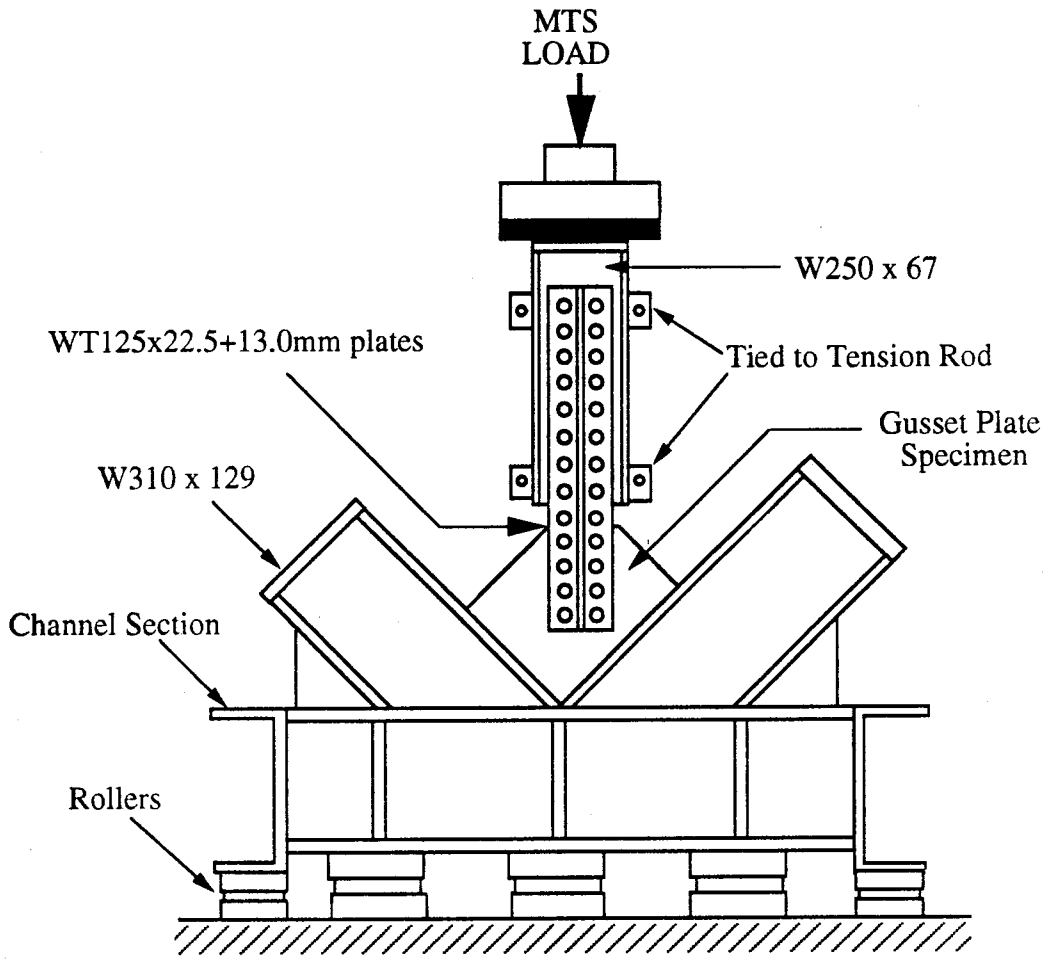


Fig. 1.3 Schematic of Test Setup for Scheme I

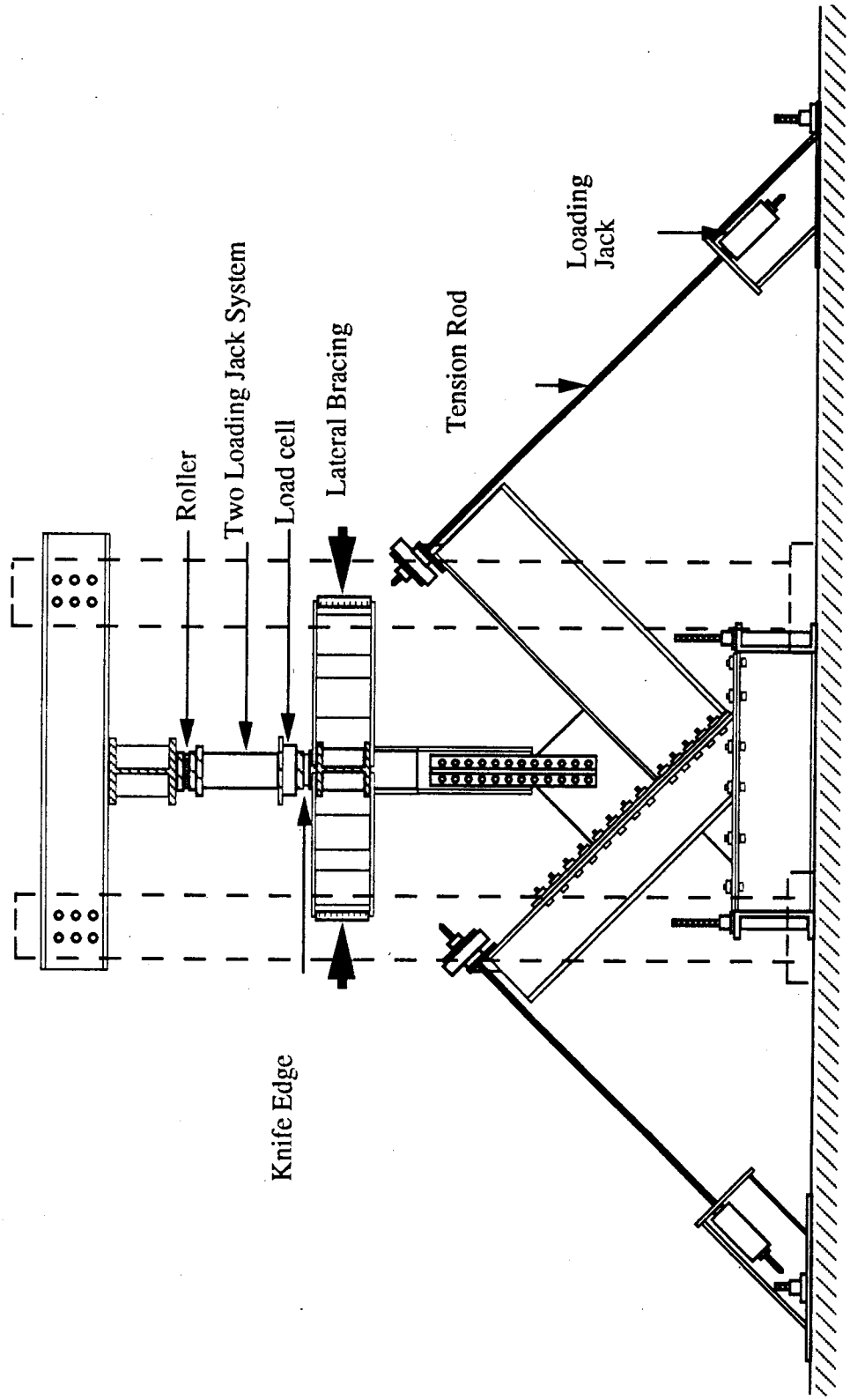


Fig. 1.4 Schematic of Test Setup for Scheme II

# 2. ANALYSIS OF TEST SPECIMENS

## 2.1 General

The compressive behavior of gusset plate connections has been investigated experimentally and the test results were presented in the previous chapters. To evaluate the ultimate strength of the specimens analytically, the finite element method was employed. It can be seen from the test results that the majority of the specimens experienced a significant yielding and out-of-plane deflection prior to reaching the ultimate loads. Since the failure mode of most of the specimens involved both a material nonlinearity and instability phenomenon, the most appropriate analysis is to trace the actual nonlinear load-deflection behavior of the specimens. However, the high computation expense of this approach prohibits its use in analyzing all the specimens. Therefore, it was decided to employ the method of plastic bifurcation buckling to evaluate the compressive strength of the GP, SP, AP, and MP type specimens. For the eccentrically loaded specimens (EP), a load deflection analysis was used to predict the ultimate strength of the specimens, since the main failure mode of the test specimens was yielding of the splice plate at the conjunction of gusset-to-splice. A rigid-plastic analysis was also performed on specimens EP1 and EP2 since a plastic collapse mechanism was observed from the test results of these specimens. The plastic bifurcation buckling method will be presented in detail in the following section.

## 2.2 Finite Element Analysis - Plastic Bifurcation Buckling

The general bifurcation buckling analysis in the context of the finite element method will be discussed first, followed by the procedure of conducting plastic bifurcation buckling analysis. Bifurcation buckling is characterized by the fact that, as the load passes through its critical stage, the structure passes from its unbuckled equilibrium configuration to an

infinitesimally close buckled equilibrium configuration. The bifurcation buckling analysis in matrix form (Cook, Malkus and Plesha 1988) can be described as :

$$([K] + \lambda[K_\sigma])\{D\} = \{0\} \qquad [2.1]$$

where the matrix [K] is the conventional structural stiffness matrix, $[K_\sigma]$ is the stress stiffness matrix to account for the in-plane stress distribution, {D} is the displacement vector corresponding to the buckling shape, and $\lambda$ is an arbitrary scalar multiplier. This equation described the problem of classical buckling analysis (Chang and Chen 1986) in which the prebuckling rotations of the structure are either neglected or are zero. Equation [2.1] can also be described as an eigenvalue problem with {D}being the eigenvector and $\lambda$ being the eigenvalue. To evaluate $[K_\sigma]$, a reference load level {R} is applied to the structure, and a standard linear static analysis is performed. The in-plane stress distribution resulting from this analysis is then used to generate $[K_\sigma]$. This $[K_\sigma]$ is subsequently multiplied by $\lambda$, an arbitrary scalar multiplier, to account for the applied load level which causes bifurcation buckling to occur. It should be noted that, since $[K_\sigma]$ is independent of displacement, multiplying $[K_\sigma]$ by $\lambda$ implies evaluating $[K_\sigma]$ based on a stress intensity corresponding to the applied load level of $\lambda\{R\}$. However, the in-plane stress distribution remains the same. The lowest value of $\lambda$ and the associated {D}(buckling shape) satisfying equation [2.1] defines the critical stage of the system, and the corresponding bifurcation buckling load is $\lambda\{R\}$.

In general, the method of plastic bifurcation buckling analysis is similar to the classical buckling analysis, except that material nonlinearity is considered in the former analysis method. In order to include the material nonlinearity existing prior to buckling, a nonlinear in-plane static analysis based on a applied trial load level and the actual material properties of the structure is performed. The resulting displacement field and the in-plane stress distribution from this analysis are used to evaluate the current values of [K] and $[K_\sigma]$,

respectively. The matrix [K], evaluated including the effects of material nonlinearity, is termed the tangent stiffness matrix. Then a classical buckling analysis based on these current stiffness values is conducted according to equation [2.1]. If $\lambda$ evaluated based on the classical buckling analysis is equal to 1.0, then the applied trial load level is the critical load. However, if $\lambda$ is greater than 1.0, a larger trial load level will be applied to the structure to perform the nonlinear in-plane static analysis again . A new set of current stiffness values is obtained and the classical buckling analysis is conducted to evaluate the new $\lambda$. This procedure continues until $\lambda$ equals 1.0. This procedure is also illustrated schematically in Fig. 2.1.

## 2.3 Finite Element Model

The commercial program ANSYS (1989), version 4.4a, installed in a 486 personal computer was used to perform the analysis. A four node quadrilateral shell element (STIF 43 in ANSYS) with six degrees of freedom at each node was used to model the gusset plate. A beam element (STIF 4) and an elastic quadrilateral shell element (STIF 63) were used to model the flanges and webs of the beam and column respectively for the analysis of MP and AP types specimens. The STIF 43 element has the capability of handling plasticity, stress stiffening and large deflection problems. A multilinear stress-strain curve, based on the coupon tests results, as shown typically in Fig. 2.2a, was used as the material properties in the analysis. The von Mises yield criteria with the associated flow rule and isotropic hardening were employed in the multilinear material model. The full Newton-Raphson method was used to solve the nonlinear equilibrium equations in the static analysis. The full subspace iteration method was used to evaluate the eigenvector (D) and eigenvalue ($\lambda$) in the classical buckling analysis.

The typical finite element model of the GP and SP types specimens is shown in Fig. 2.2a. Three-dimensional mesh was used to model the connection, with the splice plates placed on

both sides of the gusset plate, as shown in Fig. 2.2a. The beam and column boundaries were fully restrained to simulate a rigidly welded connection. At the conjunction of the bracing member and gusset plate, infinite rotational restraint was assumed to be provided by the bracing member along the element x-axis. A load was applied as the element pressure on the splicing member and transferred from the splicing member to the gusset plate, at the bolt locations as shown in the figure. Constraint equations were used at the bolt locations to simulate a rigid line tied across the splice plates and the gusset plate such that the same in-plane displacements were shared at these locations and the connection rotated about the centerline of the gusset plate during buckling. It should be noted that the shear deformation of the bolts was neglected in the analysis due to its complex nonlinear behavior. It is also believed that this assumption will have negligible effects on the ultimate strength of the specimens. This belief is based on the fact that the critical region of the gusset plate at which inelastic buckling occurred is located directly underneath the splice member. Hence, the distribution of the bolt forces is believed to have insignificant effects on the stress distribution and intensity at this region.

For the AP and MP type specimens, a similar finite model as the GP type specimens was used; however, the beam and column supporting the gusset plate specimens were also included in the model, as shown in Fig. 2.3a. This particular model provides more realistic boundary conditions for the AP type specimens and allows the application of beam and column moment for the MP type specimens. Concentrated forces were applied at the end of the beam and column to produce the required moment at the connection. For the EP type specimens, the typical finite element mesh is shown in Fig. 2.3b. It can be seen from this figure that the bracing member was also included in the model in order to provide a more realistic boundary and loading conditions for the splice member. The bracing member was modeled by using a beam element (STIF 4) for the flanges and shell elements (STIF 43) for the web. The actual material properties of the gusset plate and the splice plate were used in the load deflection analysis.

Since plasticity introduced a nonconservative aspect to the problem, the applied load increment was selected to be as close to the actual loading sequence used in the experiments as possible. However, in some cases the incremental loads may have to be decreased in order for the nonlinear solution to converge. For the plastic bifurcation buckling analysis, in general, a single load step was applied to the gusset plate model such that the finite elements in the highly stressed area were almost beginning to yield. The load level was usually chosen as approximately 90% of the corresponding Whitmore load of the specimens. Then, load increments were applied to capture the effect of material nonlinearity. As the applied load approached about 90% of the experimental ultimate load, a classical buckling analysis was performed, based on the current stiffness values as mentioned above. This whole procedure was terminated when $\lambda$, evaluated by the classical buckling analysis, was equal to 1.05 or less. For the load vs. deflection analysis, a displacement controlled method was used to load the specimens in order to achieve the convergence of the solution, especially in the region of the ultimate load level and the unloading part of the curve. A uniform incremental displacement was imposed at the nodes of the bracing member, as shown in Fig. 2.3b.

The finite element mesh employed for this analysis was based on a mesh study of the GP type specimens. The plastic bifurcation buckling loads of the GP type specimens, evaluated using a coarse mesh, were within two percent of those of a fine mesh. However, since the computation time required to analyse the fine mesh was not significantly increased relative to the coarse mesh, the fine mesh was used for the analysis of the test specimens.

## 2.4 Finite Element Analysis Results

### 2.4.1 General

The analytical ultimate loads of the specimens, based on plastic bifurcation buckling analysis, are shown together with the test results in Table 2.1. However, the analytical

results of the specimens with out-of-plane restraint are not included, since the solution of the in-plane stress analysis for these specimens converged extremely slow. In fact, the load increment had to be made so small that it became impractical to continue the analysis. Hence, it was decided to abandon the analysis of the specimens with out-of-plane restraint. In general, it can be seen from the table that the analytical predictions are in reasonable agreement with the test results. The test to predicted ratios range from 0.76 (AP1) to 1.12 (MP3B), with a mean value of 0.94 and the corresponding standard deviation of 0.11. These ratios are also shown graphically in Fig. 2.4. For comparison purposes, the elastic buckling loads of all the specimens were also evaluated and are shown in Table 2.1. It can be observed that, in general, the elastic buckling loads of the specimens are significantly higher than the test ultimate loads, except for specimen SP2, which was governed by the elastic buckling mode.

To examine the analytical results, the in-plane stress contour plots, the principal stress vector plots, and the in-plane deformation plots of the specimens (except those of the EP type) will be discussed in the following sections according to the types of specimen. Since there is no significant difference in the buckling shapes for the specimens, only a general discussion of the buckling mode will be presented. The analytical results of the EP type specimens will be presented following the section of the discussion of buckling shapes. Comparisons of the analytical results among test parameters will also be included.

### 2.4.2 GP and SP Type Specimens

#### 2.4.2.1 In-Plane Stress Distribution

To investigate the compressive behavior of the specimens, their in-plane stress distributions from the analysis are examined. The postprocessing routine of ANSYS allows the display of the in-plane stress distributions in terms of stress contour lines. In producing these contour plots, the von Mises effective stress was used. Since the experimental yielding

behavior of specimen GP1 was recorded thoroughly at various load levels during testing, the analytical yielding behavior of specimen GP1 will be examined in detail and compared with the test results. The effective stress contour plots of specimen GP1 are shown in Figs. 2.5a to 2.5e at various load levels as indicated. As a reminder, the unit of the effective stress is MPa. As can be seen from Fig. 2.5a, the yielding of the gusset plate area near the last row of bolts (Whitmore effective width section) was observed at a load level of 1370 kN. However, at this stage of loading most of the gusset plate area was still in the elastic range. It can also be seen that the short free edge was loaded more severely than the long free edge. At a load of 1500 kN, the effective stress distribution of the gusset plate changed moderately indicating that a redistribution of load had occurred due to inelastic action. The maximum effective stress at this stage occurred at the top right corner of the gusset plate, as indicated in Fig. 2.5b. A slight yielding was also observed at the plate area about the sides of the splicing member. Approximately 30% of the gusset plate area was in the inelastic range when the applied load was 1700 kN, as shown in Fig. 2.5c. General yielding of the plate was observed at the area around the last row of bolts and about the sides of the splice member. The yielding at the area around the last row of bolts extended towards the beam and column boundary when compared with the yielding zone at the previous load level. For the gusset plate area along the sides of the splicing member, the yielding progressed upwards and also towards the free edges. At a load of 1950 kN, about 65% of the area was in the inelastic range, as shown in Fig. 2.5d. A significant increase in stress levels when compared to that of the previous load level was also observed at the plate along the sides of the splicing member. Figure 2.5e shows the effective stress plot for specimen GP1 at an ultimate load of 2336 kN. It can be seen from this figure that about 85% of the gusset plate area was yielded. The yielding basically extended from the Whitmore effective width section to the entire area, except near the column boundary and the fixed end of the free edges. A similar yielding behavior and process were recorded during the testing of specimen GP1.

Based on the above discussion, it can be seen that a significant part of the gusset plate can reach the yield strength of the material. However, the connection must be stiff enough to avoid early instability failure. If the connection is relatively slender, elastic buckling may occur before the gusset plate can even reach the corresponding Whitmore load (Cheng et al. 1994).

For specimens GP2 and GP3, similar yielding patterns and stress distributions as those of specimen GP1 at the early loading stage were observed. However, the extent of yielding was not as significant. In particular, for specimen GP3, only minor yielding occurred at the plate area near the last row of bolts when the specimen reached the ultimate load. Since the analytical elastic buckling load of specimen GP3 was very close to the experimental ultimate load, it would not require a significant amount of inelastic deformation to cause plastic bifurcation buckling. For specimen SP1, a similar stress pattern to that of GP1 was observed since the same brace angle and similar plate aspect ratio were used for both types of specimens. However, for specimen SP2, no yielding developed and the plate was failed in elastic buckling.

To compare the stress prediction by ANSYS in the elastic range, the test result from specimen GP1 was used. The comparison was made at the rosette gages location in the elastic range at a load level of 1220 kN. The experimental strain readings were first converted to the principal values, and then these values were used with the two-dimensional Hook's law to evaluate the corresponding principal stresses. These principal stresses were then converted to the von Mises effective stress and compared to the ANSYS effective stress contour plot as shown in Fig. 2.6. It can be seen from this figure that a good prediction of stress was obtained from the analysis.

### 2.4.2.2 Principal Stress Vector and In-Plane Deformation Plots

The principal stress vectors plots produced by ANSYS were also used to examine the flow of force through the gusset plate to the beam and column boundary and also illustrated the behavior of in-plane bending. The stress vectors indicate a compression (tension) when the arrowheads of the vectors point inward (outward). Again, specimen GP1 was used for the illustration. The principal stress vectors plots at a load level of 1370 kN and the ultimate load level of 2336 kN were used for illustrational purposes, as shown in Figs 2.7a and 2.7b respectively . These figures show that the principal stress directions in the free edges area were almost parallel to the corresponding free edges especially in the lower load level. However, the direction of the principal stress vectors approached the angle of the bracing member, especially in the area around the end of the splicing member at which the stress vectors were almost aligned with the angle of the brace. In addition, this area was the most stressed one, as can be seen from the lengths of the stress vectors which were scaled to the actual stress values. The plate area near the last row of bolts and bounded by the beam boundary was also severely loaded, and the stress vectors were oriented at approximately 60° to the horizontal, as shown in the figures. It can be seen from these figures that the beam boundary attracted more load since it was closer to the last row of the bolts.

Transverse compression was observed at the top right part of the gusset plate, which was also the location of maximum stress at ultimate. This transverse compression was due to the significant in-plane deformation at the bolt points, as shown in Figs. 2.8a and 2.8b. The in-plane deformation mode and the principal stress plot of specimen GP1 shown in Fig. 2.8a and 2.7a respectively indicate that in-plane bending occurred at both free edges. This in-plane bending can also be observed in the stress contour plot, as shown in Fig. 2.5a, which illustrates that the stress gradient occurred in the free edges. The stress vector plot shown in Fig. 2.7b also indicates that compression occurred in the other principal direction perpendicular to the applied load direction. This compression was caused by the

displacement restraint applied to the beam and column boundary, which prohibited the lateral displacement of the plate due to Poisson's ratio effect. As will be seen in a later discussion, if the beam and column are allowed to deform (in-plane) when the load is applied to the gusset plate, tension instead of compression will occur.

### 2.4.3 AP Type Specimen

#### 2.4.3.1 In-Plane Stress Distribution

For this particular type of specimen, only the in-plane stress distribution for specimen AP1 at a load level of 1380 kN is discussed. It is believed that this is sufficient to demonstrate the in-plane stress behavior of this type of specimen. The in-plane stress distribution is shown in Fig. 2.9. It can be seen from this figure that the plate area underneath the splicing member was severely loaded. In addition, this highly stressed area was extended to the beam and column boundary. A high stress gradient was also observed at the short side free edge caused by the in-plane bending, as will be discussed in the following section. For this specimen, the maximum stress occurred at the top right part of the gusset plate, as shown in the figure.

#### 2.4.3.2 Principal Stress Vector and In-Plane Deformation Plots

The principal stress vector plot and the in-plane deformation plot are shown in Figs. 2.10 and 2.11 respectively. It can be seen from Fig. 2.10 that the plate area underneath the splice member was highly stressed. Again, the principal compressive stress vectors in this area were almost aligned with the brace angle. Transverse tension was observed in the plate. As mentioned above, this tensile stress was developed due to the in-plane deformation of the supporting beam and column boundary when the axial load was applied. This in-plane deformation can be observed from the in-plane deformation plot of the gusset plate specimen, as shown in Fig. 2.11. This figure shows that the column boundary

deflected quite significantly when it is compared with the deformation at the beam boundary. It also illustrates that in-plane bending existed in both free edges, especially in the short free edge. The severity of this in-plane bending at the short free edge can also be observed from the principal stress vector plot where tensile stress existed in almost all the elements at the short free edge, as shown in Fig. 2.10.

### 2.4.4 MP Type Specimens

#### 2.4.4.1 In-Plane Stress Distribution

The general discussion of the in-plane stress distribution for the MP type specimen will be based on specimen MP1. However, the effects of the beam and column moment will be presented in the following section of discussion and comparison of analytical results. Two load levels of 300 kN and 1500 kN were considered in this section. It should be noted that full beam and column moment values were applied to the specimen at these load levels. The stress contour plots for these load levels are shown in Figs. 2.12a and 2.12b. As can be seen from Fig. 2.12a when the applied load was relatively small (300 kN), the in-plane stress distribution was predominantly influenced by the beam and column moment. This can be illustrated by the fact that maximum tensile stress occurred at the fixed ends of the free edges due to the beam and column moment at the applied load of 300 kN. On the other hand, as the applied load increased to 1500 kN, the stress distribution was significantly altered, as shown in Fig. 2.12b. Again, the highly stressed area was located underneath the splicing member, although the maximum stress occurred at the top right part of the gusset plate. A high stress gradient also existed at the short free edge area, as shown in Fig. 2.12b.

#### 2.4.4.2 Principal Stress Vector and In-Plane Deformation Plots

The principal stress vector plots and the in-plane deformation plots at the load levels of 300 kN and 1500 kN are shown in Figs. 2.13a and 2.13b respectively. It can be seen from Fig. 2.13a that the beam and column moment severely loaded the part of the plate closer to the beam and column boundary and produced principal tensile stress at this region, in particular in the area close to the fixed ends of the free edges. When the applied load increased to 1500 kN, the stress vector plot indicated that the axial load effect became more dominant. Again, the principal compressive stress vectors were almost aligned with the brace angle, especially in the area underneath the splicing member, as shown in Fig 2.13b. However, the elements near the fixed ends of the free edges still showed principal tensile stresses at this high load level.

The in-plane deformation at the load level of 300 kN is shown in Fig. 2.14a. This figure also includes the beam and column deflection. As can be seen from this figure, significant deflection was observed for the beam and column due to the applied concentrated loads at their ends. This figure also shows that the beam and column deformation stretched the gusset plate. The tensile stress produced by this stretching was oriented according to the principal tensile stress vector, as shown in Fig. 2.14a. The in-plane deformation plot at the load level of 1500 kN is shown in Fig. 2.14b. Again, in-plane deflection was observed at the beam and column boundary.

### 2.4.5 Buckling Shapes of Specimens

The typical buckling shapes of each type of specimens (except EP type) are shown in Figs. 2.15a to 2.15d. For illustrational purposes, the splicing members were removed from the model. It can be seen from these figures that, in general, similar buckling shapes were observed for the specimens. Since the bracing member was allowed to sway out-of-plane, the buckling shapes of these specimens at the free edges and the plate area underneath the

splicing member resembled the buckling shape of a fixed-guided column. However, a slight twisting at the conjunction of gusset-to-splice was observed, especially with the AP type specimens. This slight twisting was mainly caused by the unsymmetrical gusset plate section for all the specimens and, in addition, the 30° brace angle for the AP type specimens. However, it can be seen from these figures that the spliced region remains relatively straight for all the specimens.

### 2.4.6 EP Type Specimens

#### 2.4.6.1 Load Deflection Behavior

As mentioned above, load deflection analysis was employed to evaluate the ultimate strength of the EP type specimens. The experimental and analytical load deflection curves for the specimens are shown in Figs. 2.16 to 2.18. It can be seen from these figures that the analysis predicts very well the experimental ultimate load of the specimens. The test to predicted ratios range from 0.97 to 1.05. However, the predictions by ANSYS show a stiffer load deflection behavior for the specimens. This may be due to the effects of the assumed idealized boundary conditions in the finite element model and the initial imperfections that could exist in the connection. Nevertheless, for specimens EP1 and EP2 the predicted load deflection curves are generally in good agreement with the test results.

#### 2.4.6.2 In-Plane Stress Distribution

Since specimens EP1 and EP2 are similar, except for the splice plate thickness, only the discussion of the in-plane stress distribution of specimen EP1 will be presented. The in-plane stress distributions of the splice plate for specimen EP1 are shown in Figs 2.19 and 2.20. Fig 2.19 illustrates the in-plane stress for the top surface of the splice plate and Fig. 2.20 shows the bottom surface stress. The in-plane stress shown in these figures is in the local element x-axis, as illustrated in Fig. 2.3b. It can be seen from these figures that the

splice plate area near the last bolt line from the end of the brace member was stressed significantly. The bottom stresses at this location were well above the static yield strength of the material, and the top stresses were very close to yield. The test results also indicated that significant yield lines occurred in this region when the applied load was near ultimate. To illustrate that a significant bending stress existed in the splice plate, a plot of surface stresses along the centerline of the length of the splice plate is shown in Fig. 2.21. This figure shows that the bending of the splice plate was mainly concentrated in the vicinity of the last bolt line. It should be noted that high compressive stresses existed in the top surface of the splice plate for the part of the splice plate connected to the gusset plate, whereas the compressive stresses in the bottom surface were reduced in this region. This is due to the bending action of this region, which induced significant compressive bending stress to the top surface and tensile bending stress to the bottom surface of the splice plate.

The top and bottom surface in-plane stress distributions of the gusset plate are shown in Figs. 2.22 and 2.23. It can be seen from these figures that the gusset plate was stressed significantly from the effects of bending in a strip of area joining the two fixed ends of the free edges . The top stress levels in this strip of area were generally greater than the static yield strength of the gusset plate material. The test results also showed that yield lines in the gusset plate originating from the end of the splice plate to the beam boundary were observed . For the bottom surface stress, stress levels very close to yield were observed in this strip of gusset plate area. It can be seen from the analytical results of specimens EP1 and EP2 that plastic hinges were developed at the splice plate near the end of brace and along the strip of gusset plate area as mentioned above. These plastic hinges provided a failure mechanism for the connection, which was also observed in the test results. This plastic collapse mechanism will be discussed in the following section.

For specimen EP3, compressive yielding was observed for the 2.5 mm thick splice plate on both the top and bottom surfaces, as shown in Figs. 2.24a and 2.24b. The tee-section

splice member showed tensile yielding near the tip of the web at the conjunction of the gusset-to-splice at the ultimate load. As shown in Fig. 7.15, these observations compared well with the test results for the plot of load versus strain gauge readings recorded at the splice plate and the web of the tee-section. The gusset plate in-plane stress distributions for specimen EP3 are shown in Fig. 2.25a and 2.25b. Again, the strip of area joining the fixed ends of the free edges was highly stressed for both top and bottom surfaces. In particular, the gusset plate area underneath the splice members was severely stressed as indicated by the contour lines. This observation also confirms the test results wherein diagonal yield lines resulting from the applied axial load and yield lines resulting from the bending effects were observed.

#### 2.4.6.3 Principal Stress Vector and Out-of-Plane Deformation Plots

Since the principal stress vector plots for the gusset plate of the EP type specimens are similar, only specimen EP1 will be discussed. The principal stress vector plots for both the top and bottom surfaces of specimen EP1 are shown in Figs. 2.26 and 2.27. It can be seen from these figures that significant bending of the gusset plate was observed. The top surface of the gusset plate, which was connected to the bottom surface of the splice plate, was in severe compression, due to the combination of the axial compressive stress and the compressive bending stress. On the other hand, the bottom surface of the gusset plate was loaded in tension due to the significant bending effects.

The out-of-plane deformation plots for the EP type specimens are shown in Figs 2.28 to 2.30. It can be seen from these figures that significant bending deformation was observed at both the gusset plate and the splice member at the conjunction of gusset-to-splice. To examine closely the deformation mode of the splice member, a plot of out-of-plane displacement along the centerline of the splice plate for specimens EP1 and EP2 are produced, as shown in Figs. 2.31 and 2.32. These figures illustrate that a significant

rotation of the splice plate occurred in the vicinity of the location of gusset-to-splice and also at the gusset plate near the end of the splice plate. These observed rotations substantiated that plastic hinges were developed at these locations.

## 2.5 Discussion and Comparison of Analytical Results

### 2.5.1 General

As mentioned in the previous section, the predictions by ANSYS were in reasonable agreement with the test results. The test to predicted ratios varied from 0.76 to 1.12, as illustrated in Table 2.1 and Fig. 2.4. As can be seen from this figure, conservative predictions are always observed for the 6.5 mm thick specimens except for specimen MP3. However, the ultimate loads for the rest of the specimens were over-estimated. This is probably due to the use of the bifurcation buckling concept and also the nature of finite element method that usually produces a stiffer model of the structure. Nevertheless, these predictions do provide a reasonable estimate of the compressive strength of the specimens. A design method will be proposed, based on the test and analytical results and presented in the following chapter. The effects of various parameters on the compressive behavior and strength of the gusset plate specimens will be discussed in the following sections.

### 2.5.2 Effects of Gusset Plate Thickness and Size

As can be seen in Table 2.1, as the gusset plate thickness increased, the ultimate load of the specimens increased. In order to compare with the test results, a linear regression line was fitted to the analytical results and the test results were also plotted on the same graph, as shown in Fig. 2.33. As mentioned above, the predictions were in general higher than the experimental ultimate loads, except for the 6.5mm thick specimens. This figure also shows that as the plate thickness increases, the difference between the test results and the analytical predictions increases. However, no reason can be found to explain this observation. In

general, for the same plate size the amount of yielding observed from the specimens in the analysis decreased with decreasing plate thickness, as described in the previous section. As the plate thickness decreases, the specimen may fail by instability before reaching the load level which causes inelastic deformation.

Table 2.1 shows that the predicted ultimate loads of the specimens decreases with increasing plate size. As expected, the slenderness of the gusset plate increases with increasing plate size and thus leads to a decrease in ultimate load. The amount of inelastic deformation also decreased with increasing plate size, as indicated from the analysis. It was also observed from both the tests and the analysis that elastic buckling occurred in specimen SP2 (850 x 700 x 2.8).

### 2.5.3 Effects of Angle of Diagonal Brace Member (45° and 30°)

In general, the analytical ultimate loads of the AP type specimens (30° brace angle) are slightly lower than those of the corresponding GP type specimens (45° brace angle), except for specimen AP3. However, Table 2.1 illustrates that the test results showed an appreciable difference between the ultimate loads of the AP and GP type specimens. Nevertheless, it can be seen that the ultimate loads of the specimens were not significantly affected by changing the brace angle from 45° to 30°. On the other hand, changing the brace angle affected the in-plane stress distribution of the specimens.

The effective stress distribution of specimens GP1 and AP1 are shown in Figs. 2.5a and 2.9 respectively. It can be seen that for specimen AP1, the severely loaded area underneath the splicing member was significantly increased, when compared to that of specimen GP1. In addition, a higher stress gradient for specimen AP1 existed in the free edges, as shown in Fig. 2.9. In fact, tensile stress was observed at the fixed end of the short free edge as shown by the principal stress vector plot in Fig. 2.10. This observation was also recorded from the strain gage readings from the test results. As mentioned in the previous chapter of

test results, this tensile stress was probably caused by the in-plane bending resulting from the larger horizontal component of the applied force for the AP type specimens. However, this was not observed in the GP type specimens.

### 2.5.4 Effects of Beam and Column Moments

As can be seen from both the test and the analytical results, in general the beam and column moments did not significantly affect the ultimate loads of the specimens. In fact, the predictions by ANSYS showed very similar ultimate loads for the specimens with the same thickness and size, regardless of the presence of beam and column moments. The effects of beam and column moment levels on the ultimate loads of the specimens were also examined by varying the moments applied to the 6.5 mm thick MP type specimens. As can be seen from Table 2.1, the analytical ultimate loads of the these specimens did not vary substantially when the beam and column moment levels were increased. However, as mentioned in the test results, the beam and column moments influenced the in-plane behavior of the specimens. To examine this observation in detail, the analytical results of MP3 specimens (MP3, MP3A and MP3B) are used. Figs 2.34a to 2.34c show the effective stress contour plots for the specimens at the same applied load level of 630 kN. One significant observation from these figures is that the effective stress increased when the applied beam and column moments increased. This explains the test results which demonstrate that when the beam and column moments were applied to the specimens, a significant additional increase in compressive strains was detected in the rosette gages. The additional increase in compression also contributed to the decrease in the in-plane stiffness of the specimens due to the early yielding initiated by this compression, as illustrated in the test results. The stress contour plots for specimens MP3 and MP3A also indicated that a high stress level existed at the fixed ends of the free edges due to the applied moments. Tensile strains close to yielding were also recorded at the strain gages located in the fixed ends of the free edges.

The principal stress vector plots shown in Figs. 2.35a to 2.35c indicate that a significant transverse tension due to the applied moments was observed in the specimens. As expected, this transverse tension increased with increasing applied moments, as indicated by the lengths of the stress vector. Again, significant tension was observed at the fixed ends of the free edges for the specimens (MP3 and MP3A) with applied moments. However, this tension was not observed from the specimen (MP3B) without applied moments, as shown in Fig. 2.35c. Different in-plane deformation modes are also observed for the specimens as shown in Figs. 2.36a to 2.36c. It can be seen from these figures that stretching of the plate was observed for the specimens with applied moments. This stretching is evident at the plate along the beam and column boundary and the free edges.

Based on the above discussion, it can be seen that beam and column moment produced both tensile and compressive stresses to the gusset plate. Since there was no significant increase or decrease in the ultimate loads of the specimens due to the applied moments, it is speculated that, although the increase in compression would have detrimental effects on the ultimate loads, the tensile stress would produce a beneficial stiffening effect on the specimens. Therefore, these two opposite stresses compensated each other and no significant change in ultimate loads was thus observed, due to the applied moments.

### 2.5.5 Effects of Loading Eccentricity

The test and analytical results both indicated that the presence of loading eccentricity significantly reduced the strength of the gusset plate connection and also produced a large out-of-plane deflection. It can be seen from the analysis that the loading eccentricity induced significant bending moment to both the splice member and the gusset plate. At the ultimate, plastic hinges were developed at the critical section of the splice member and also at the gusset plate. When the in-plane stress contour plots for specimens GP1 and EP3 are compared, it can be seen that the bending moment due to the loading eccentricity

significantly altered the in-plane stress distribution of the gusset plate. In particular, the gusset plate area underneath the splice member was stressed severely by both the axial load and the bending moment, which also produced high bending stresses in the vicinity of the fixed ends of the free edges, as typically shown by the stress vector plots of specimen EP1 in Figs. 2.25 and 2.26.

When the analytical load-deflection curves of the specimens were compared, it was found that the out-of-plane stiffness of the specimens increased as the thickness of the splice plate increased. In particular, the stiffness of specimen EP3 increased significantly due to the tee-section splice which provided bending rigidity to the connection.

## 2.6 Rigid Plastic Analysis of Specimens EP1 and EP2

As mentioned above, both the test and analytical results indicated that plastic hinges were formed in the splice plate at the conjunction of gusset-to-splice and along a strip of gusset plate area joining the fixed ends of the free edges for specimens EP1 and EP2. Since a failure mechanism was developed by these plastic hinges, a rigid-plastic analysis of the specimens may provide useful information, especially in estimating the ultimate load of the connection. Kitipornchai et al. (1993) also employed the rigid plastic collapse analysis to evaluate the ultimate strength of the eccentrically loaded cleat plates. The rigid-plastic analysis provides an unloading line which represents the changes in the plastic collapse load due to the change in the plate geometry (Korol et al. 1972). The intersection of this unloading line with the elastic loading curve of the connection provides an upper bound estimate of the ultimate load of the structure.

The plastic collapse model for the specimens is shown in Fig. 2.37. The plastic hinges were assumed to be located at the splice plate and the gusset plate, as mentioned above. It should be noted that the plastic hinge in the gusset plate was assumed to be a horizontal line originating from the fixed end of the long free edge to the beam boundary (hinge A), as

shown in Fig. 2.37. A more appropriate plastic hinge would be the one labeled as hinge B, shown in Fig. 2.37. Nevertheless, the assumed plastic hinge (hinge A) provided a simple mechanism and also simplified the evaluation of the plastic moment capacity of the plate.

The equilibrium approach was used to derive the equation of the rigid-plastic unloading line of the connection. A free body diagram of the mechanism is shown in Fig. 2.37. The connection was assumed to have deflected $\Delta$, and plastic moment capacity was developed in both plastic hinges. However, the plastic moment capacity of the section was reduced by the interaction of the axial load and applied moment, according to:

$$M_{pc} = M_p\left(1.0 - \left(\frac{P}{P_y}\right)^2\right) \qquad [2.2]$$

where P is the applied axial load, $P_y$ is the yield load of the section, $M_{pc}$ is the reduced plastic moment, and $M_p$ is the plastic moment capacity of the section. $M_{pcG}$ is the reduced plastic moment for the gusset plate and $M_{pcS}$ is the reduced plastic moment for the splice plate, as shown in Fig. 2.37. The loading eccentricity produced an eccentric moment of $P\cdot e$ as shown in the figure. Summing moment at the bottom plastic hinge gives:

$$M_{pcS} + M_{pcG} - P\cdot e - P\cdot\Delta = 0$$

therefore,
$$P(e+\Delta) = M_{pcS} + M_{pcG} \qquad [2.3]$$

According to eqn. 2.2, eqn 2.3 can be further reduced to:

$$P(e+\Delta) = M_{pS}\left(1.0 - \left(\frac{P}{P_{yS}}\right)^2\right) + M_{pG}\left(1.0 - \left(\frac{P}{P_{yG}}\right)^2\right)$$

where the subscripts S and G resprent the splice plate and the gusset plate respectively. The above quadratic equation can be solved simply as:

$$P = \frac{-(e+\Delta) + \sqrt{(e+\Delta)^2 + 4\left(\frac{MpS}{P_{yS}^2} + \frac{MpG}{P_{yG}^2}\right)(MpS+MpG)}}{2\left(\frac{MpS}{P_{yS}^2} + \frac{MpG}{P_{yG}^2}\right)} \qquad [2.4]$$

The unloading line can be evaluated by assuming a $\Delta$ and then solve for P from eqn. 2.3. A typical calculation of the unloading line for specimen EP1 is included in the appendix.

The rigid-plastic unloading lines for specimens EP1 and EP2 are shown in Figs. 2.38 and 2.39. As can be seen from these figures, an elastic curve was also included. The elastic curve was evaluated using ANSYS, which considered only the large deflection behavior of the connection. In general, the unloading lines for both specimens underestimated the unloading behavior of the specimens. However, for specimen EP1, the slope of the unloading curve was quite similar to that of the experimental curve. This underestimation of the unloading behavior was probably due to the assumption of the plastic hinge location in the gusset plate and also the strain-hardening of the material, aspects which were not included in the analysis. Murray (1981) investigated this effect of strain-hardening on the unloading line and concluded that if the static yield strength was increased by 20-30%, a better agreement between the tests and analysis would be achieved. To obtain an upper bound estimate of the ultimate load of the specimens, the intersection of the unloading line and the elastic curve was used. As can be seen from these figures, the intersection of the unloading line and the elastic curve for both specimens gives an ultimate load of approximately 10% higher than the test loads. The plastic collapse loads for these specimens are shown in Table 2.2. Hence, it can seen that by employing the rigid-plastic analysis and the elastic analysis (both of which do not require enormous computation time)

the upper bound of the ultimate load of the eccentrically loaded gusset plate connections can be evaluated.

Table 2.1 Analytical Plastic Bifurcation Buckling Loads of Test Specimens

| Specimen | Ultimate Load P (kN) | $P_{ANSYS}$ (kN) | $\frac{P}{P_{ANSYS}}$ | Elastic Buckling Load $P_E$ (kN) |
|---|---|---|---|---|
| GP1 | 1956 | 2336 | 0.84 | 5428 |
| GP2 | 1356 | 1483 | 0.91 | 2638 |
| GP3 | 742 | 680 | 1.09 | 836 |
| SP1 | 1606 | 1940 | 0.83 | 2169 |
| SP2 | 1010 | 940 | 1.07 | 940 |
| AP1 | 1720 | 2260 | 0.76 | 6476 |
| AP2 | 1210 | 1460 | 0.83 | 3181 |
| AP3 | 728 | 690 | 1.06 | 910 |
| MP1 | 1933 | 2320 | 0.83 | 6075 |
| MP2 | 1316 | 1450 | 0.91 | 3118 |
| MP3 | 721 | 755 | 0.95 | 985 |
| MP3A | 819 | 765 | 1.07 | 985 |
| MP3B | 821 | 735 | 1.12 | 985 |
| EP1 | 310 | 321 | 0.97 | - |
| EP2 | 334 | 342 | 0.98 | - |
| EP3 | 890 | 846 | 1.05 | - |

Table 2.2 Rigid-Plastic Collapse Load for Specimens EP1 and EP2

| Specimen | Ultimate Load P (kN) | Rigid-Plastic Collapse Load $P_{RPC}$ (kN) | $\frac{P}{P_{RPC}}$ |
|---|---|---|---|
| EP1 | 310 | 341 | 0.91 |
| EP2 | 334 | 364 | 0.92 |

**Plastic Bifurcation Buckling Analysis**

$$\{[K_T] + \lambda[K_\sigma]\}\ \{D\} = \{0\}$$

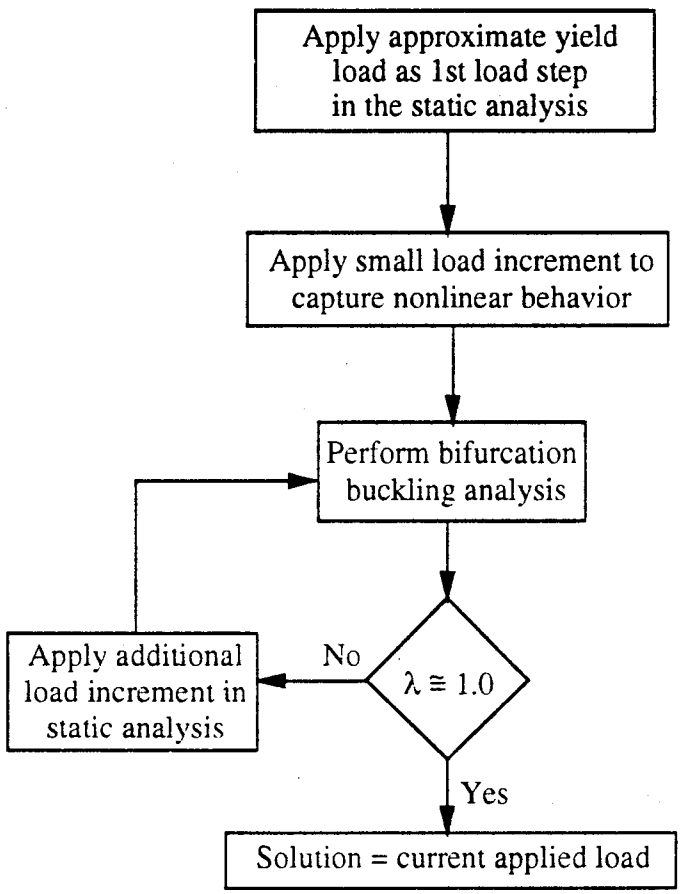


Figure 2.1 Flow Diagram for Plastic Bifurcation Buckling Analysis

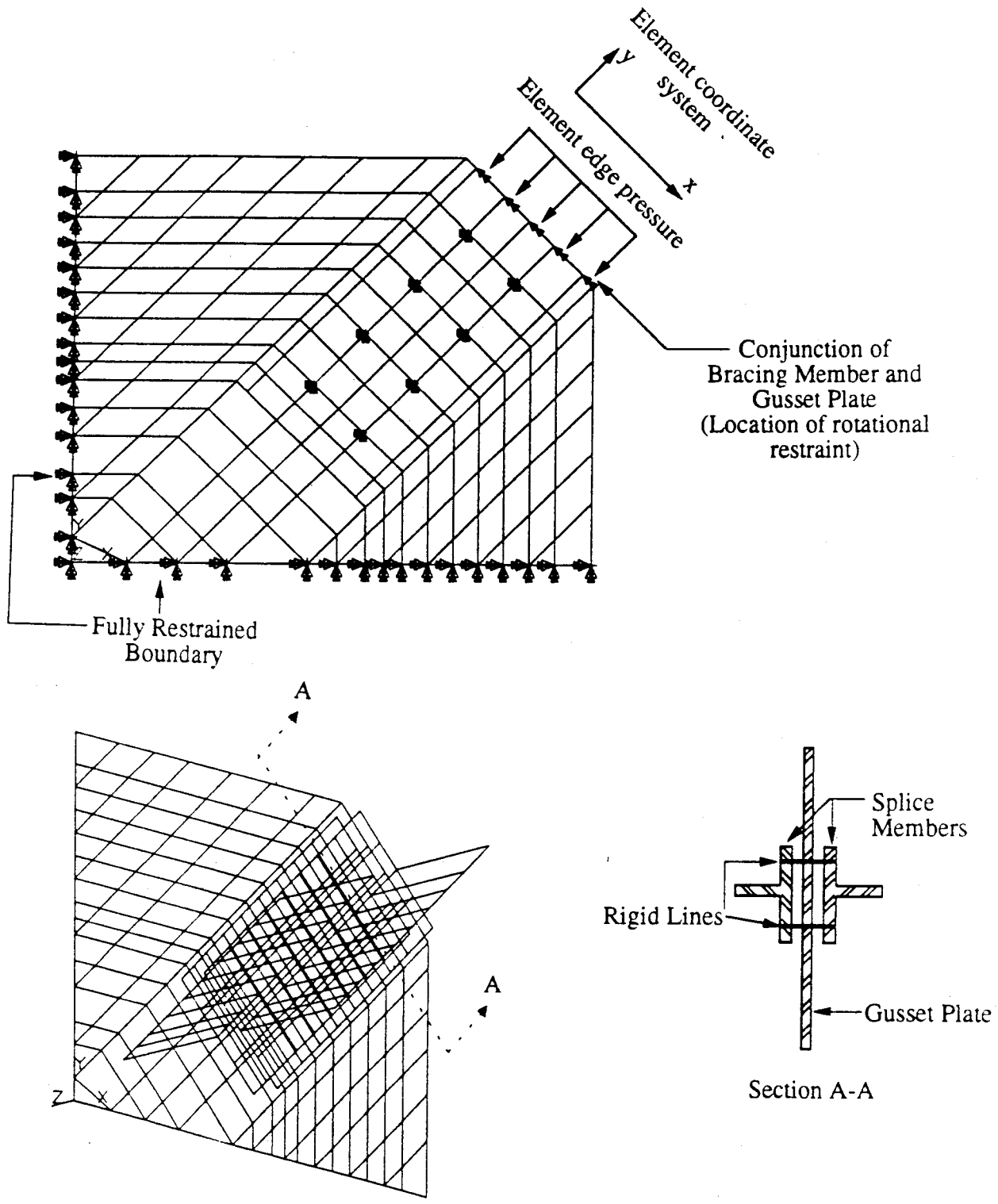


Fig. 2.2 Finite Element Model for GP and SP Type Specimens

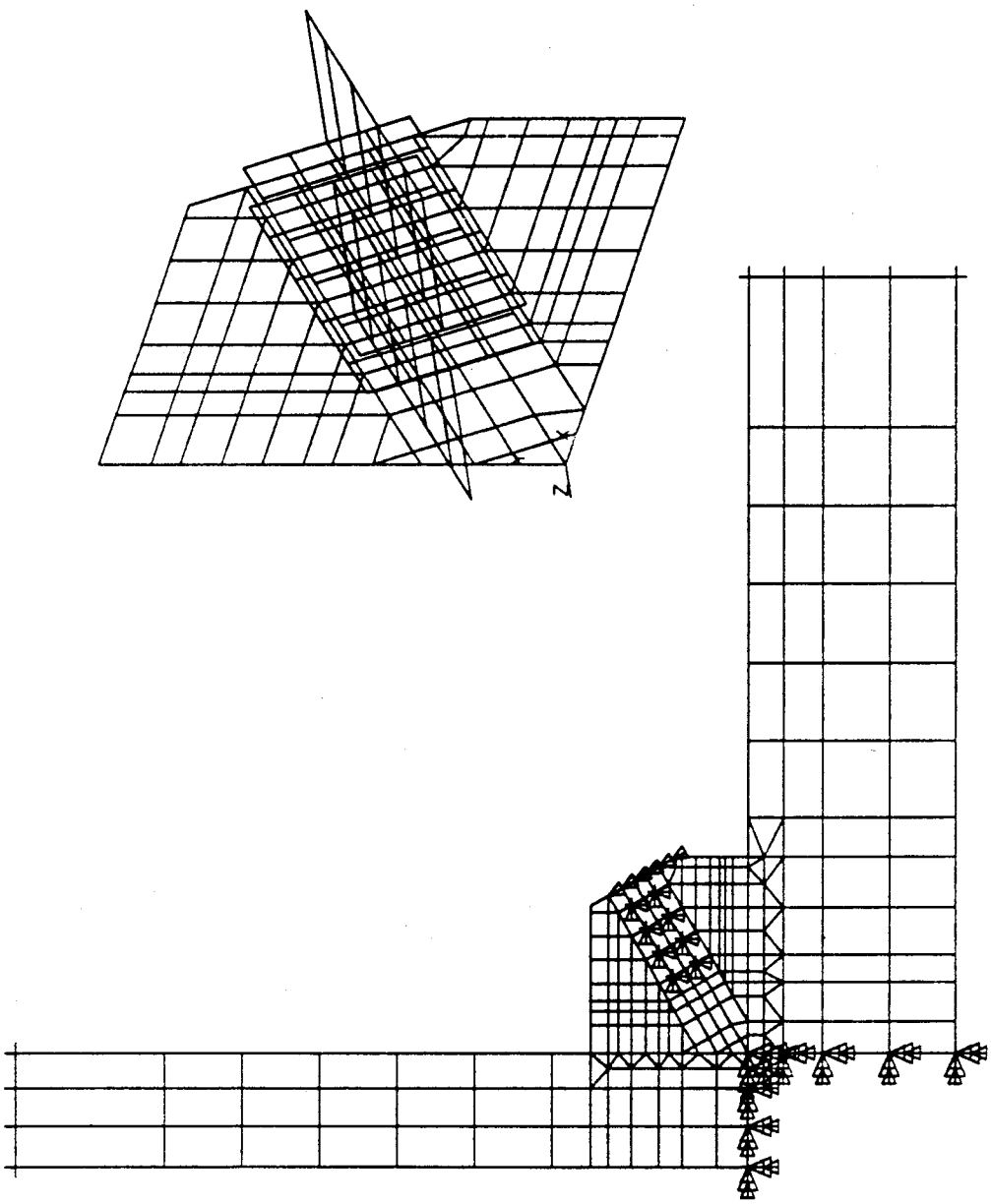


Fig. 2.3a Finite Element Model for AP and MP Type Specimens

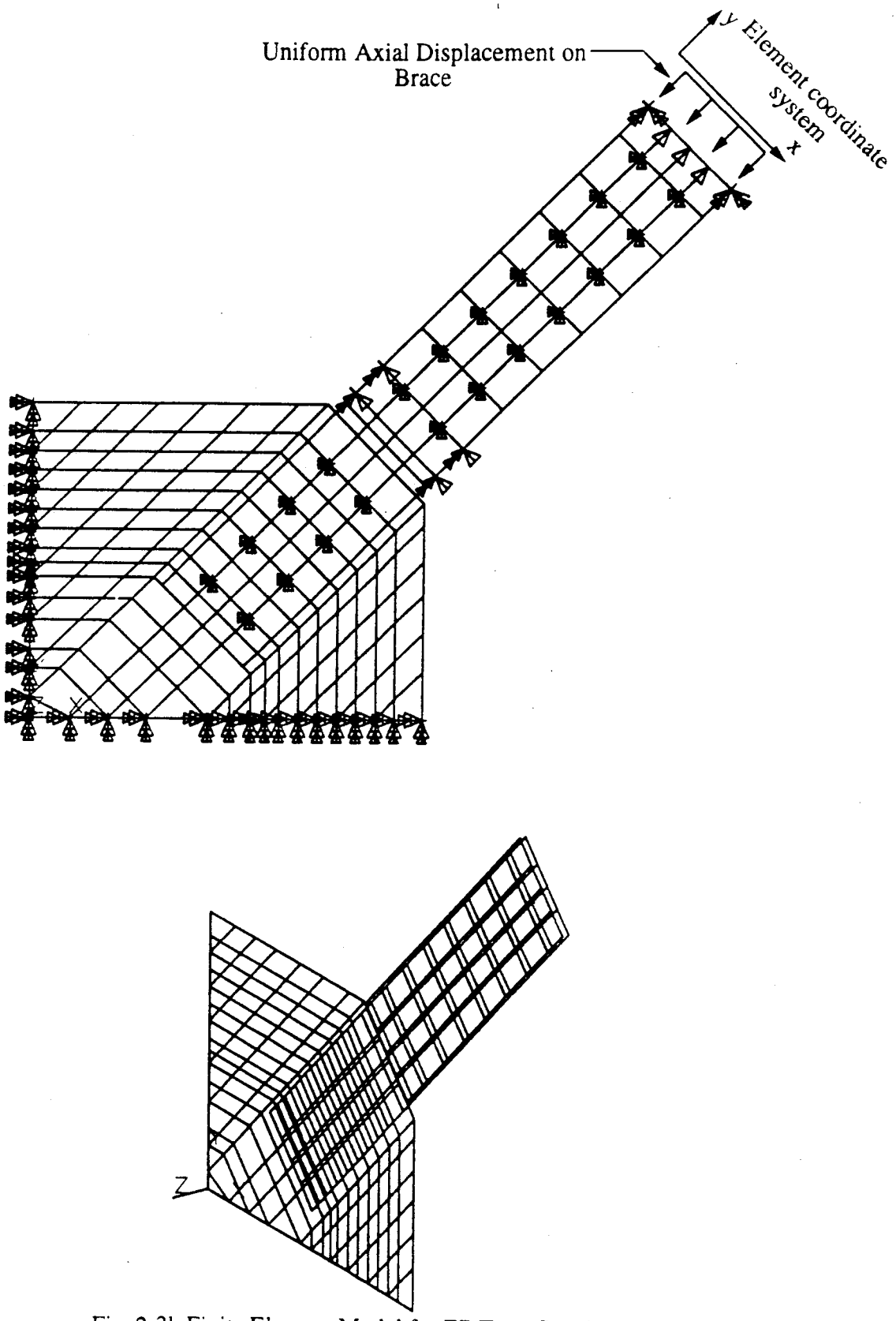


Fig. 2.3b Finite Element Model for EP Type Specimens

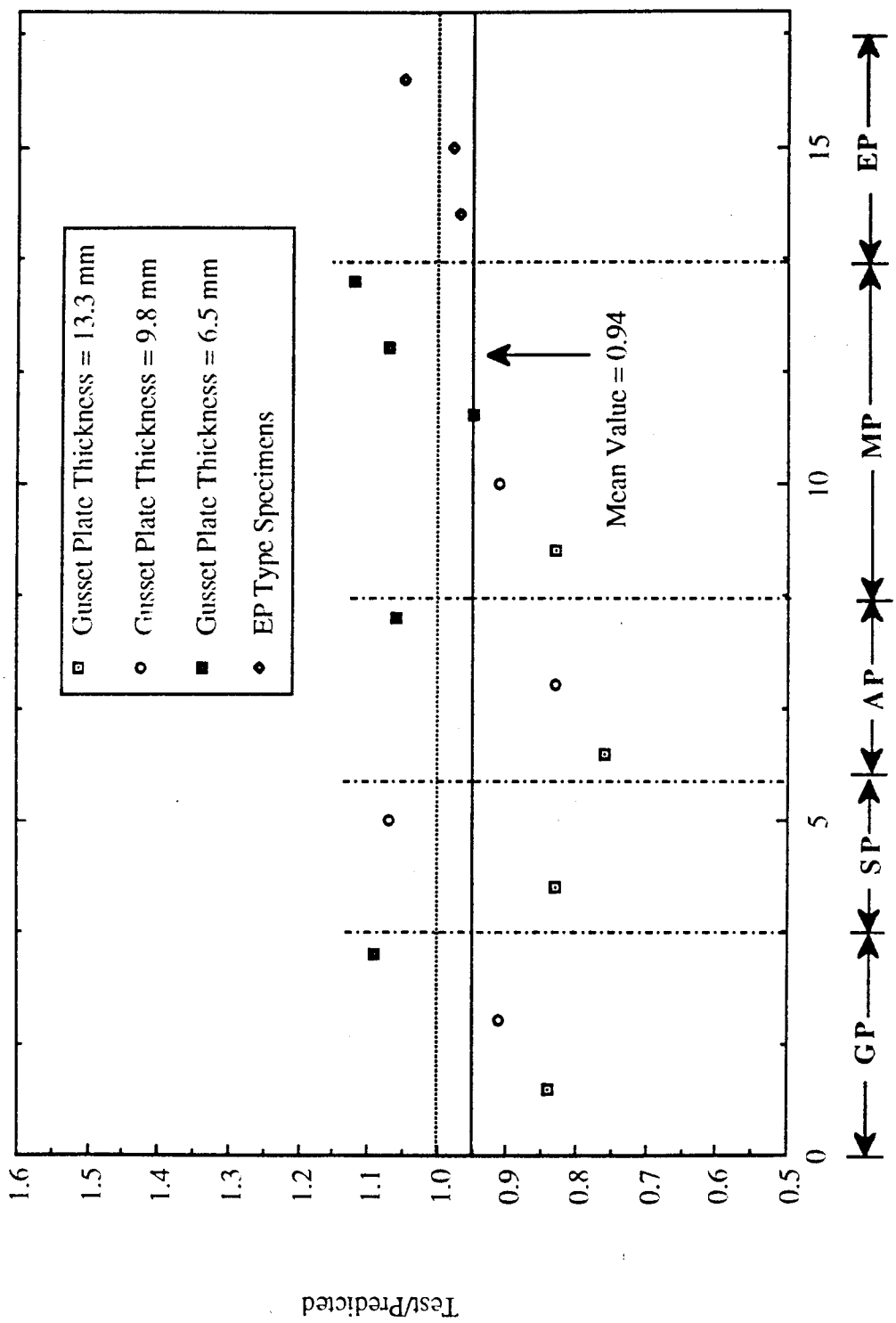


Fig. 2.4 A Plot of Test to Predicted(ANSYS) Ratios for Various Specimens

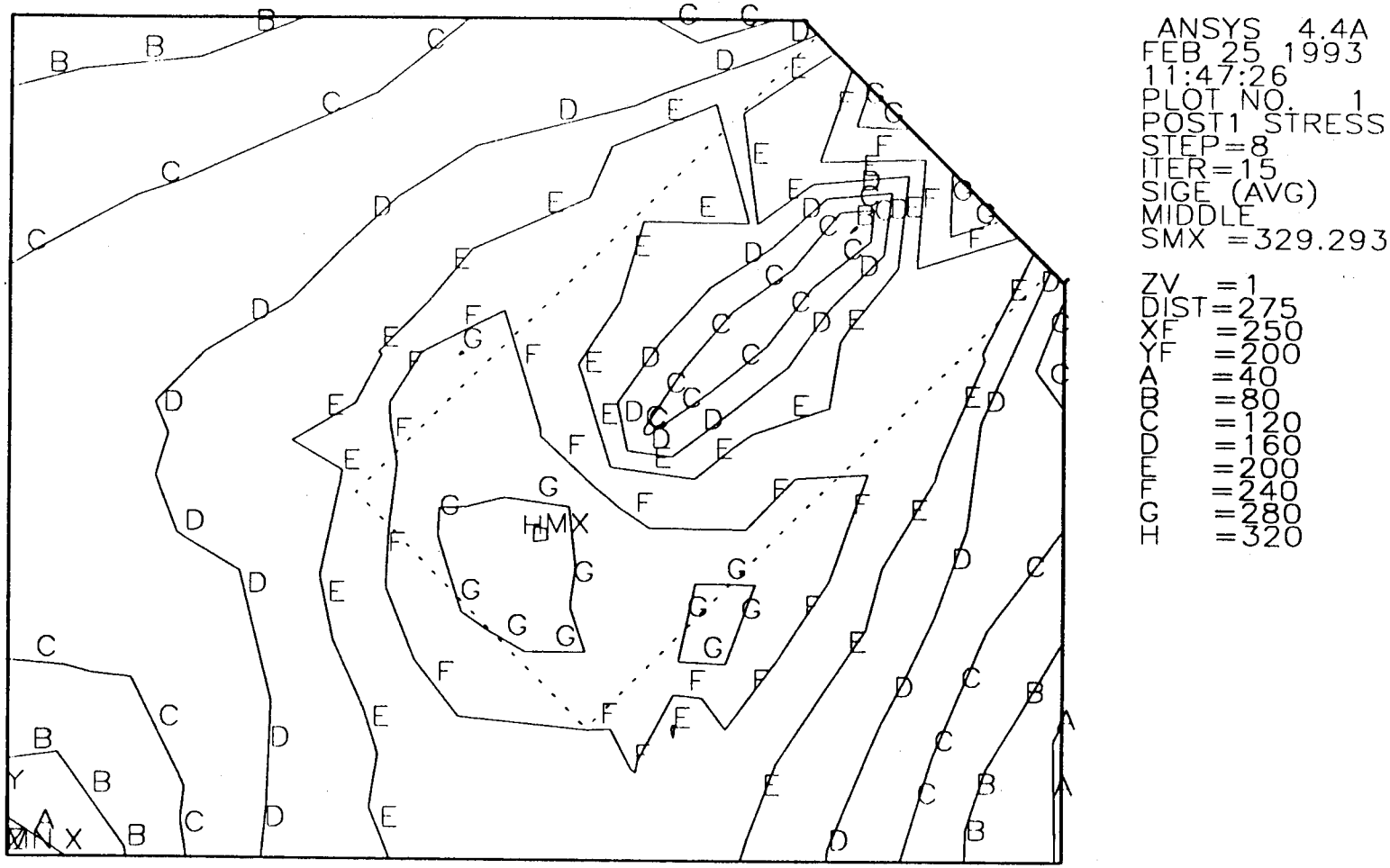


Fig. 2.5a In-Plane Stress Contour for Specimen GP1 at P = 1370 kN

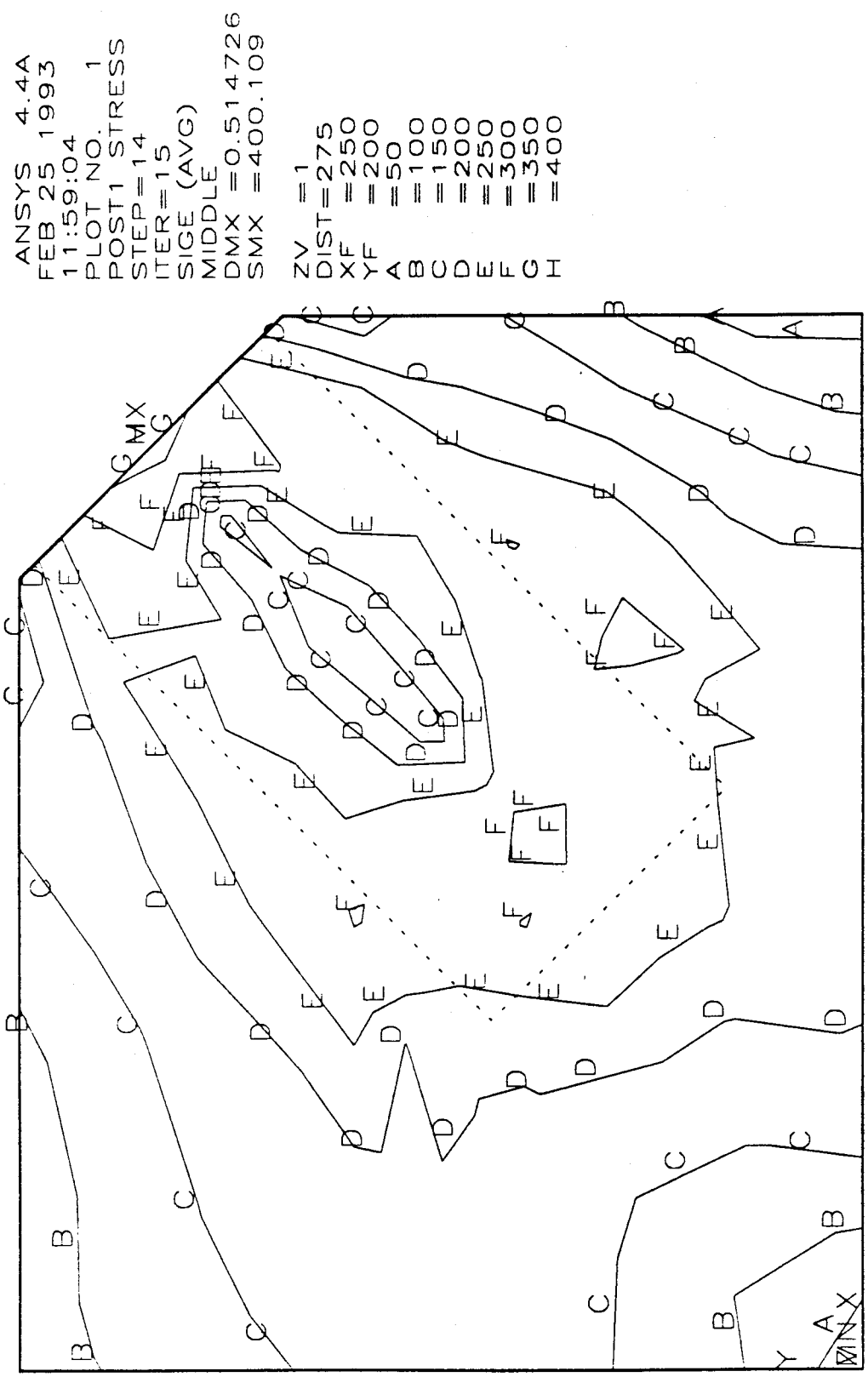


Fig. 2.5b In-Plane Stress Contour for Specimen GP1 at P = 1500 kN

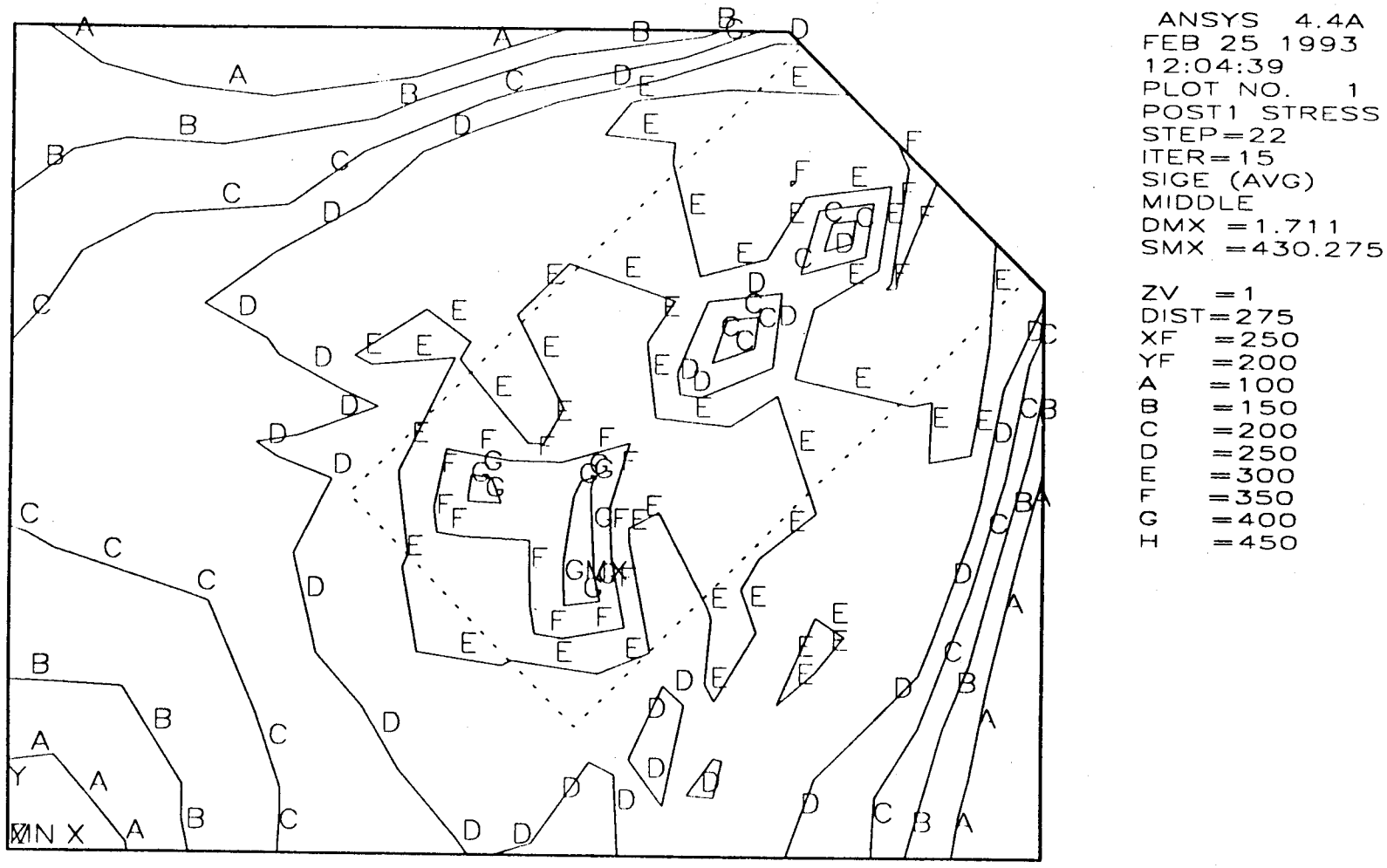


Fig. 2.5c In-Plane Stress Contour for Specimen GP1 at P = 1700 kN

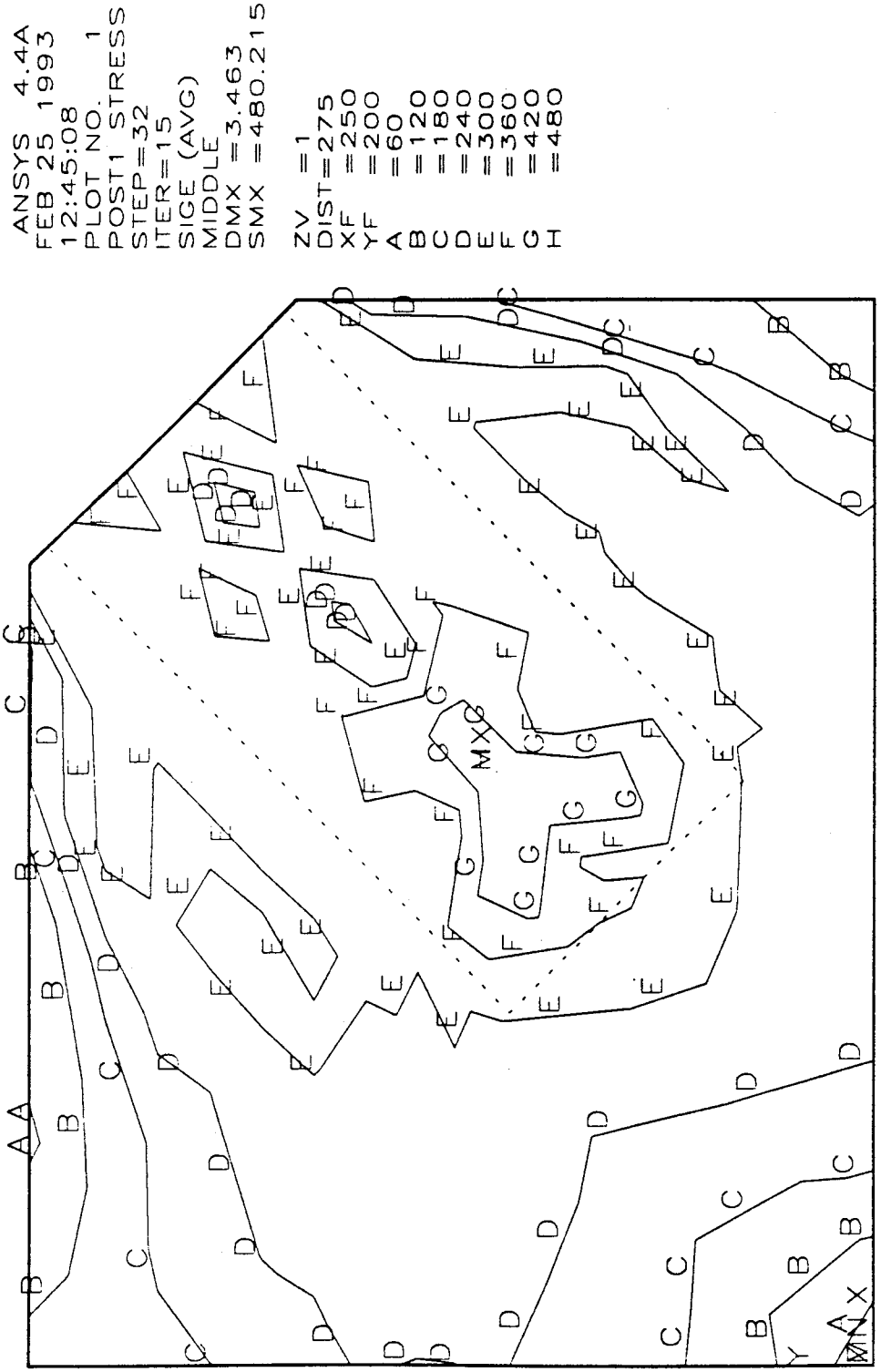


Fig. 2.5d In-Plane Stress Contour for Specimen GP1 at P = 1950 kN

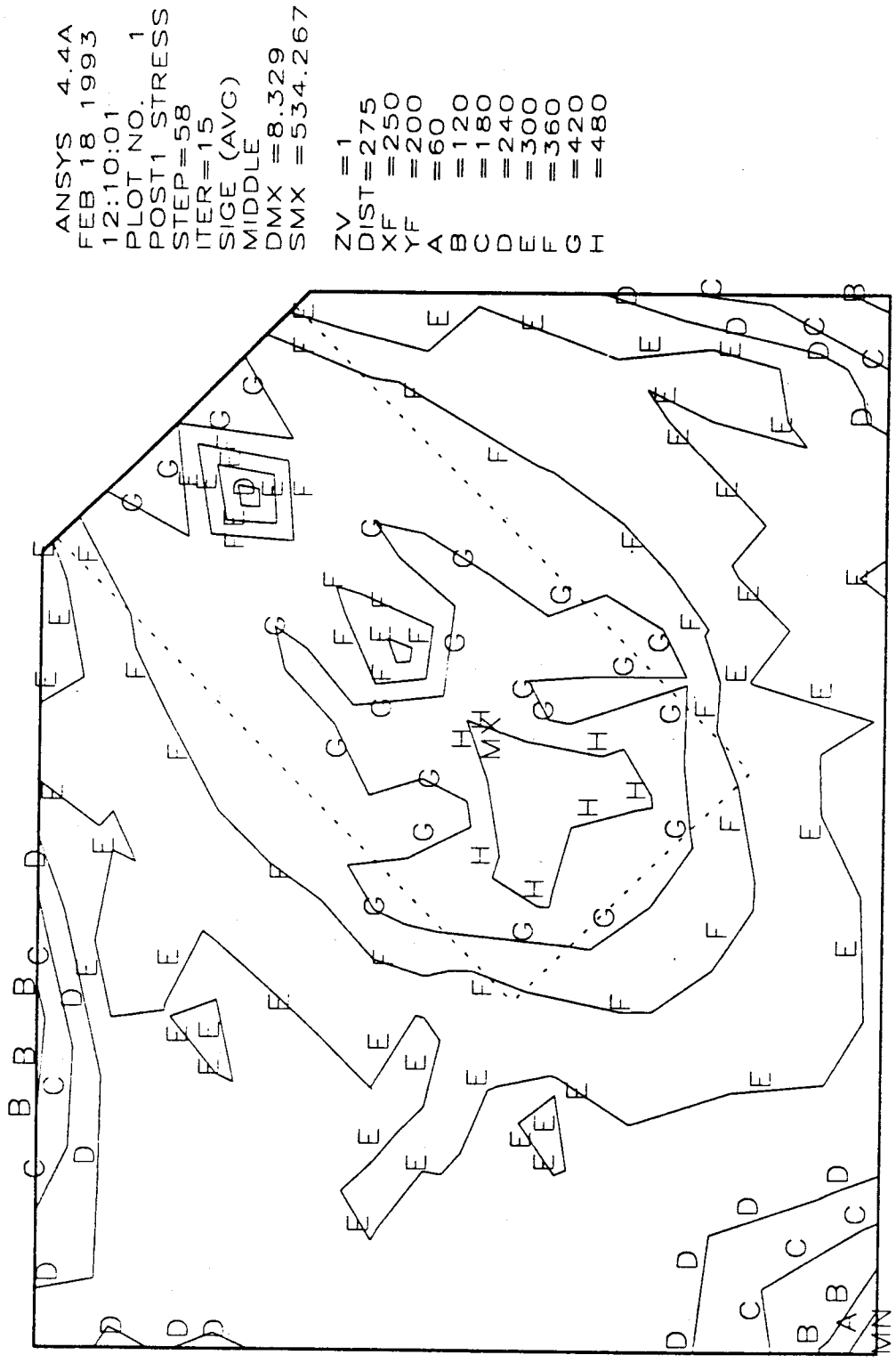


Fig. 2.5e In-Plane Stress Contour for Specimen GP1 at P = 2336 kN

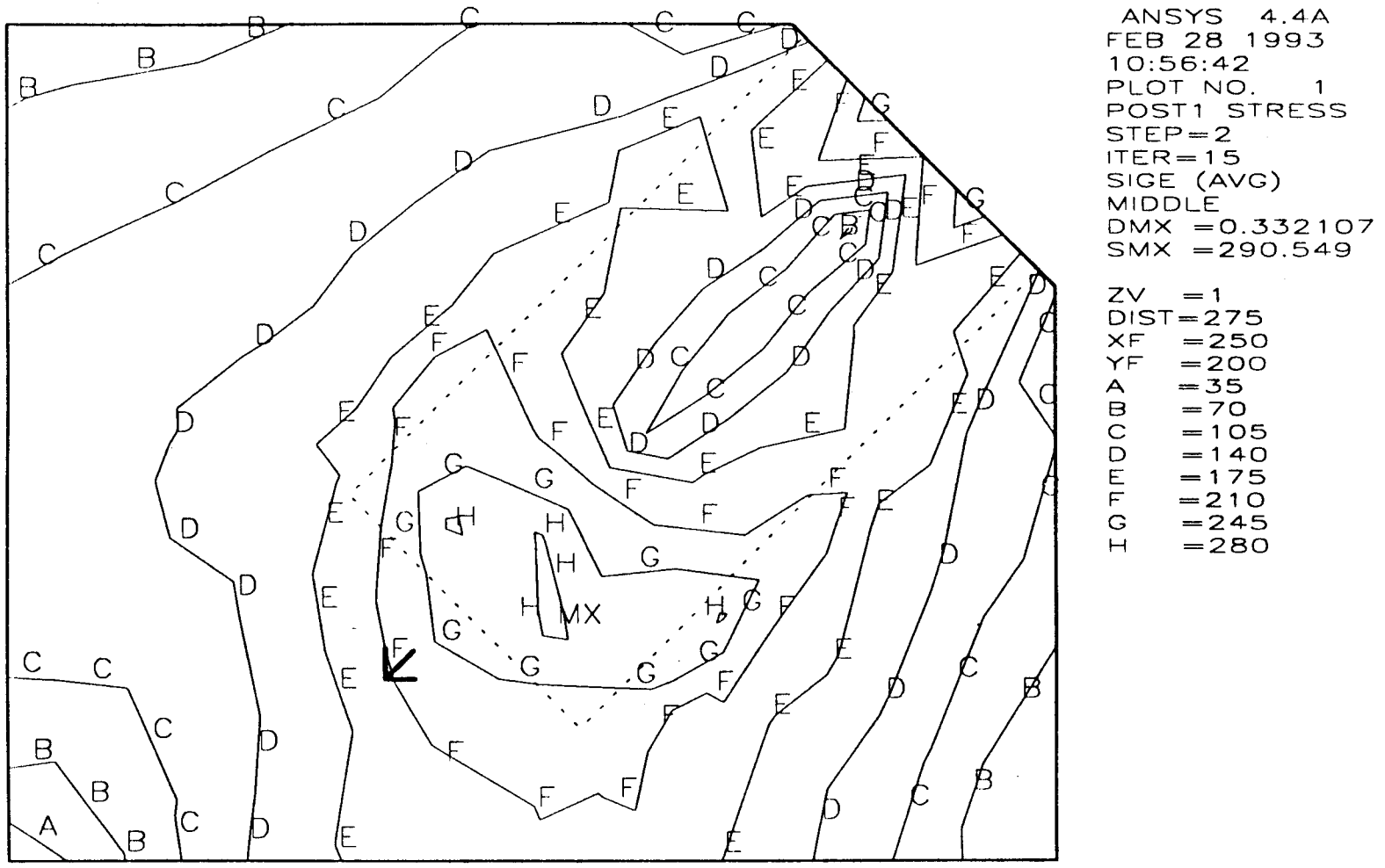


von Mises effective stress at rosette = 200 MPa

Fig. 2.6 In-Plane Stress Contour for Specimen GP1 at P = 1220 kN

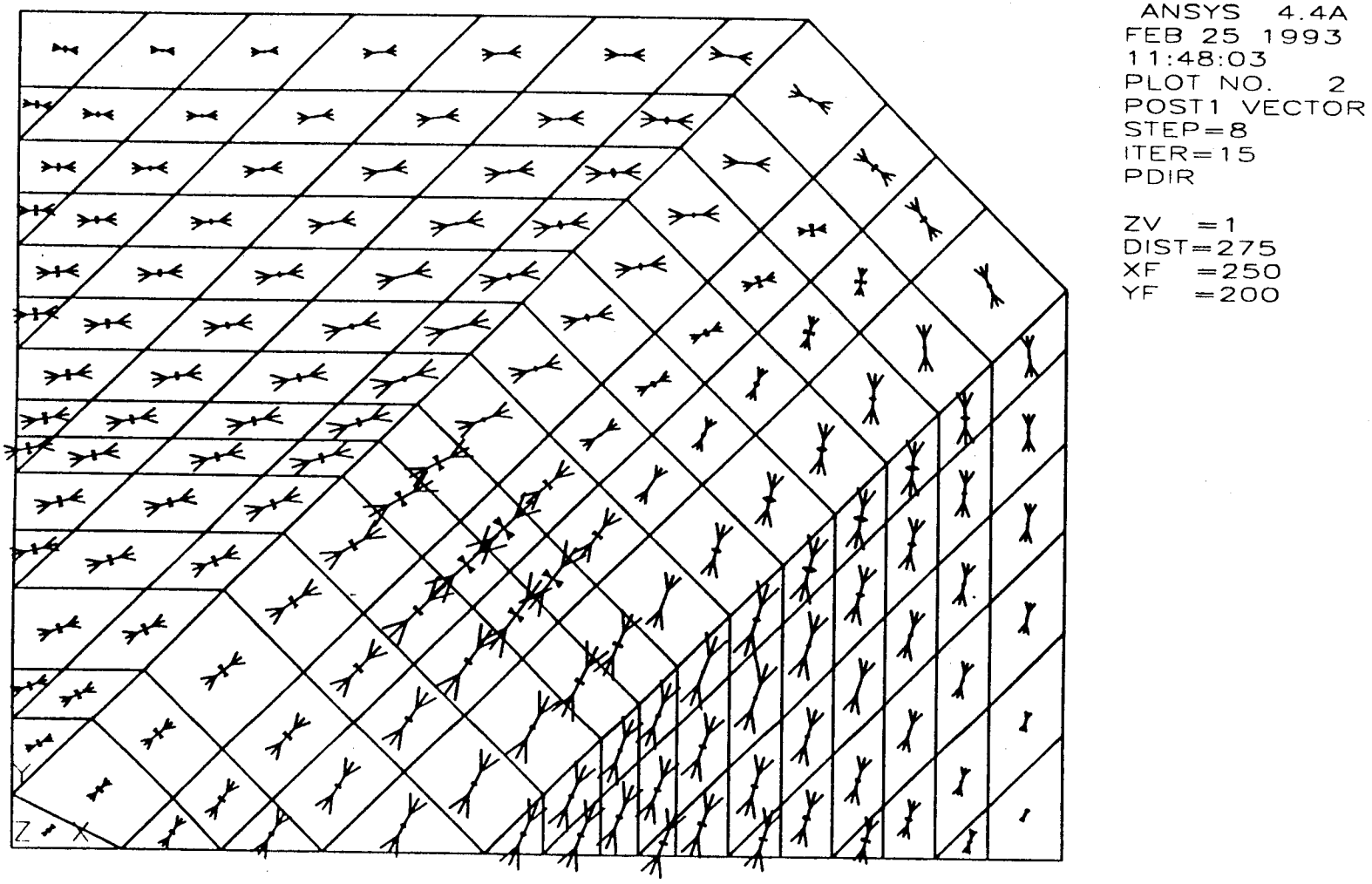


Fig. 2.7a Principal Stress Vector Plot for Specimen GP1 at P = 1370 kN

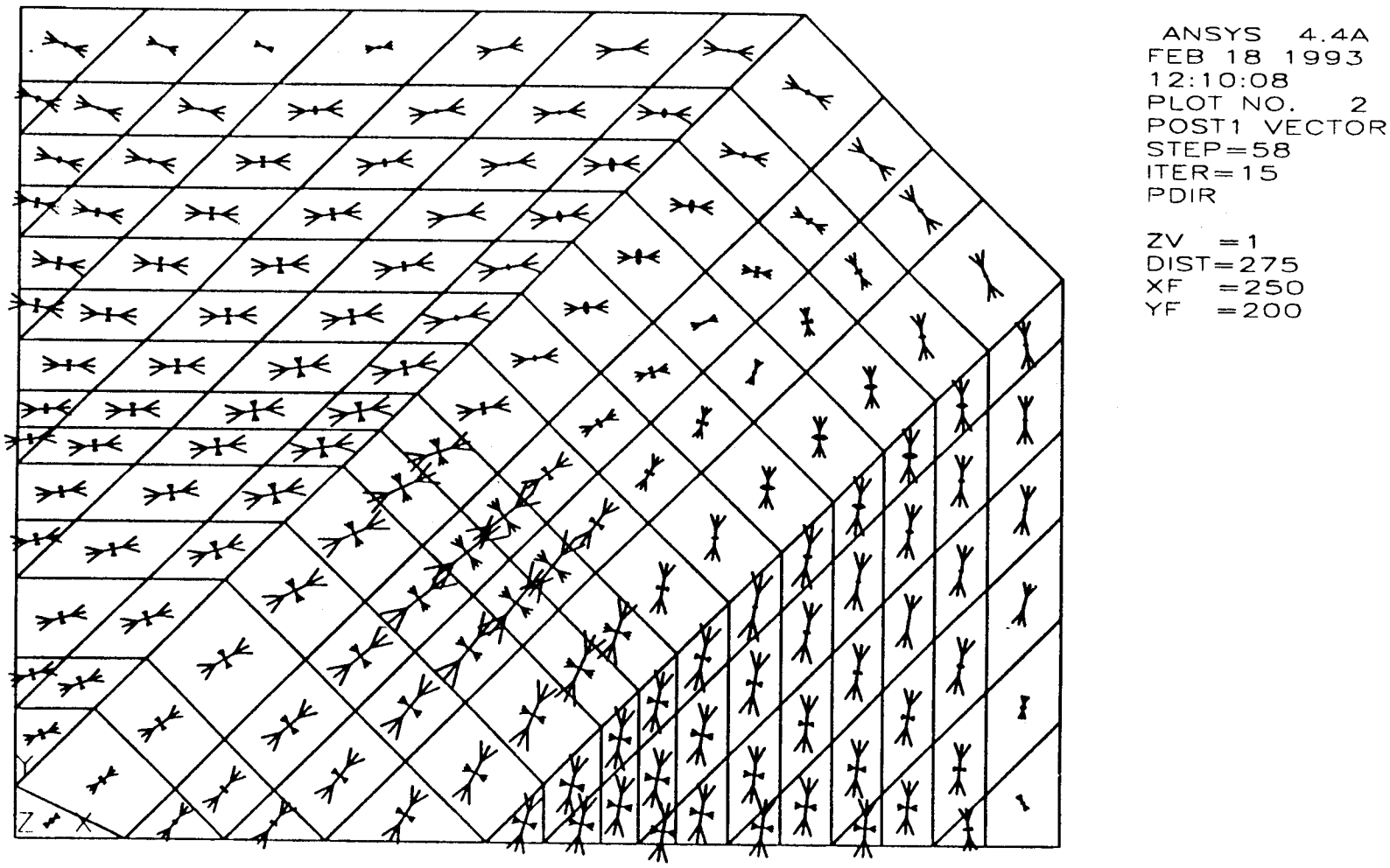


Fig. 2.7b Principal Stress Vector Plot for Specimen GP1 at P = 2336 kN

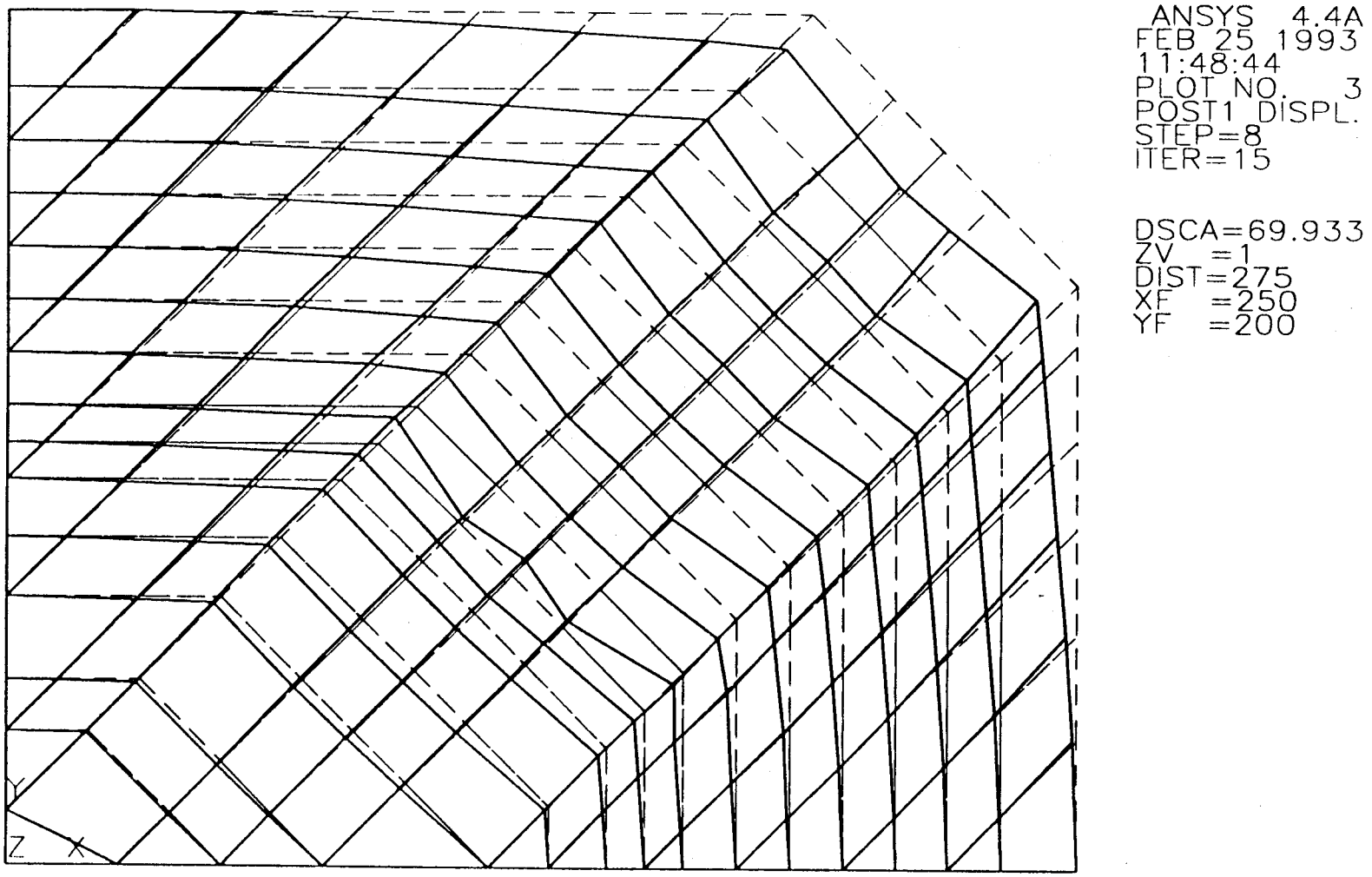


Fig. 2.8a In-Plane Deformation Mode for Specimen GP1 at P = 1370 kN

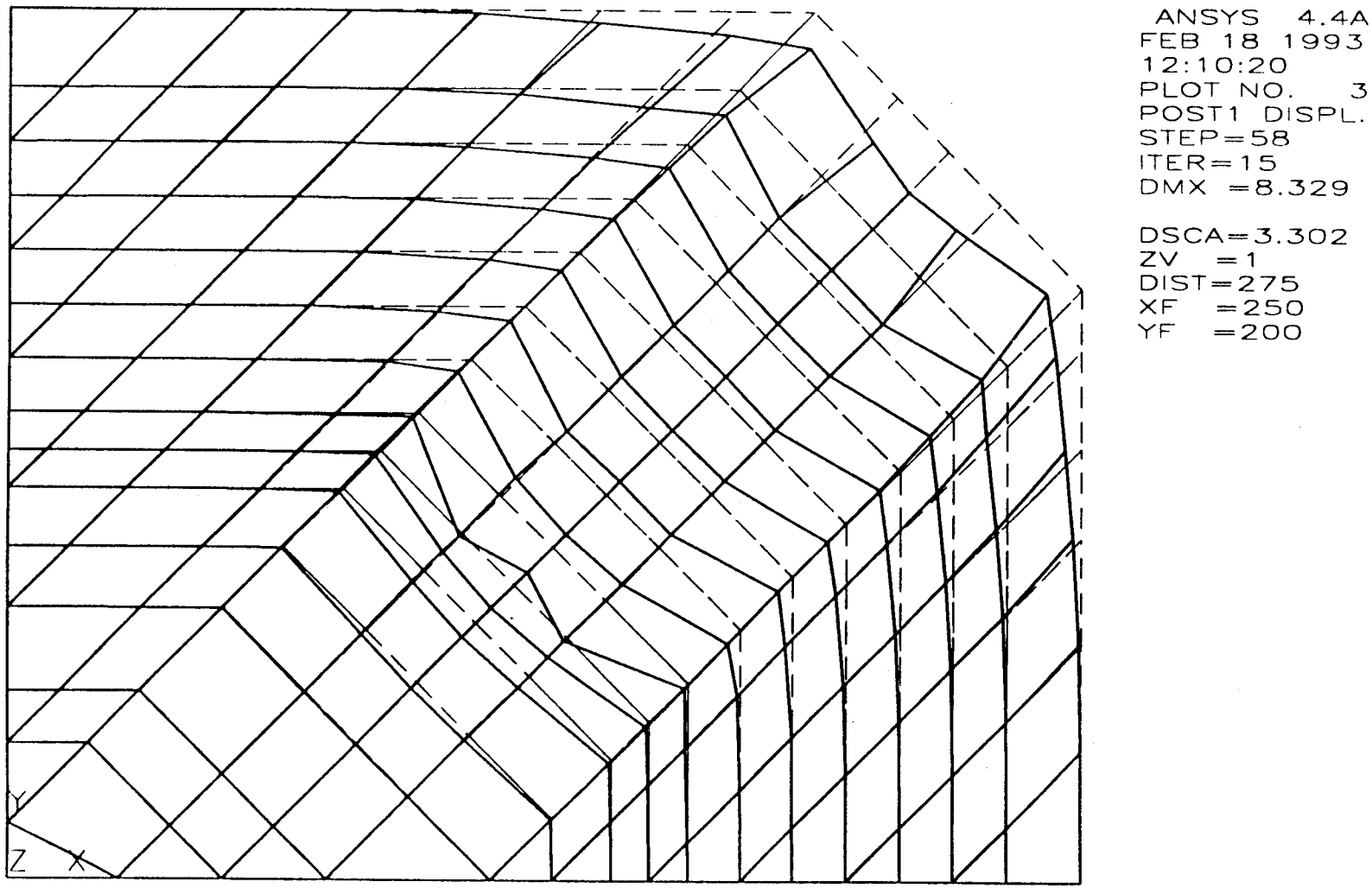


Fig. 2.8b In-Plane Deformation Mode for Specimen GP1 at P = 2336 kN

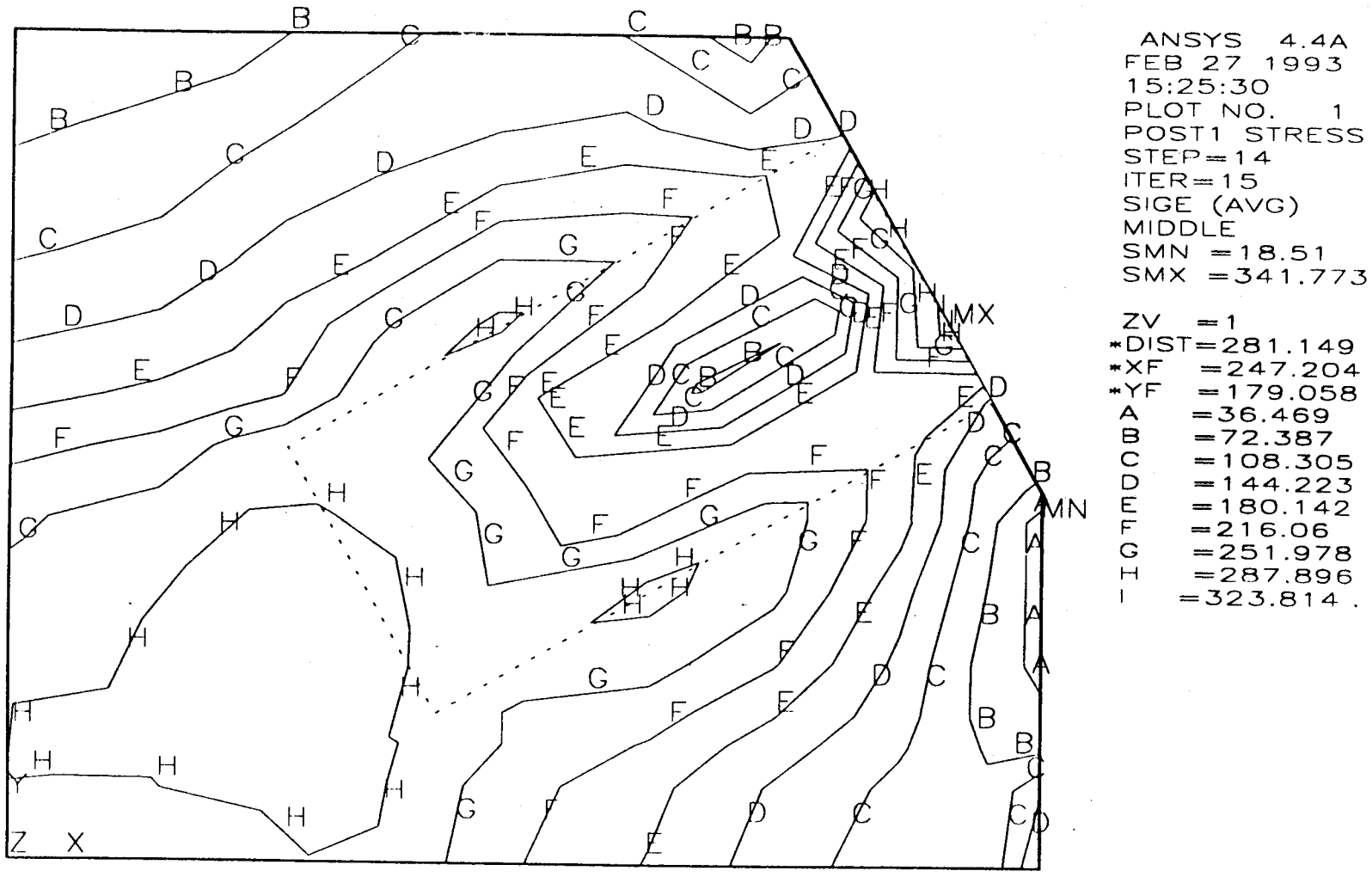


Fig. 2.9 In-Plane Stress Contour for Specimen AP1 at P = 1380 kN

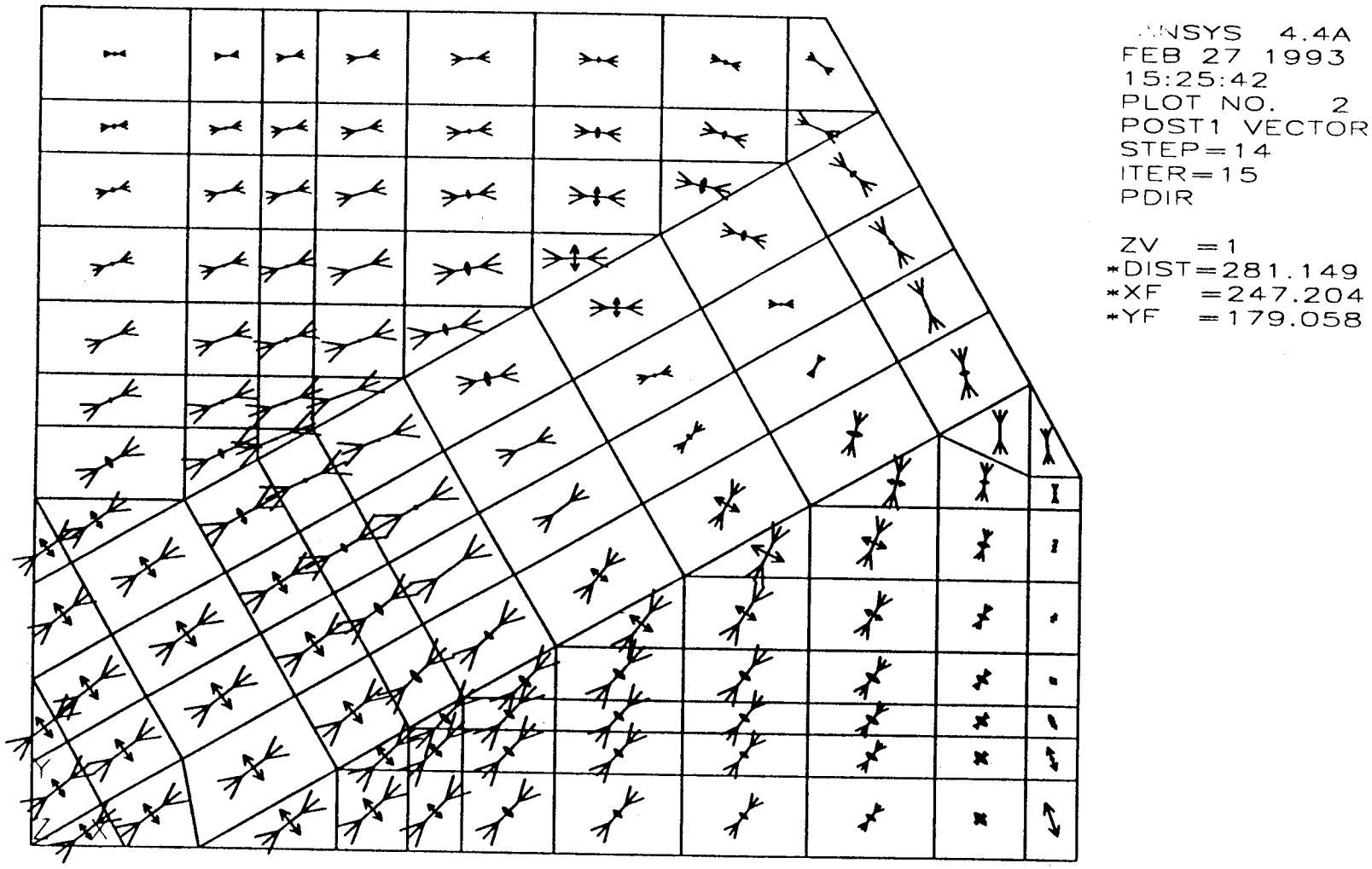


Fig. 2.10 Principal Stress Vector Plot for Specimen AP1 at P = 1380 kN

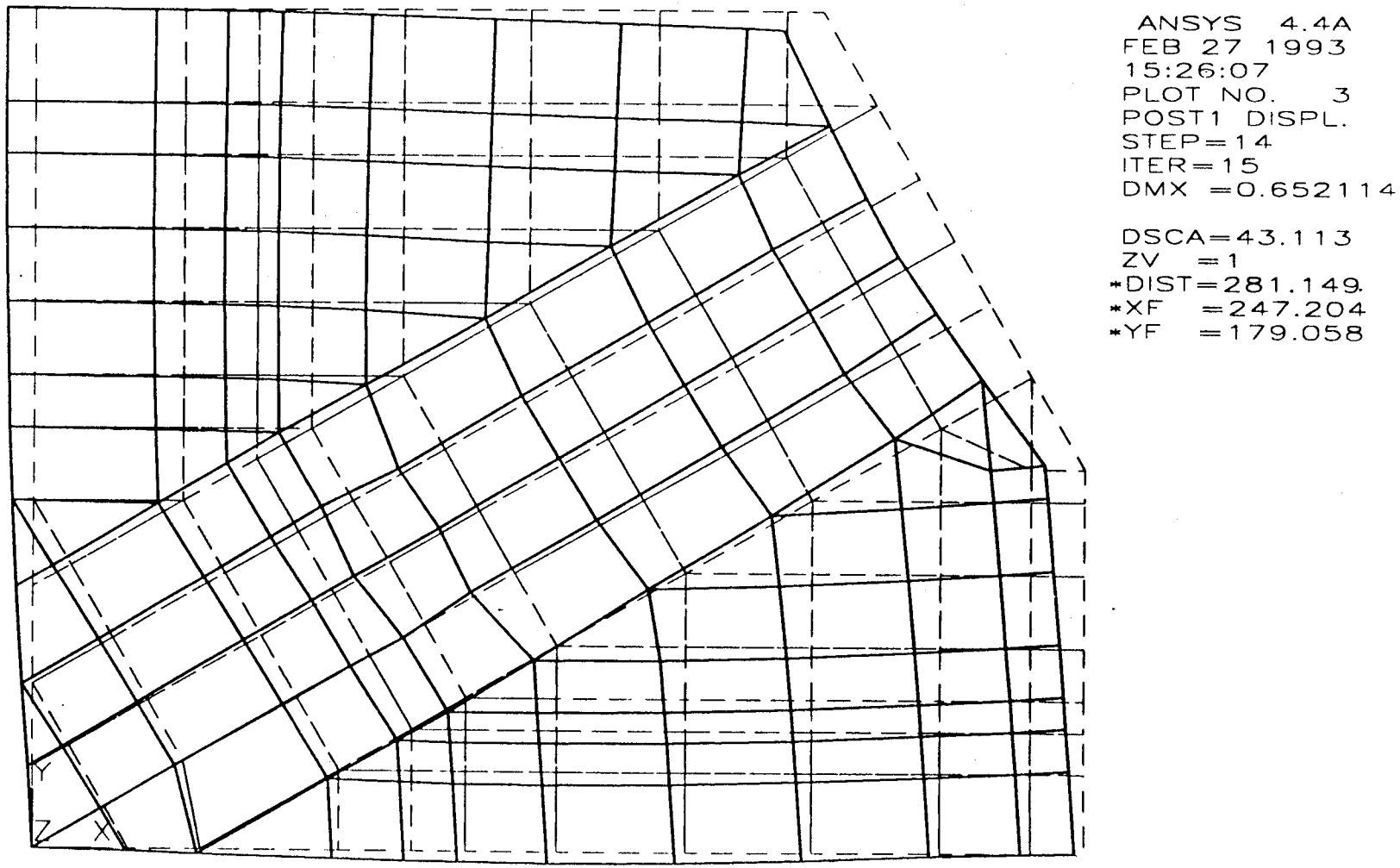


Fig. 2.11 In-Plane Deformation Mode for Specimen AP1 at P = 1380 kN

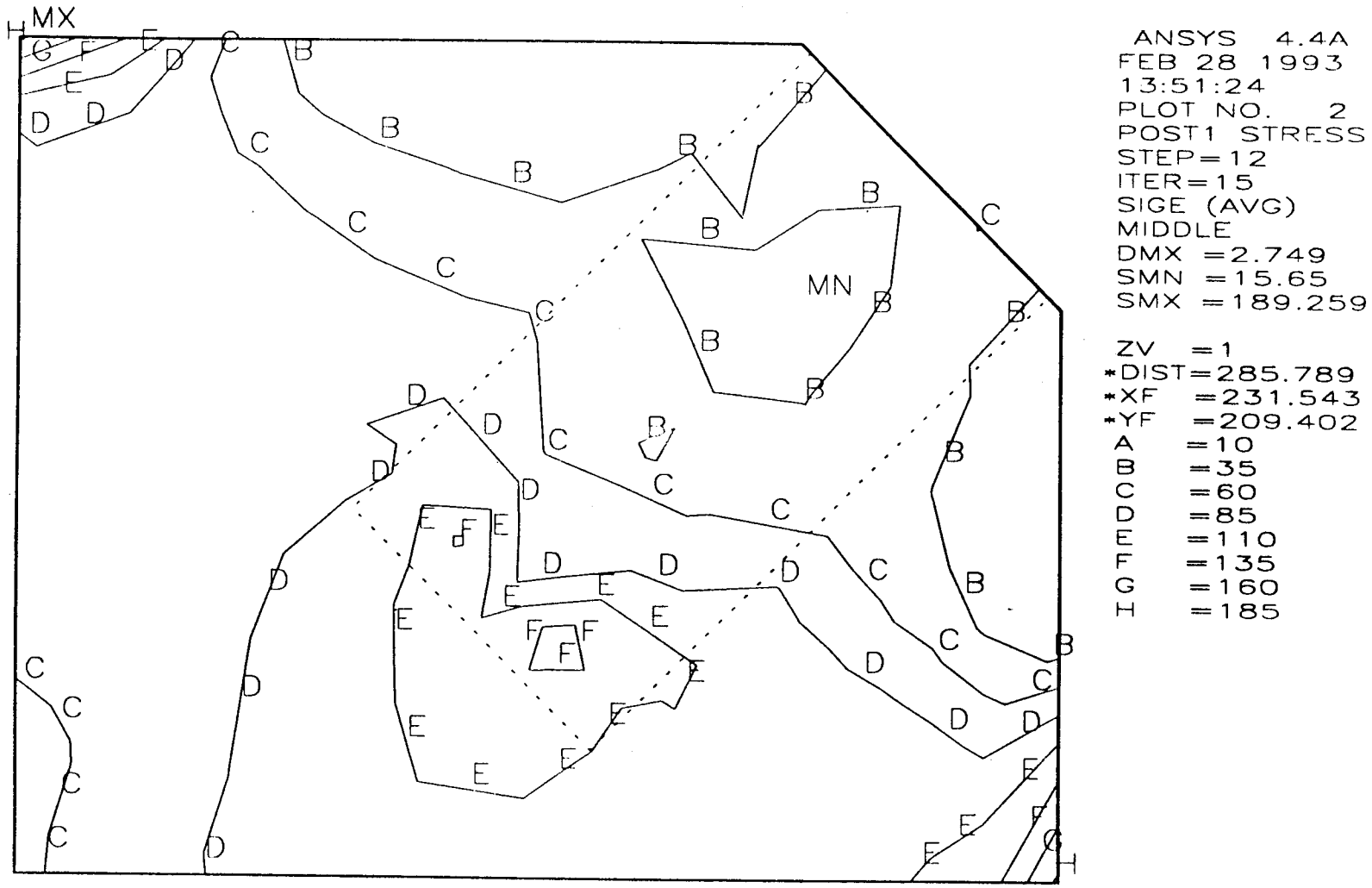


Fig. 2.12a In-Plane Stress Contour for Specimen MP1 at P = 300 kN

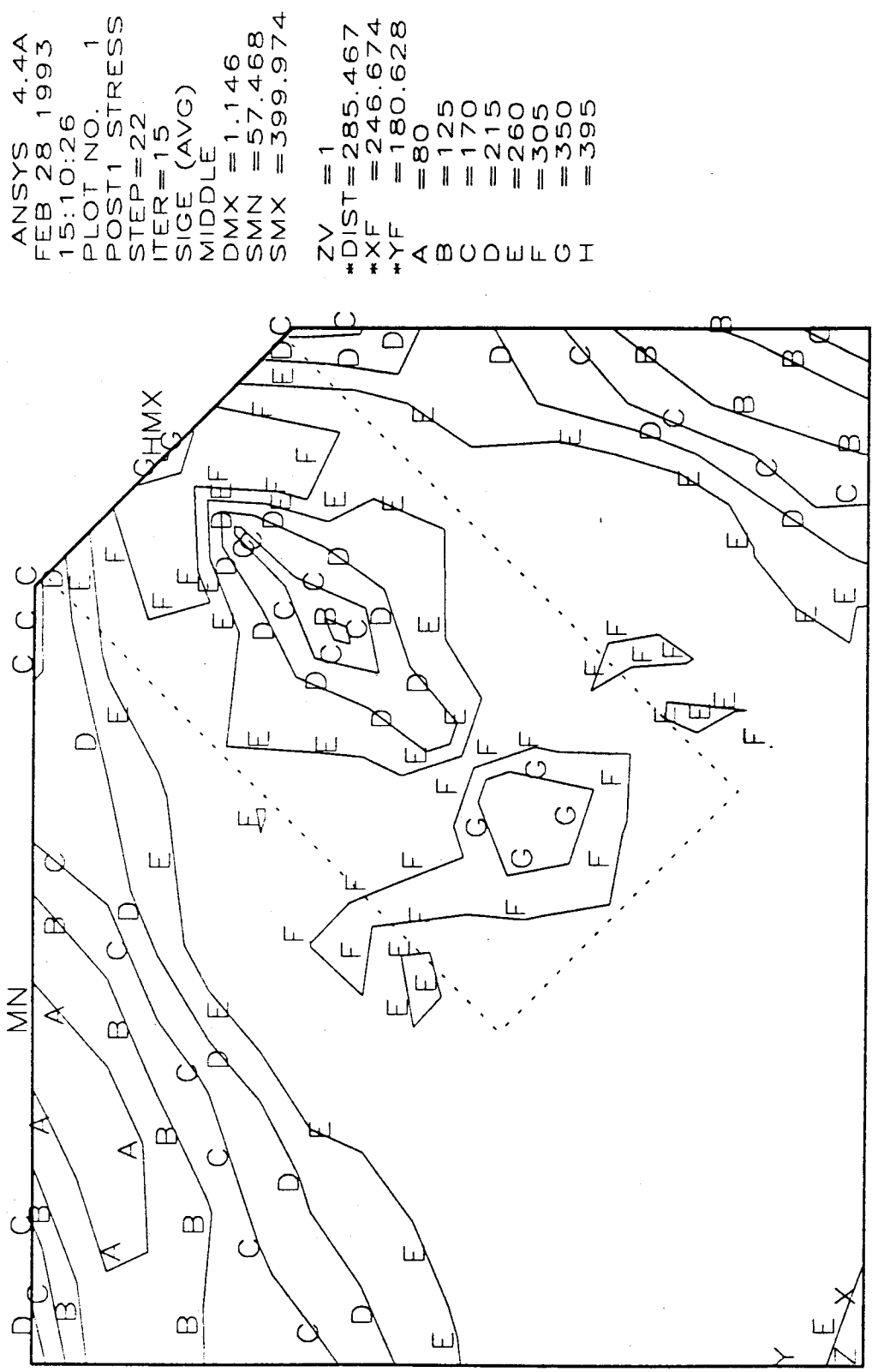


Fig. 2.12b In-Plane Stress Contour for Specimen MP1 at P = 1500 kN

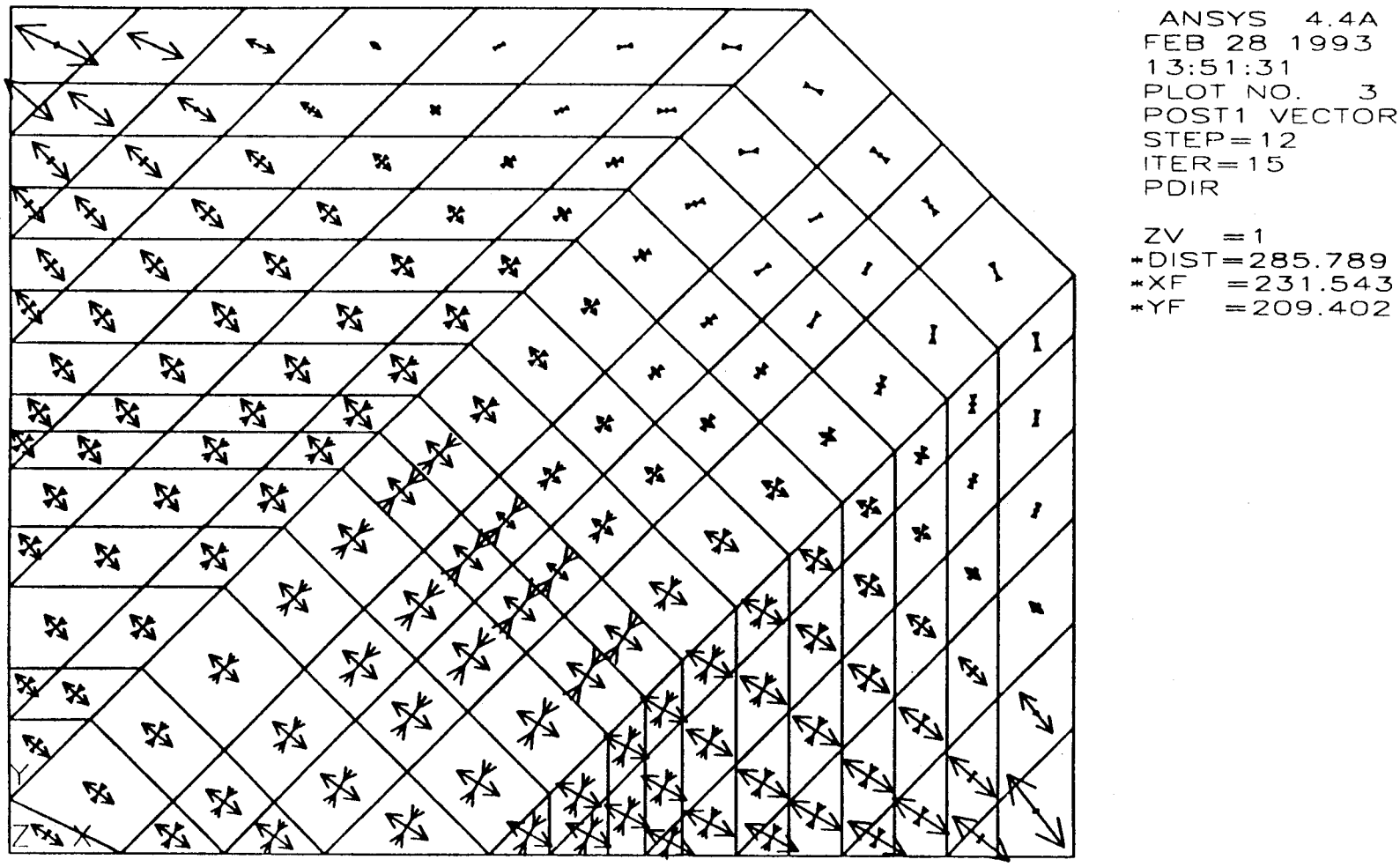


Fig. 2.13a Principal Stress Vector Plot for Specimen MP1 at P = 300 kN

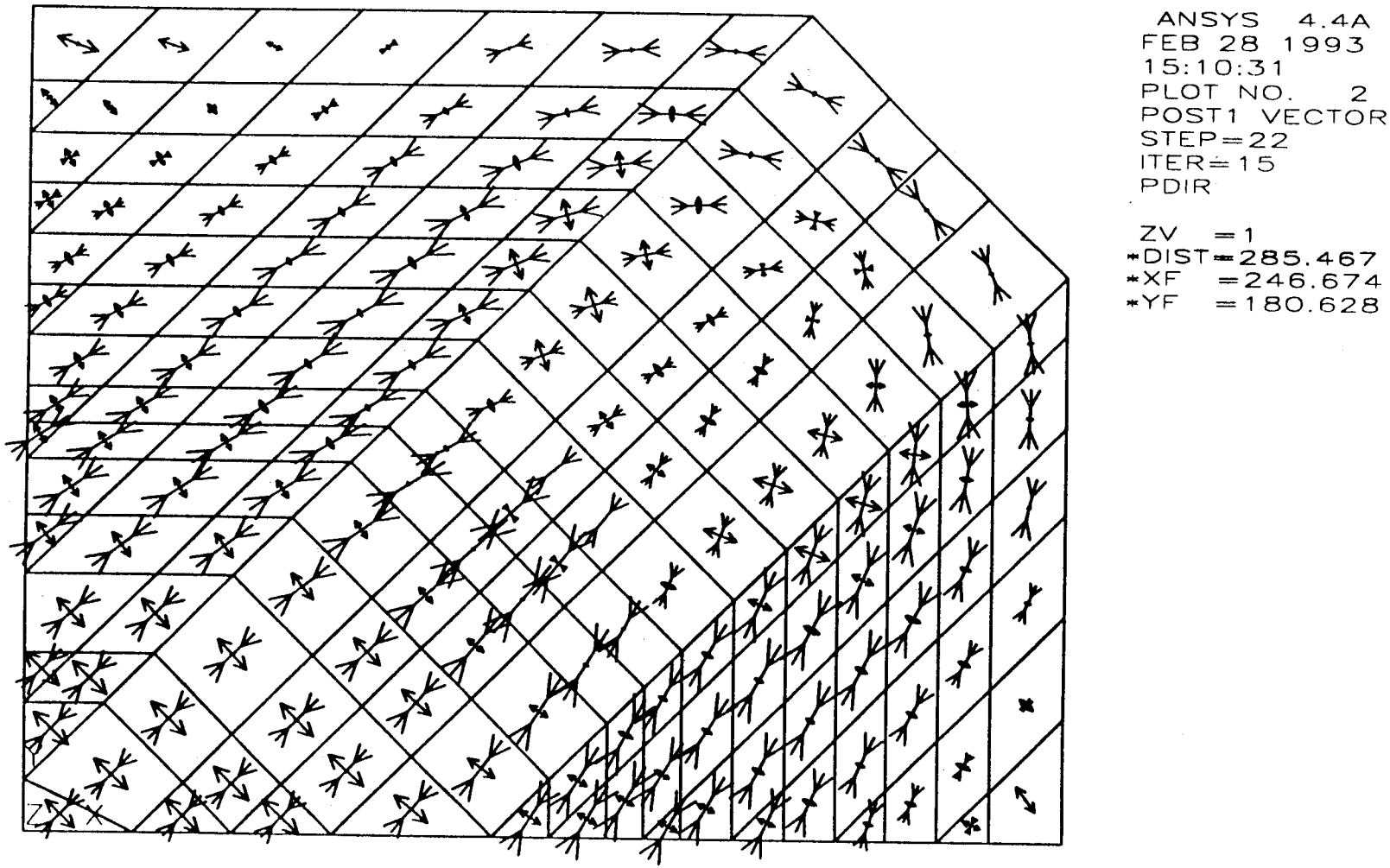


Fig. 2.13b Principal Stress Vector Plot for Specimen MP1 at P = 1500 kN

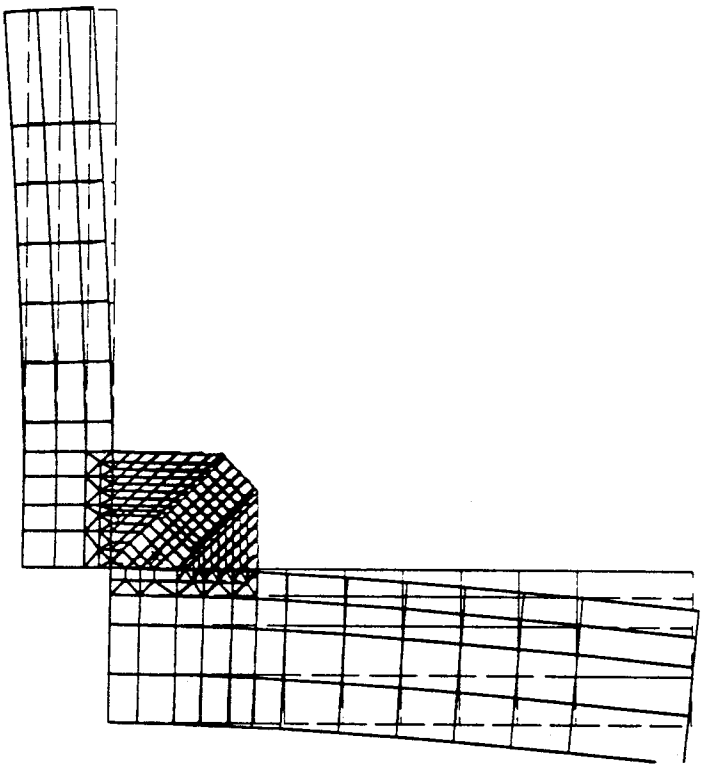

Beam and Column In-Plane Deformation

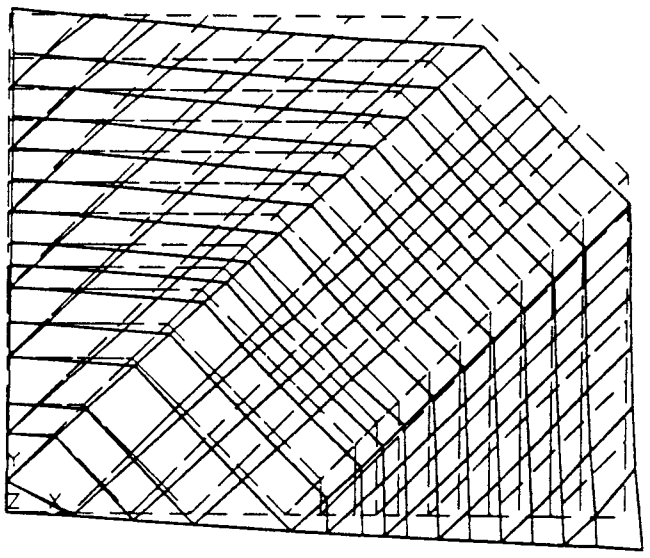

Stretching of Gusset Plate Specimens Due to Beam and Column Moments

Fig. 2.14a In-Plane Deformation Mode for Specimen MP1 at P = 300 kN

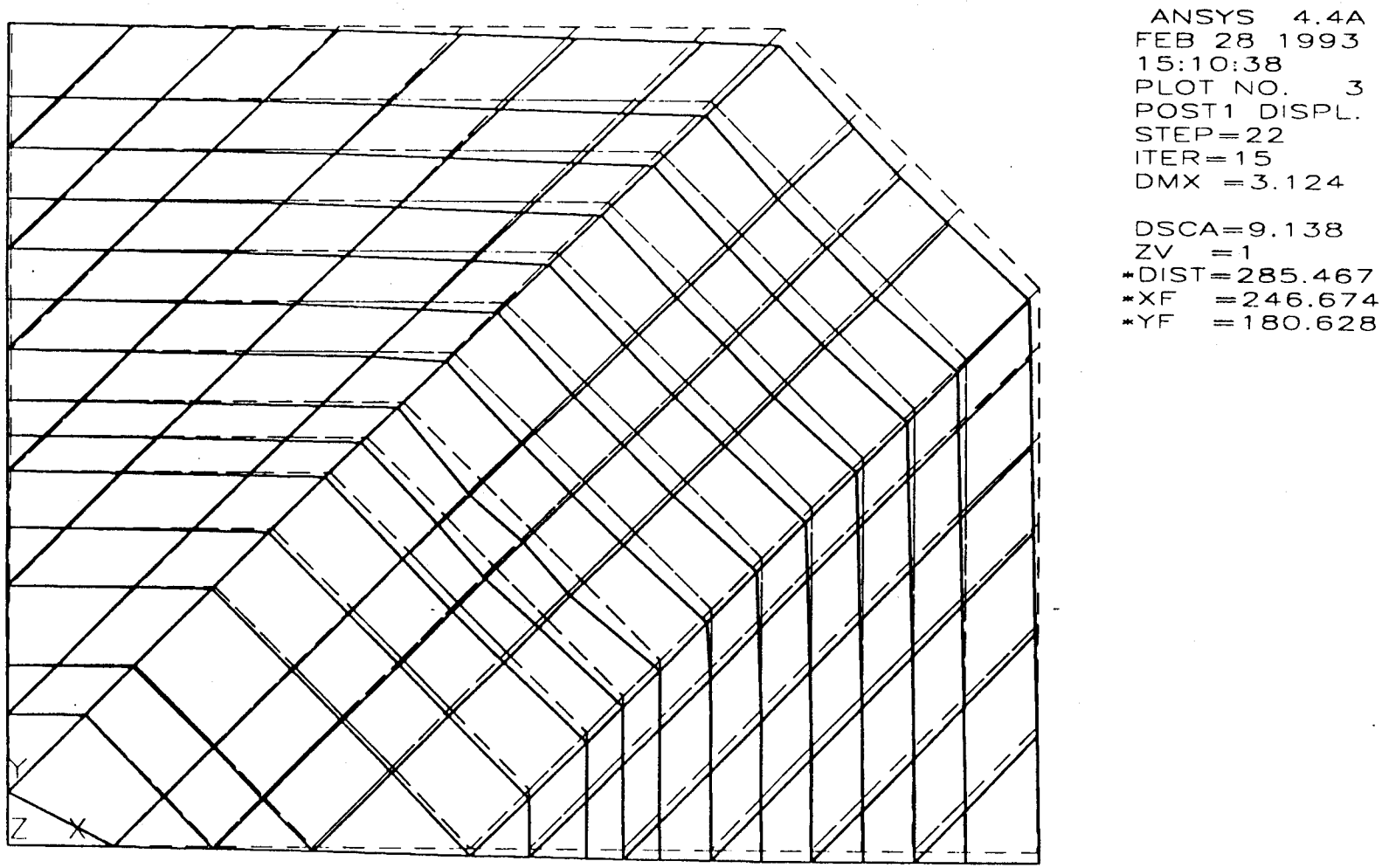


Fig. 2.14b In-Plane Deformation Mode for Specimen MP1 at P = 1500 kN

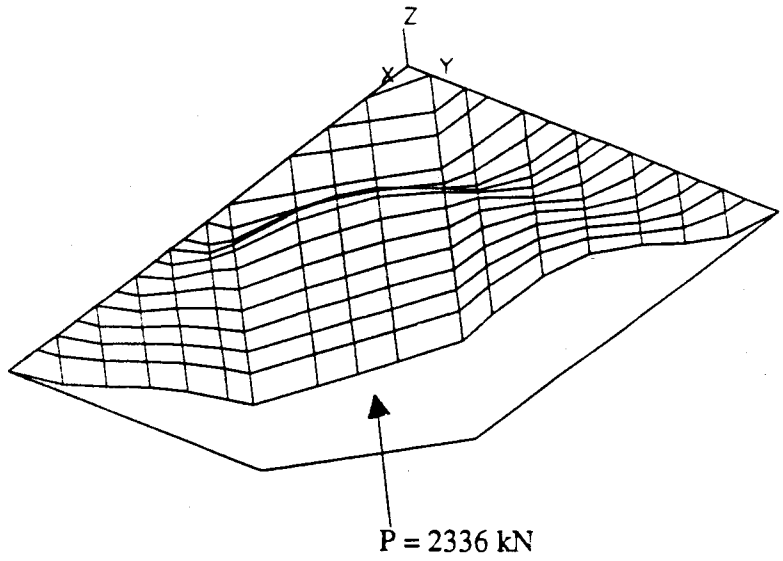


Specimen GP1

(a)

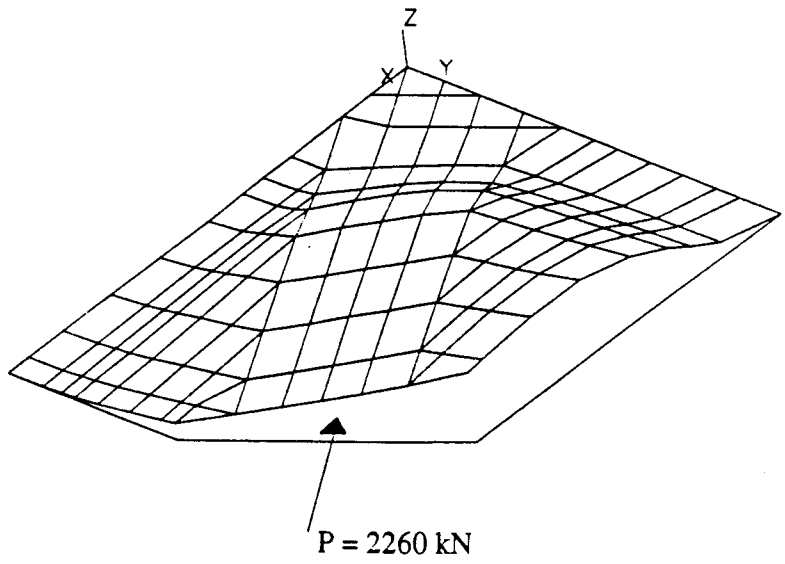


Specimen AP1

(b)

Fig. 2.15a,b Typical Buckling Shapes for Specimens GP1 and AP1

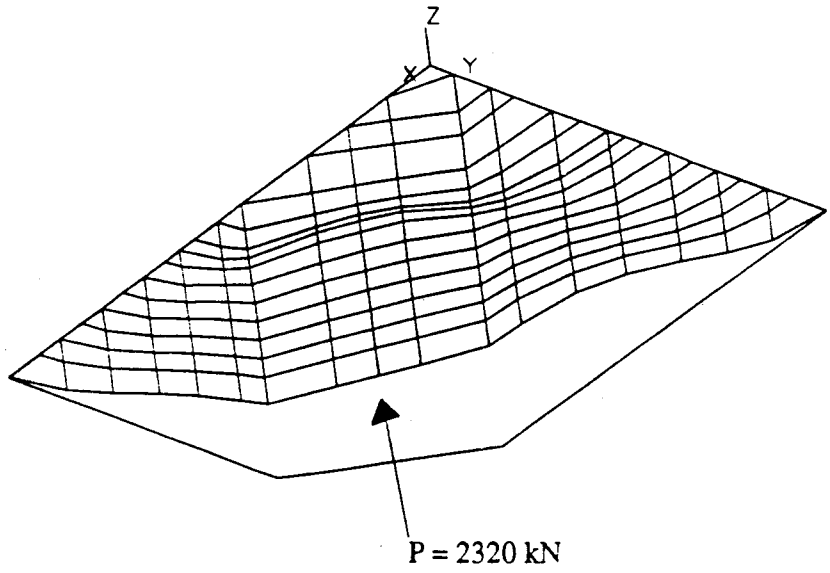


Specimen MP1

(c)

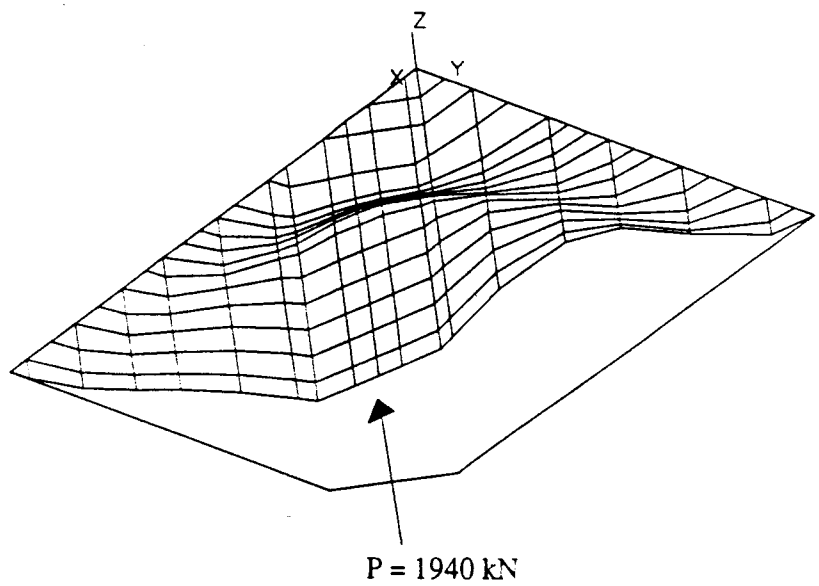


Specimen SP1

(d)

Fig. 2.15 c,d Typical Buckling Shapes for Specimens MP1 and SP1

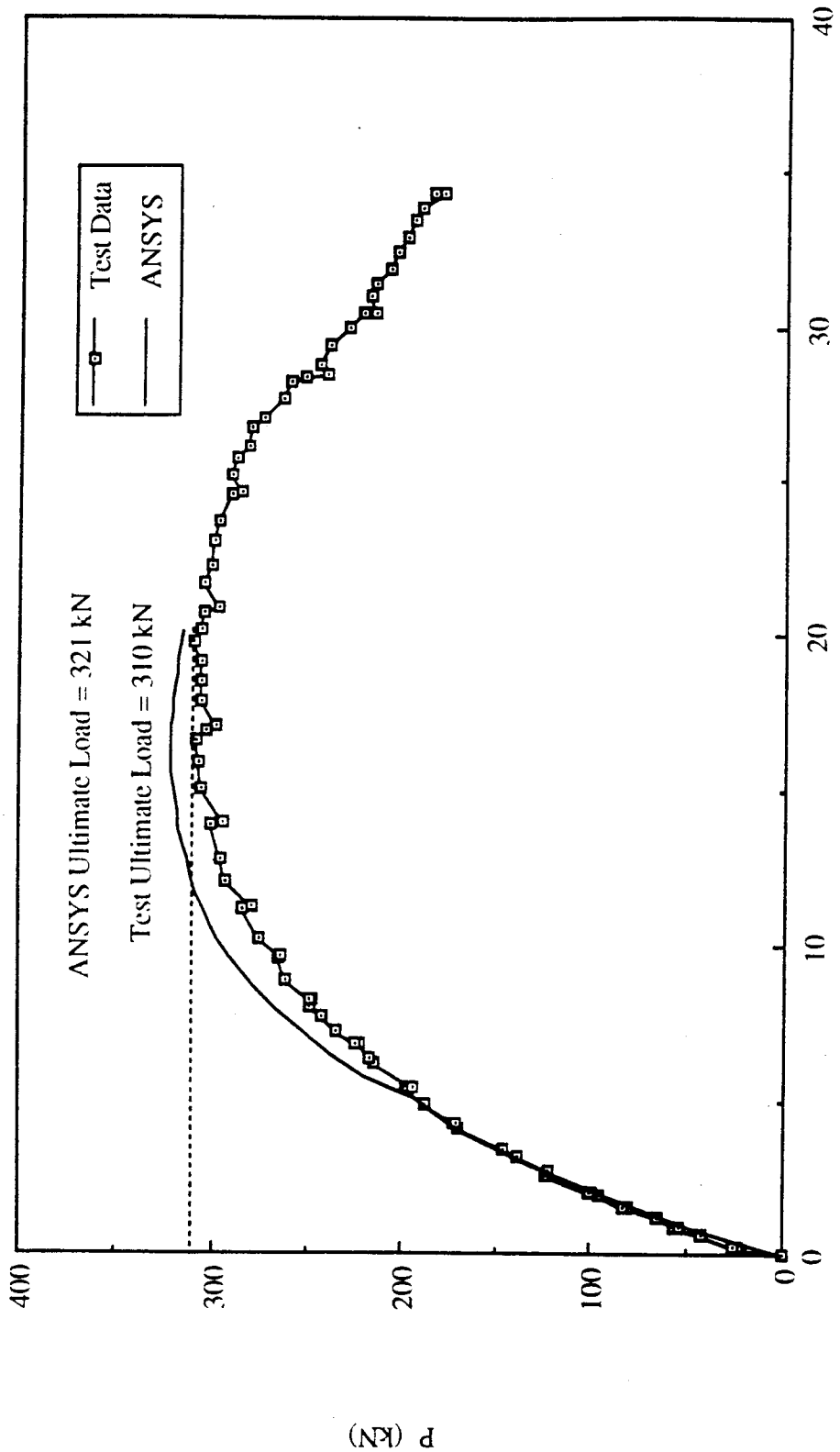


Fig. 2.16 Analytical Load Deflection Curve for Specimen EP1

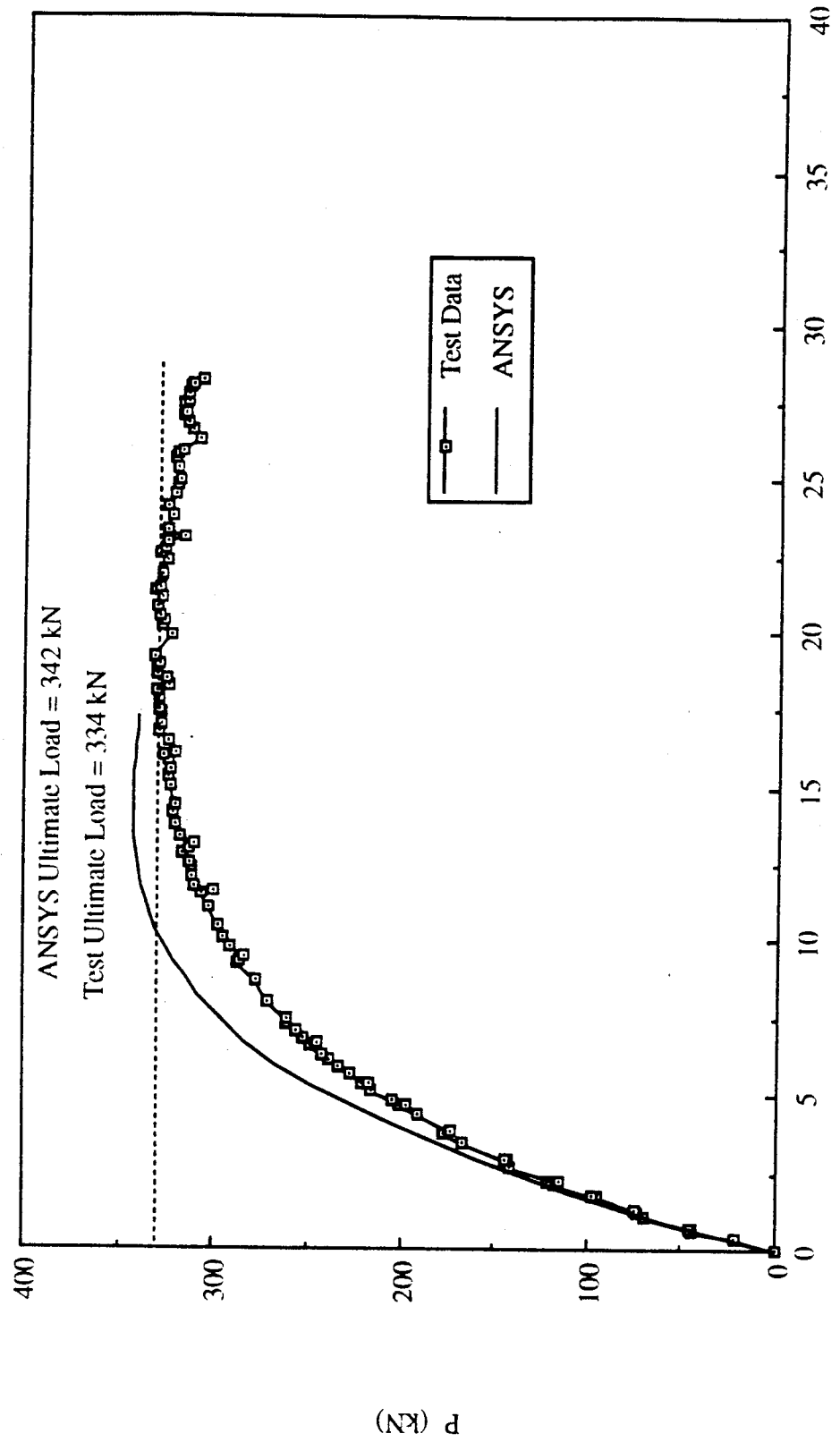


Fig. 2.17 Analytical Load Deflection Curve for Specimen EP2

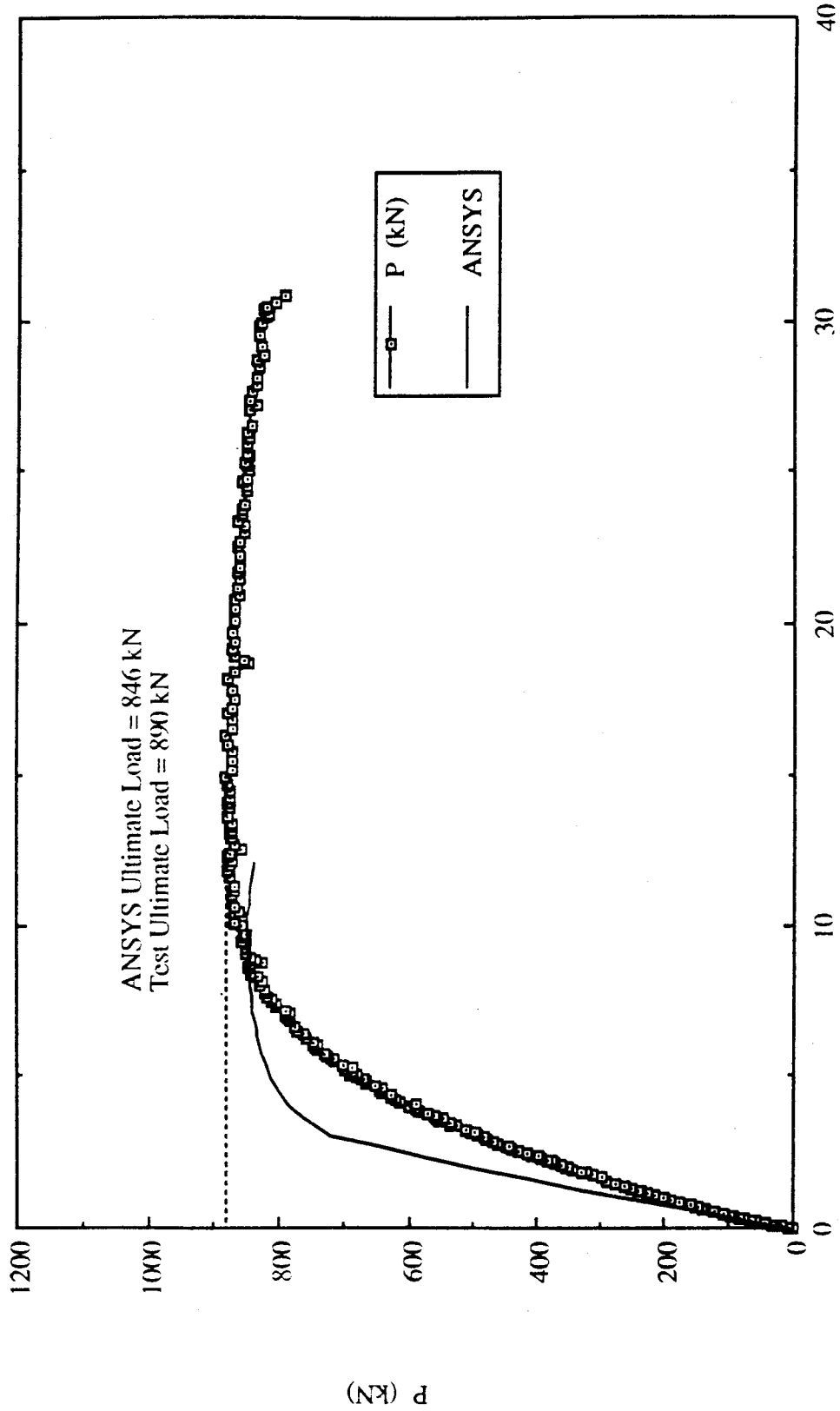


Fig. 2.18 Analytical Load Deflection Curve for Specimen EP3

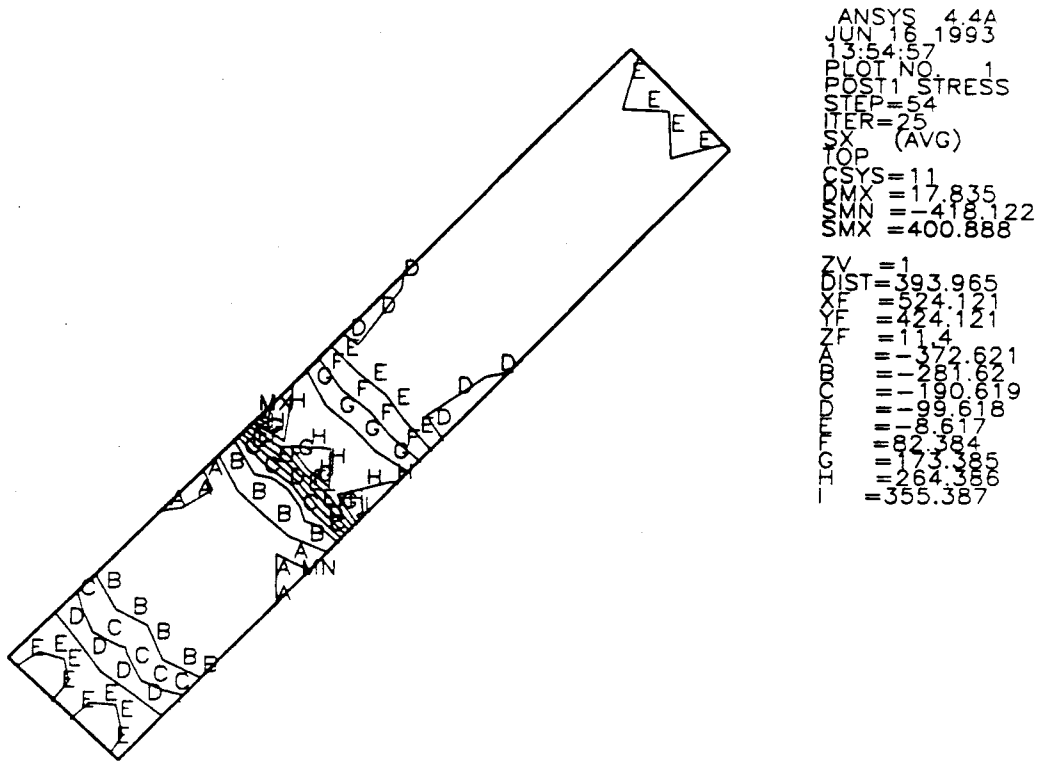


Fig. 2.19 In-Plane Stress Distribution of Splice Plate Top Surface for Specimen EP1 at Ultimate

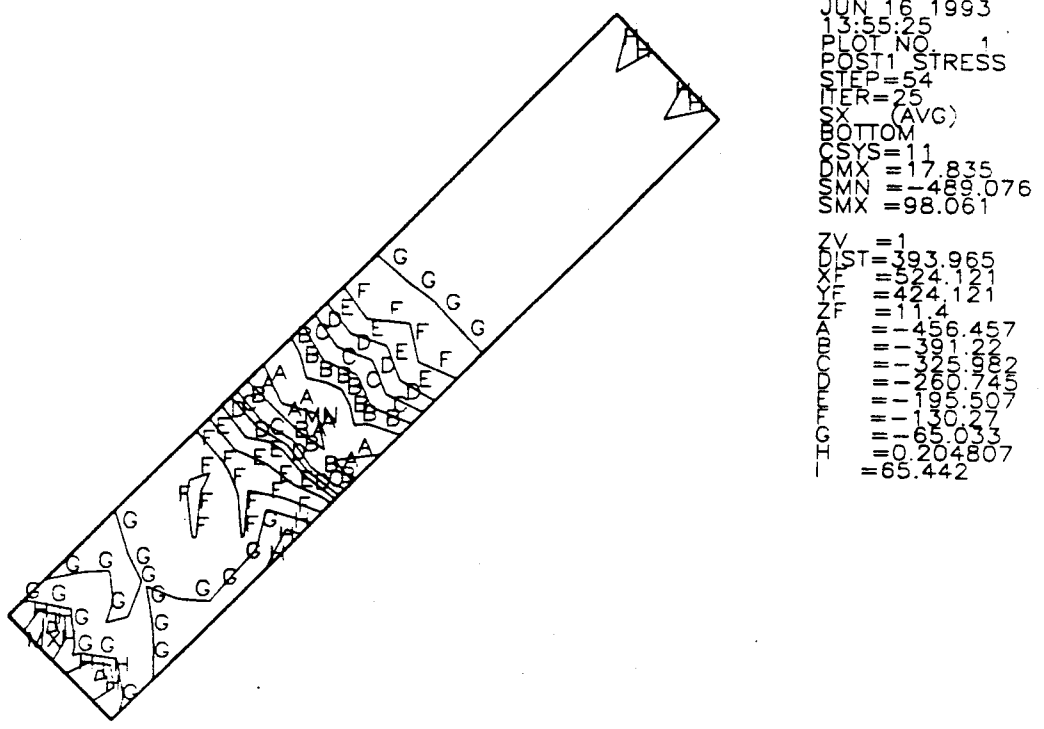


Fig. 2.20 In-Plane Stress Distribution of Splice Plate Bottom Surface for Specimen EP1 at Ultimate

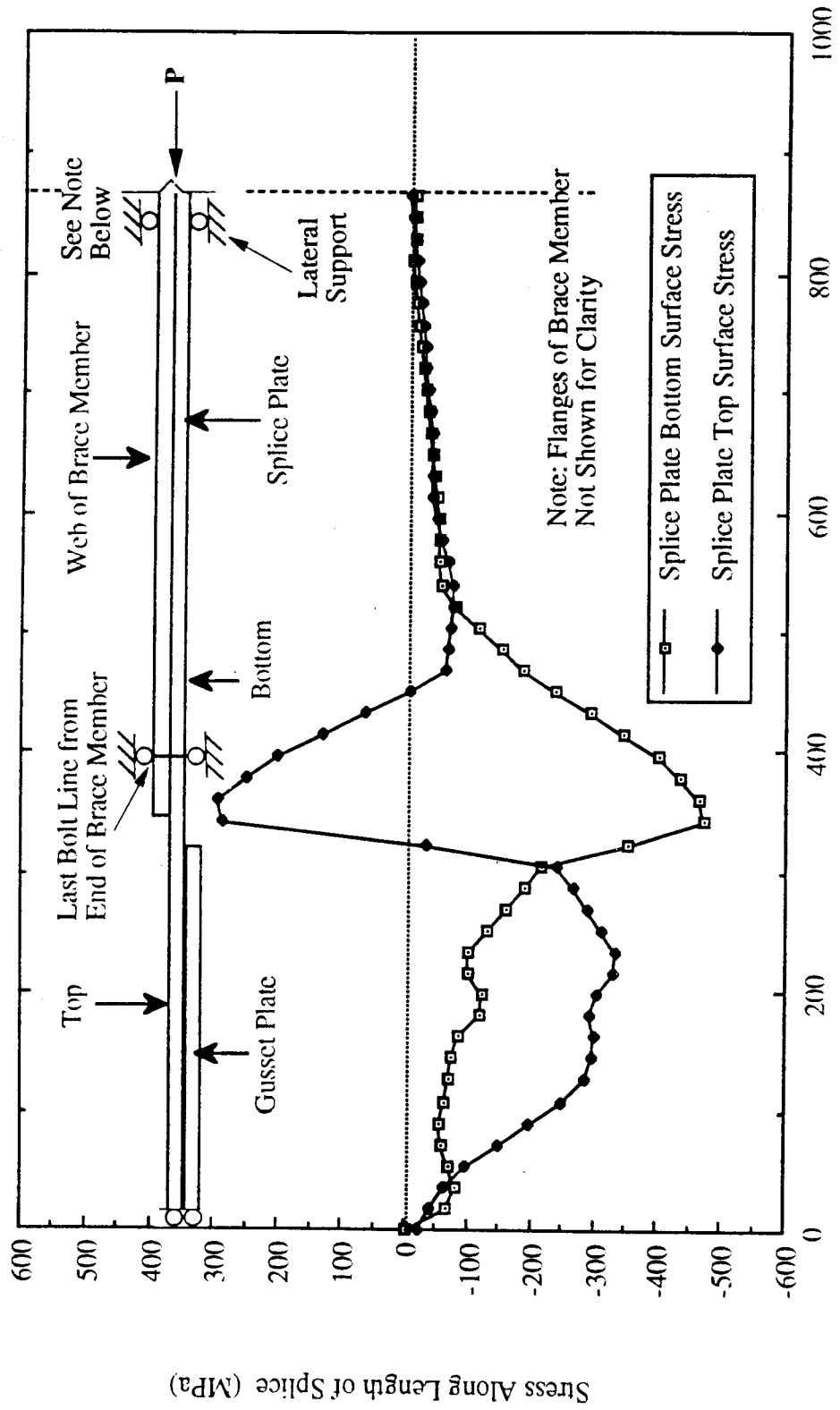


Fig. 2.21 In-Plane Stress Distribution at Centerline Along Length of Splice Plate for Specimen EP1

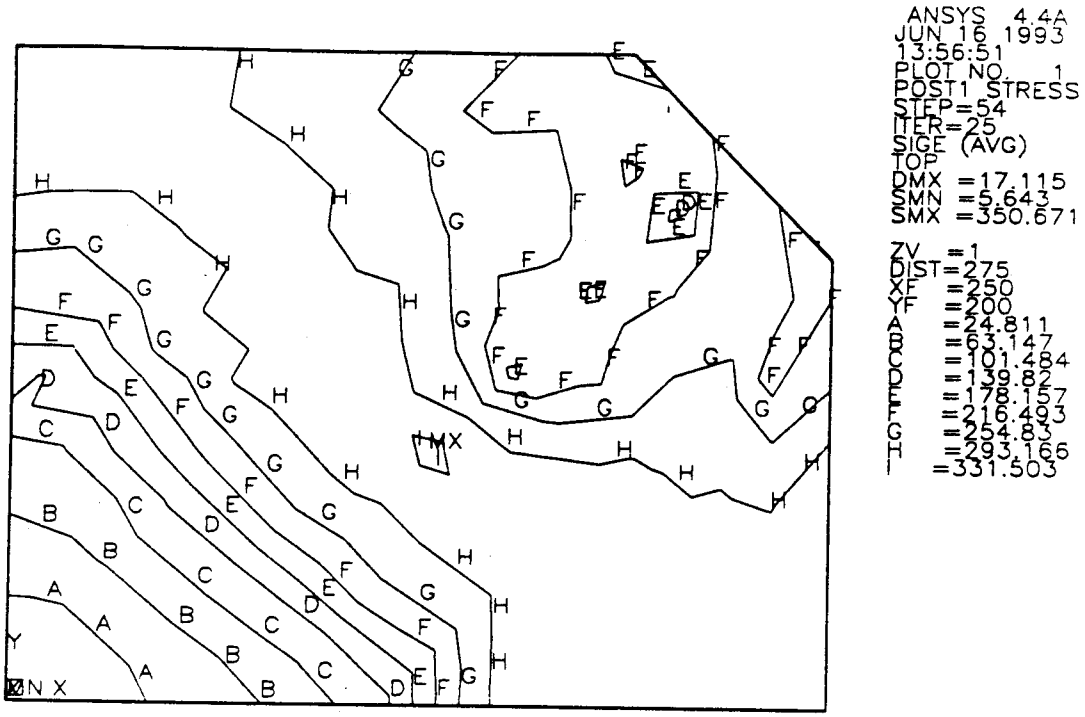


Fig. 2.22 In-Plane Stress Distribution of Gusset Plate Top Surface for Specimen EP1 at Ultimate

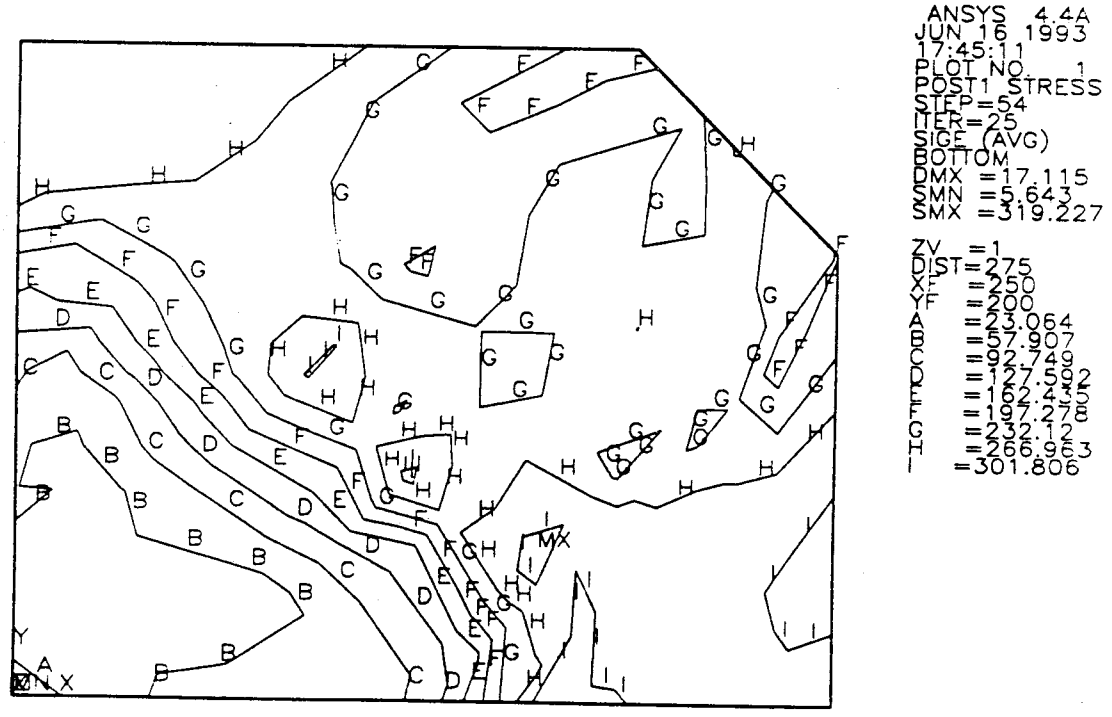


Fig. 2.23 In-Plane Stress Distribution of Gusset Plate Bottom Surface for Specimen EP1 at Ultimate

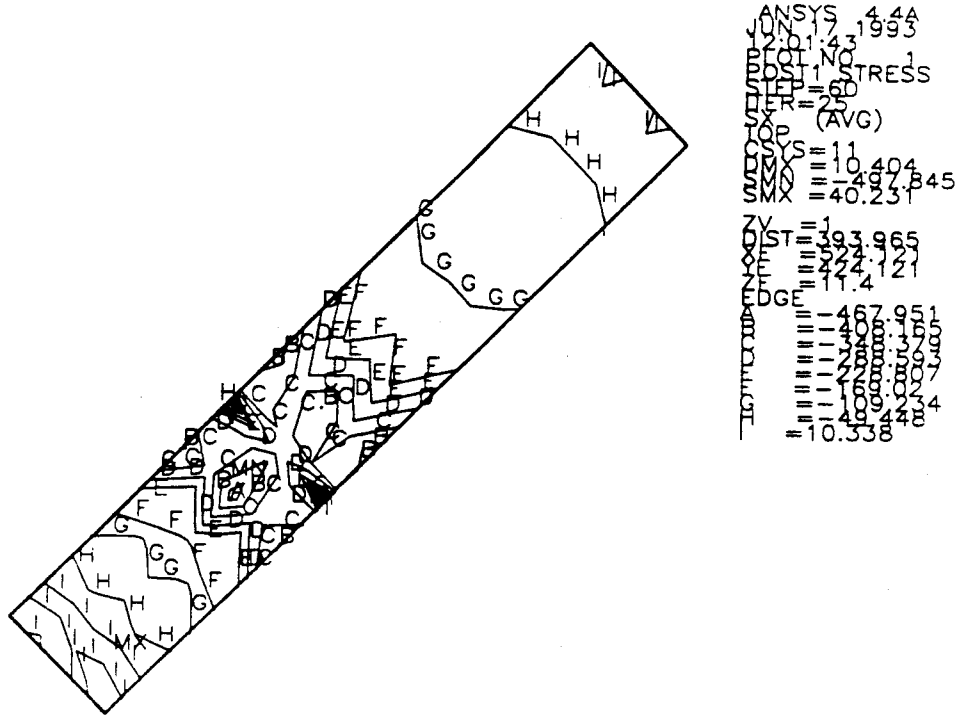


Fig. 2.24a In-Plane Stress Distribution of Splice Plate Top Surface for Specimen EP3 at Ultimate

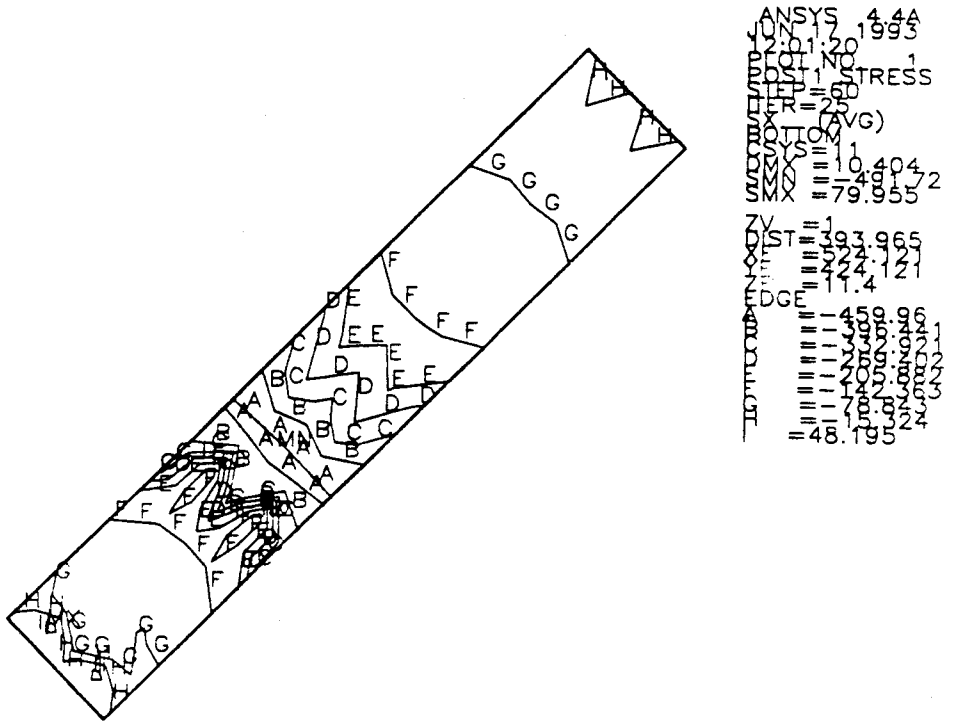


Fig. 2.24b In-Plane Stress Distribution of Splice Plate Bottom Surface for Specimen EP3 at Ultimate

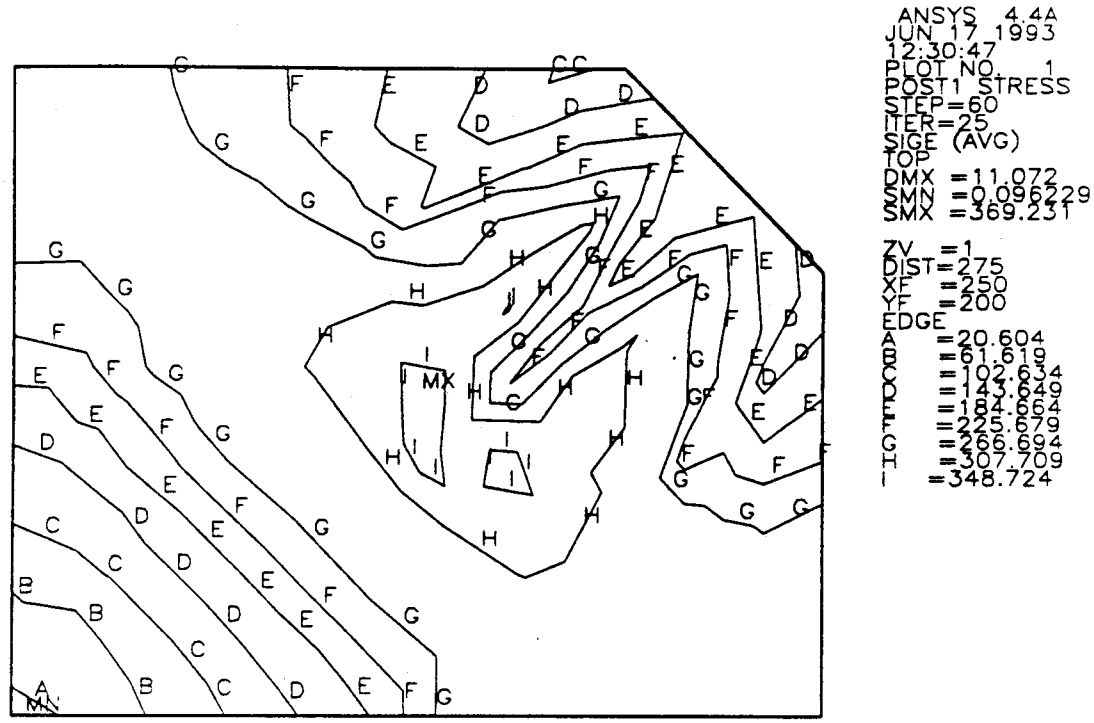


Fig. 2.25a In-Plane Stress Distribution of Gusset Plate Top Surface for Specimen EP3 at Ultimate

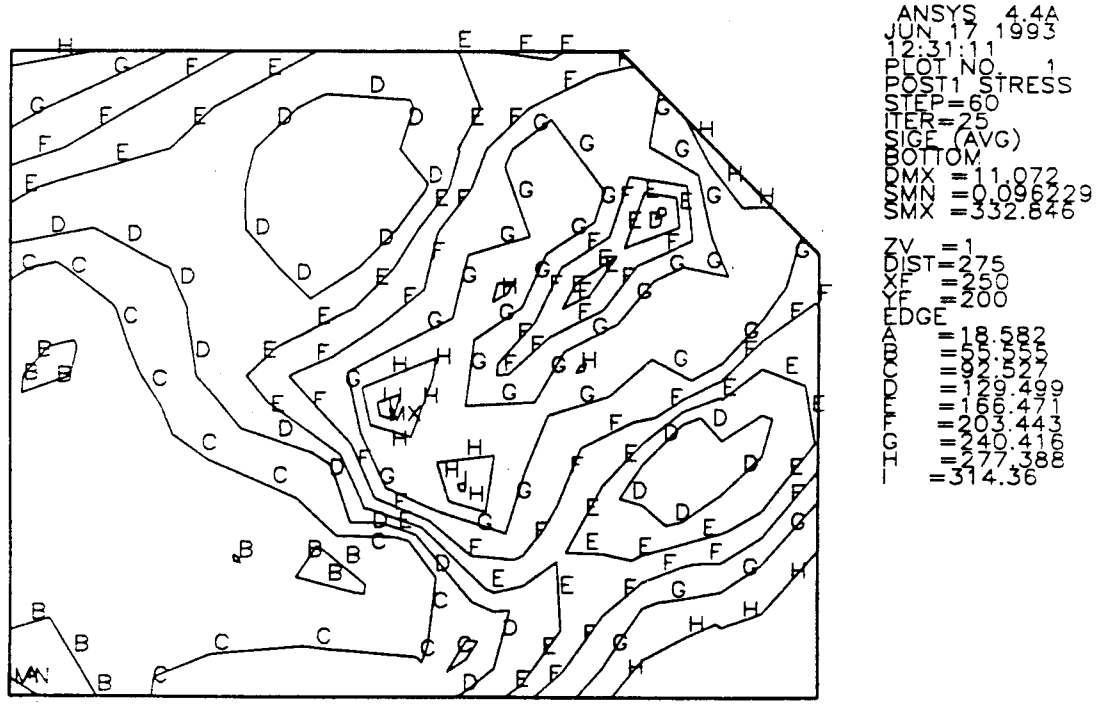


Fig. 2.25b In-Plane Stress Distribution of Gusset Plate Bottom Surface for Specimen EP3 at Ultimate

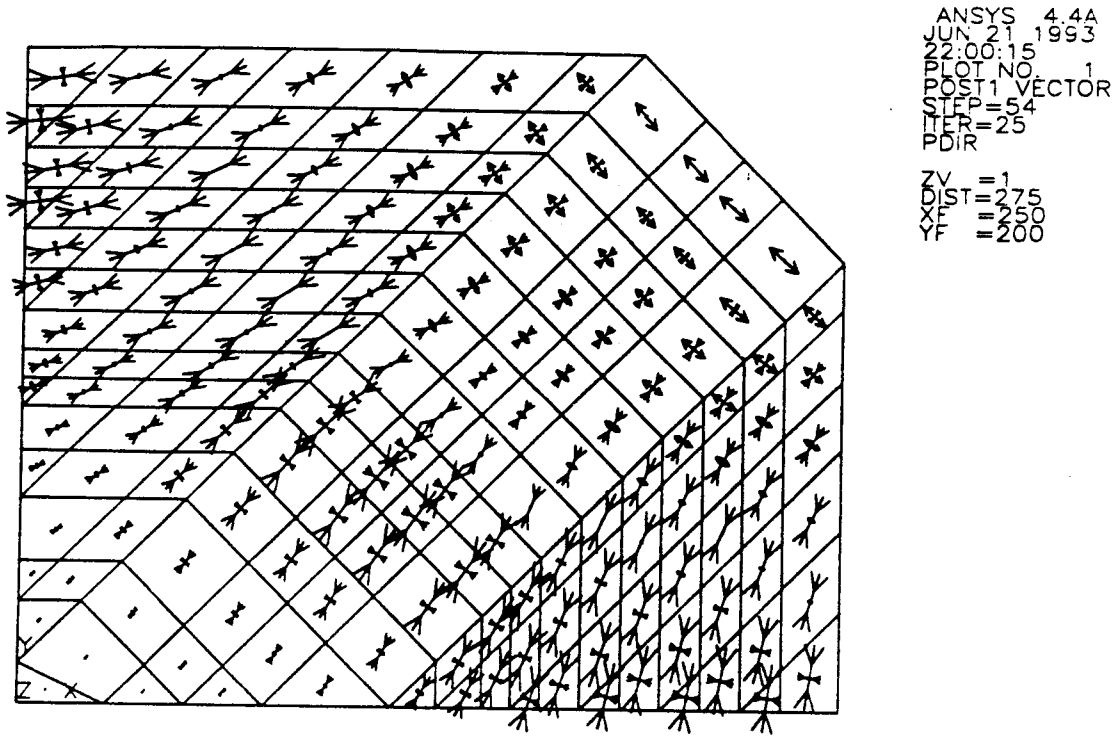


Fig. 2.26 Principal Stress Vector of Gusset Plate Top Surfcae for Specimen EP1 at Ultimate

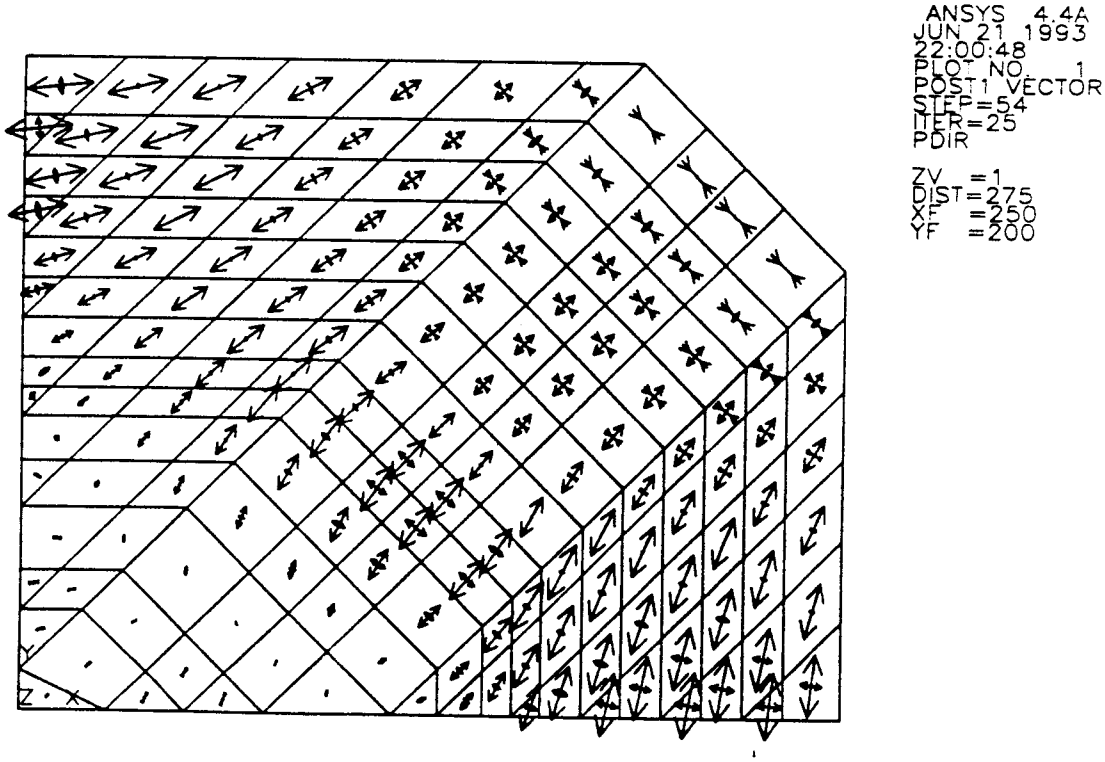


Fig. 2.27 Principal Stress Vector of Gusset Plate Bottom Surfcae for Specimen EP1 at Ultimate

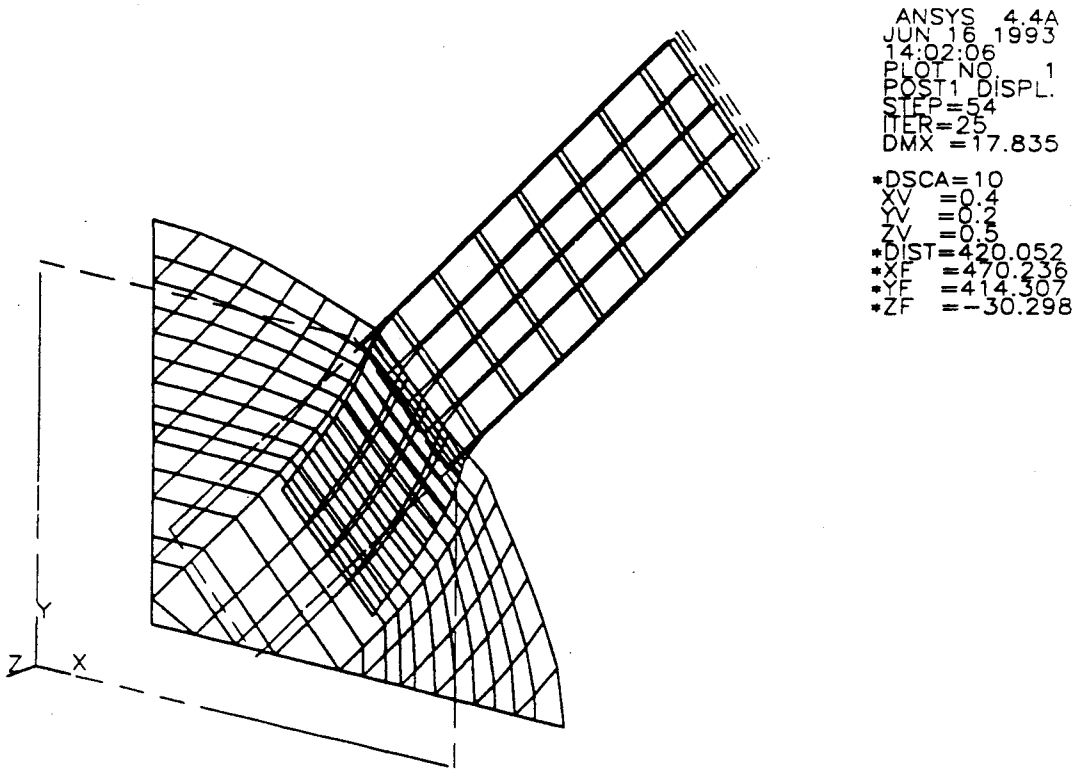


Fig. 2.28 Out-of-Plane Deformation for Specimen EP1

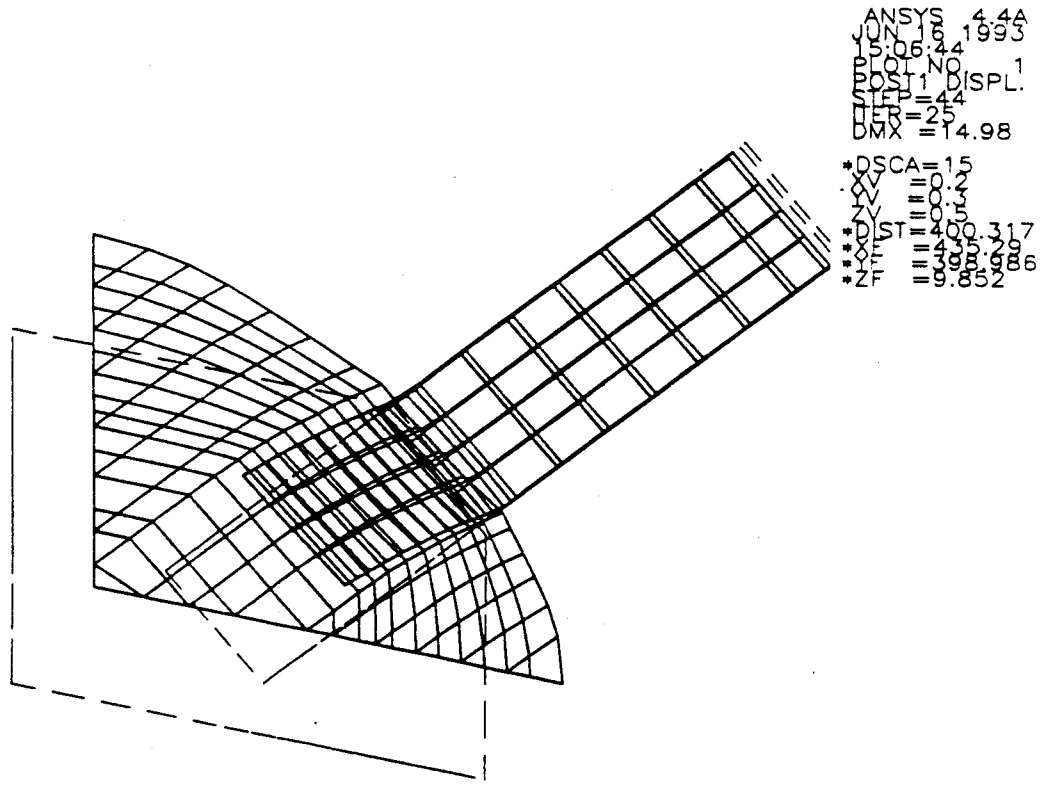


Fig. 2.29 Out-of-PlaneDeformation for Specimen EP2

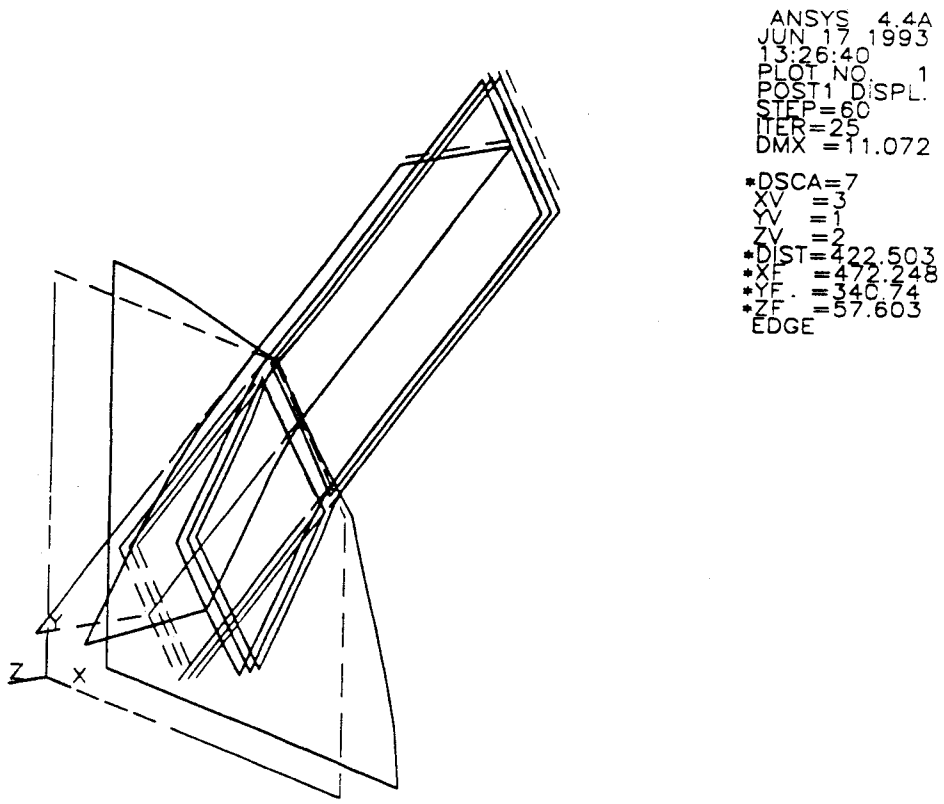


Fig. 2.30 Out-of-Plane Deformation for Specimen EP3

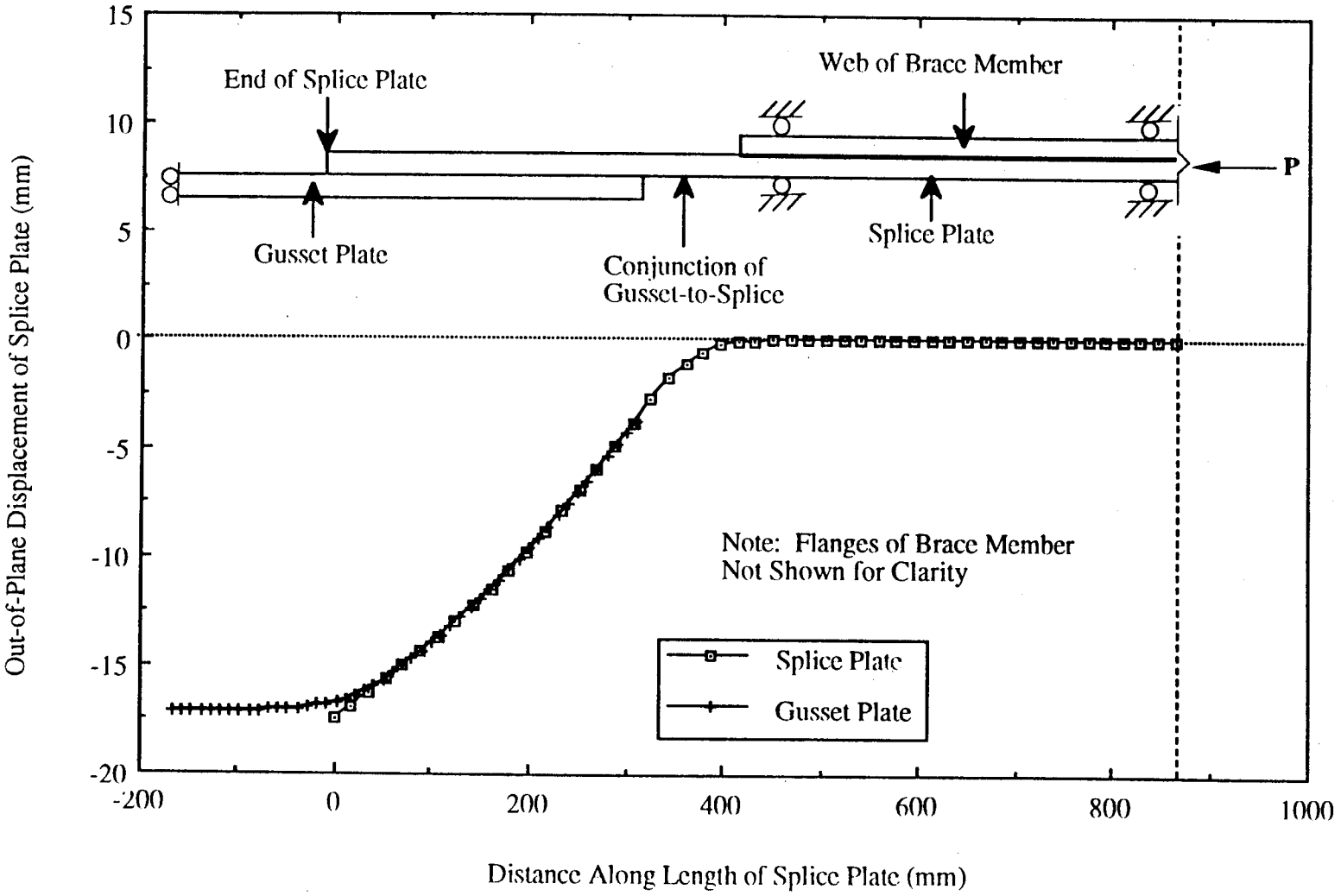


Fig. 2.31 Analytical Out-of-Plane Deflection at Centerline of Splice Plate for Specimen EP1

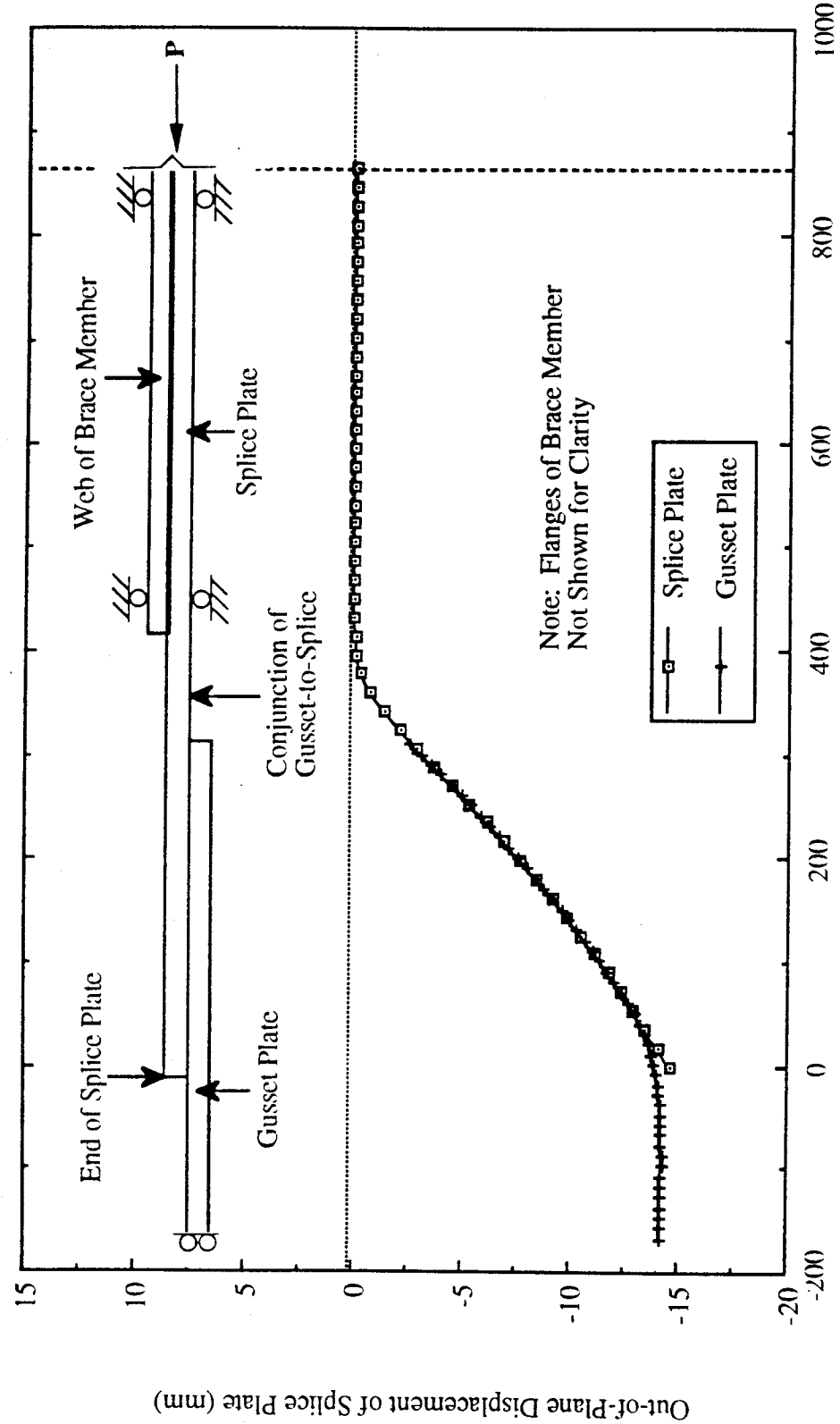


Fig. 2.32 Analytical Out-of-Plane Deflection at Centerline of Splice Plate for Specimen EP2

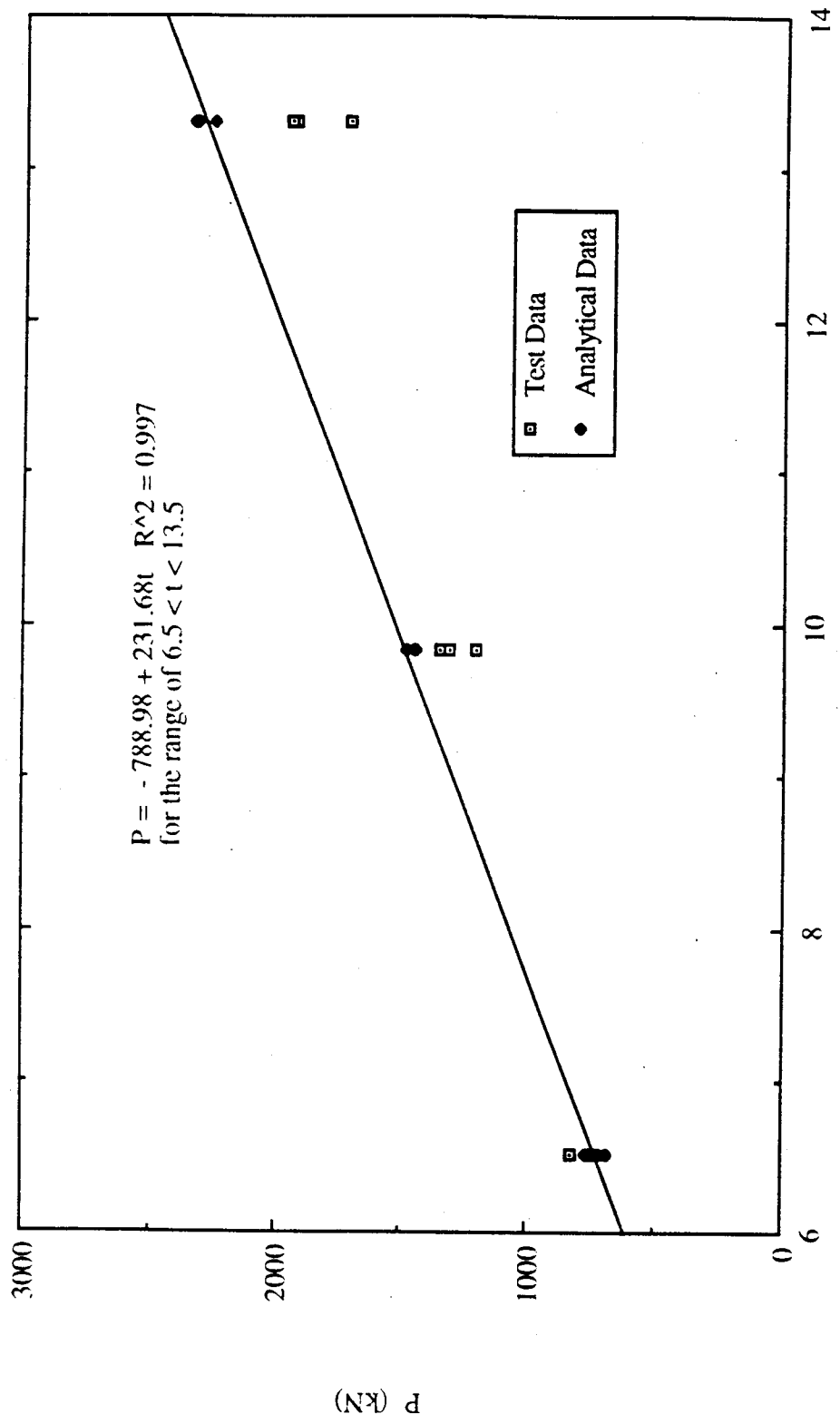


Fig. 2.33 Load vs. Gusset Plate Specimen Thickness

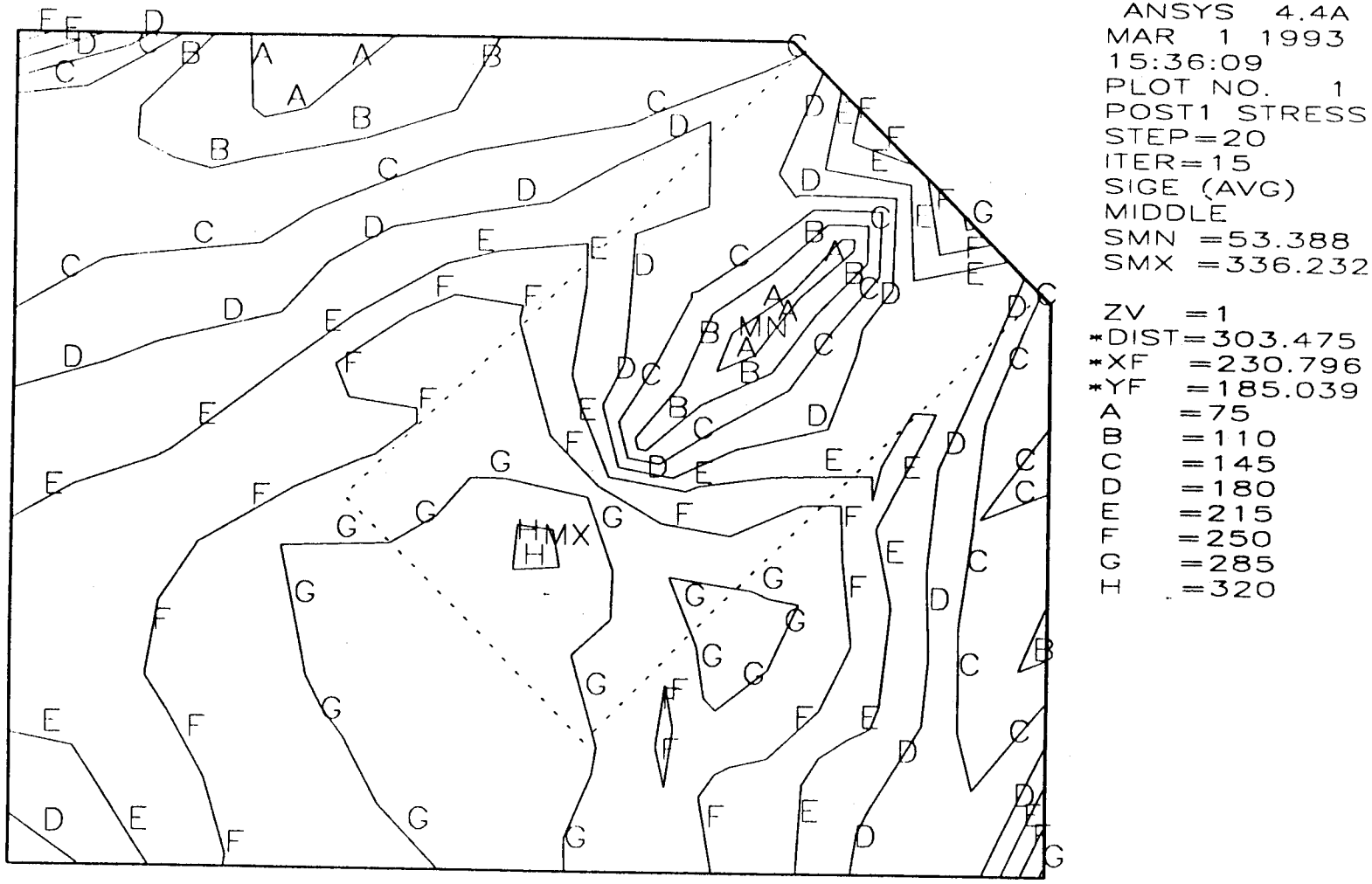


Fig. 2.34a In-Plane Stress Contour for Specimen MP3 at P = 630 kN

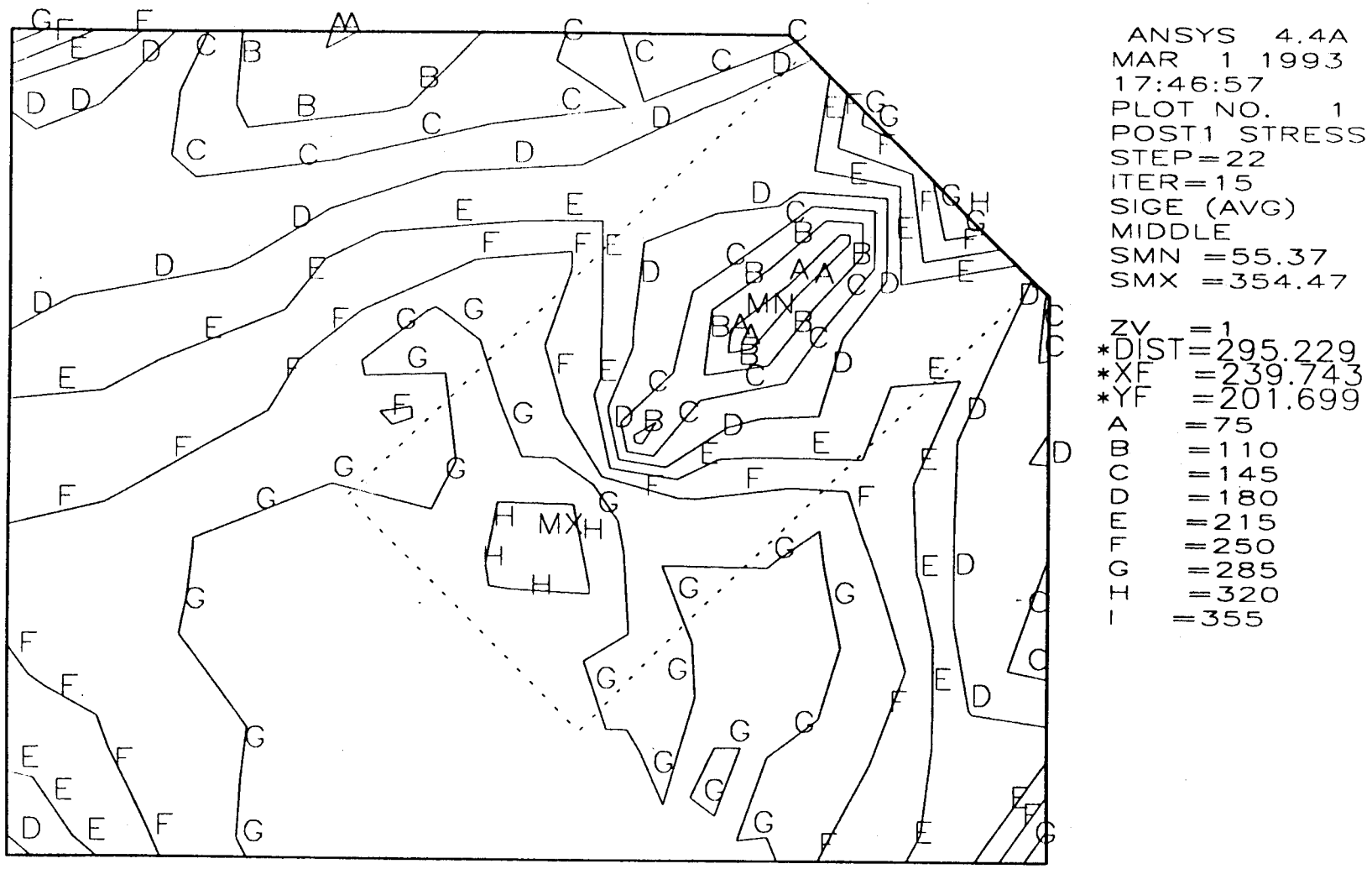


Fig. 2.34 b In-Plane Stress Contour for Specimen MP3A at P = 630 kN

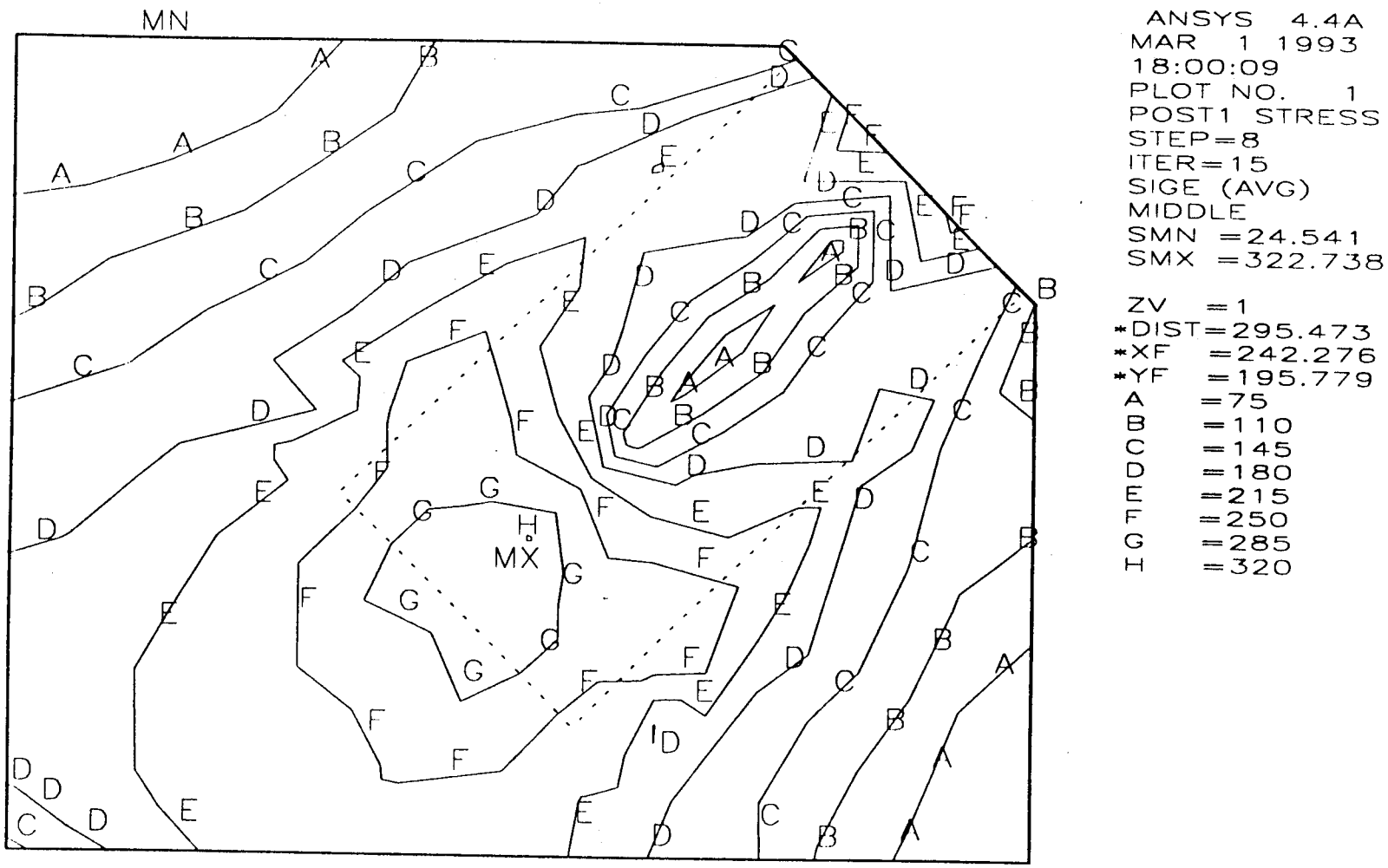


Fig. 2.34c In-Plane Stress Contour for Specimen MP3B at P = 630 kN

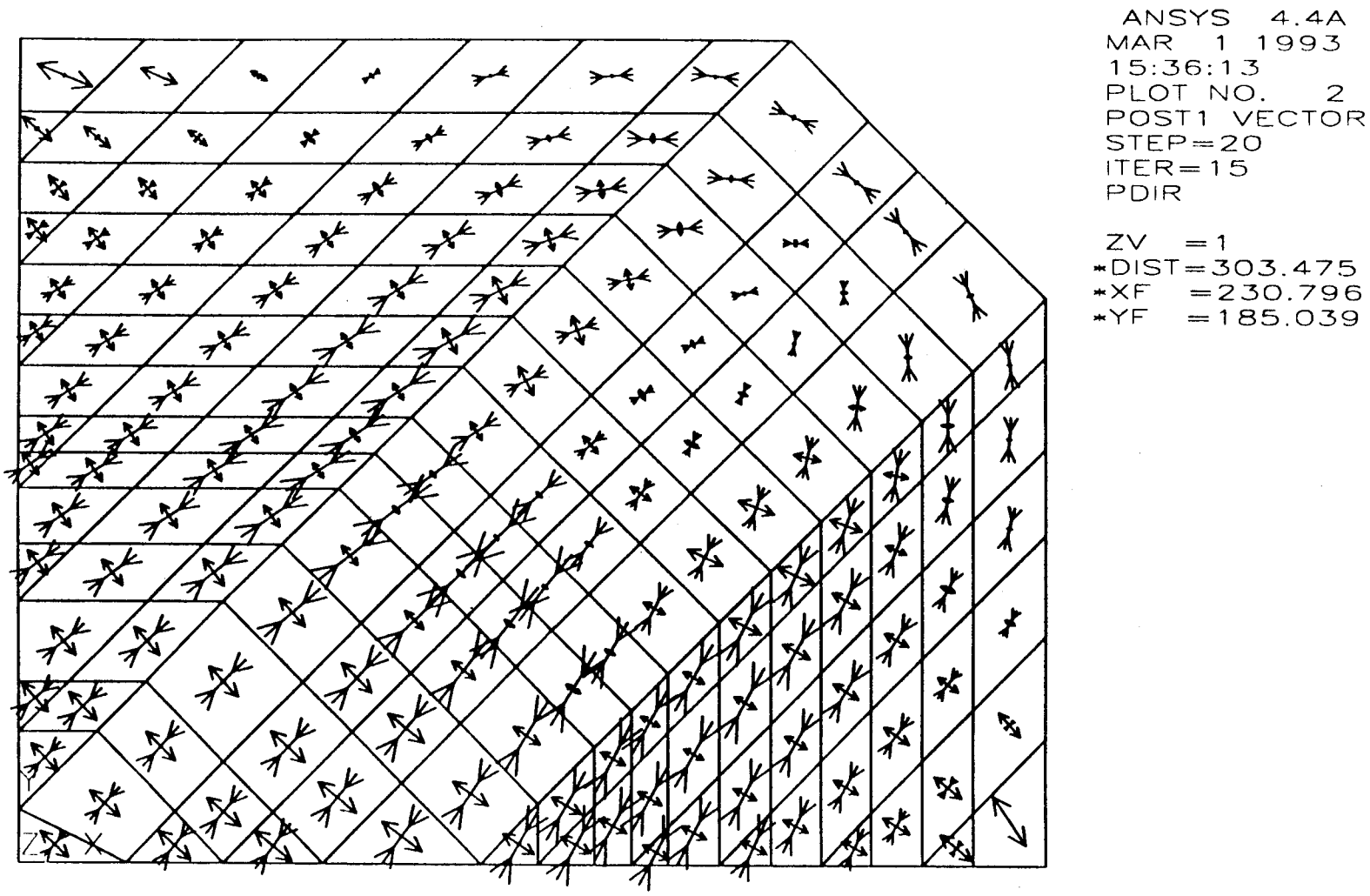


Fig. 2.35a Principal Stress Vector Plot for Specimen MP3 at P = 630 kN

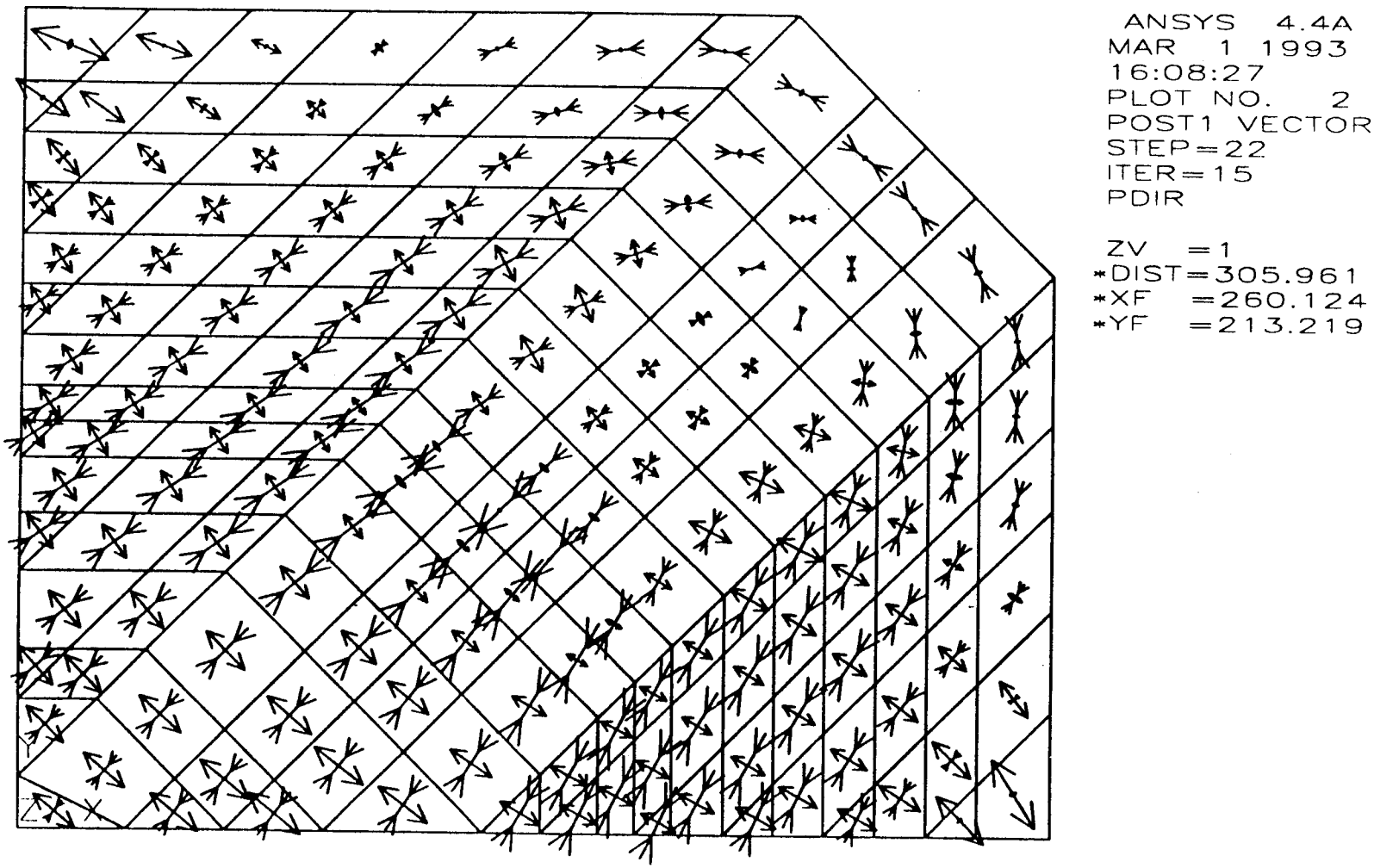


Fig. 2.35b Principal Stress Vector Plot for Specimen MP3A at P = 630 kN

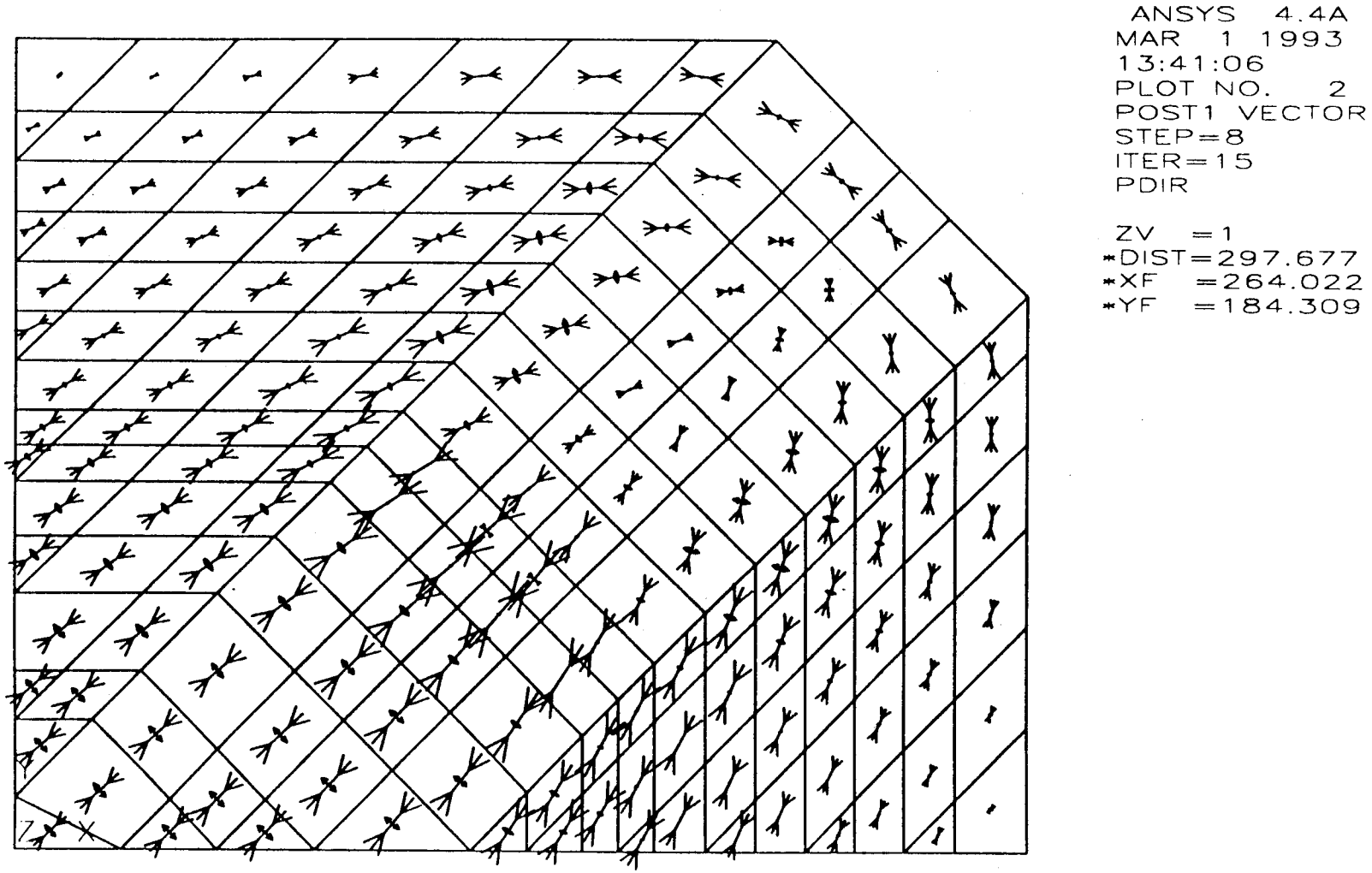


Fig. 2.35c Principal Stress Vector Plot for Specimen MP3B at P = 630 kN

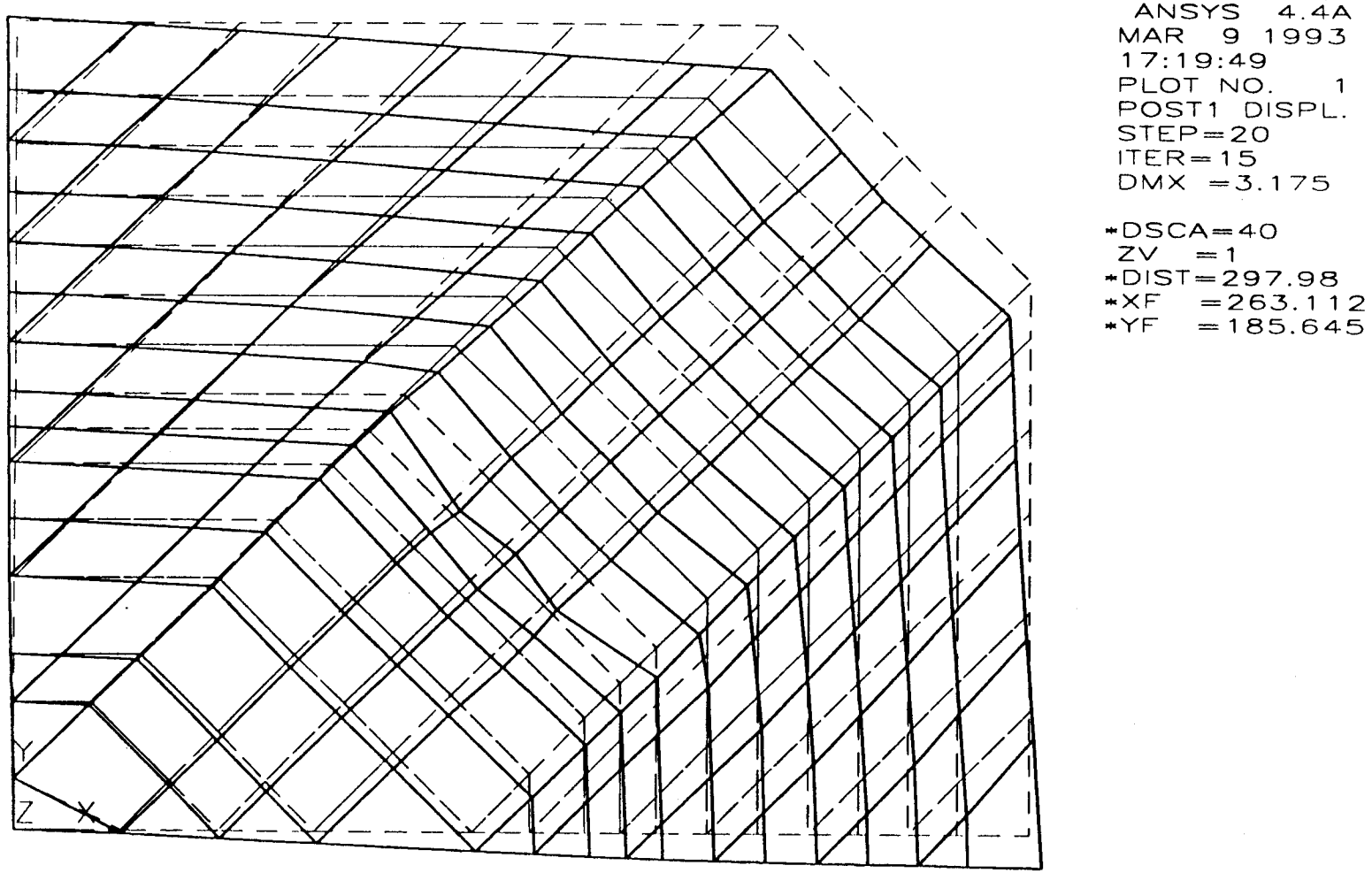


Fig. 2.36a In-Plane Deformation Mode for Specimen MP3 at P = 630 kN

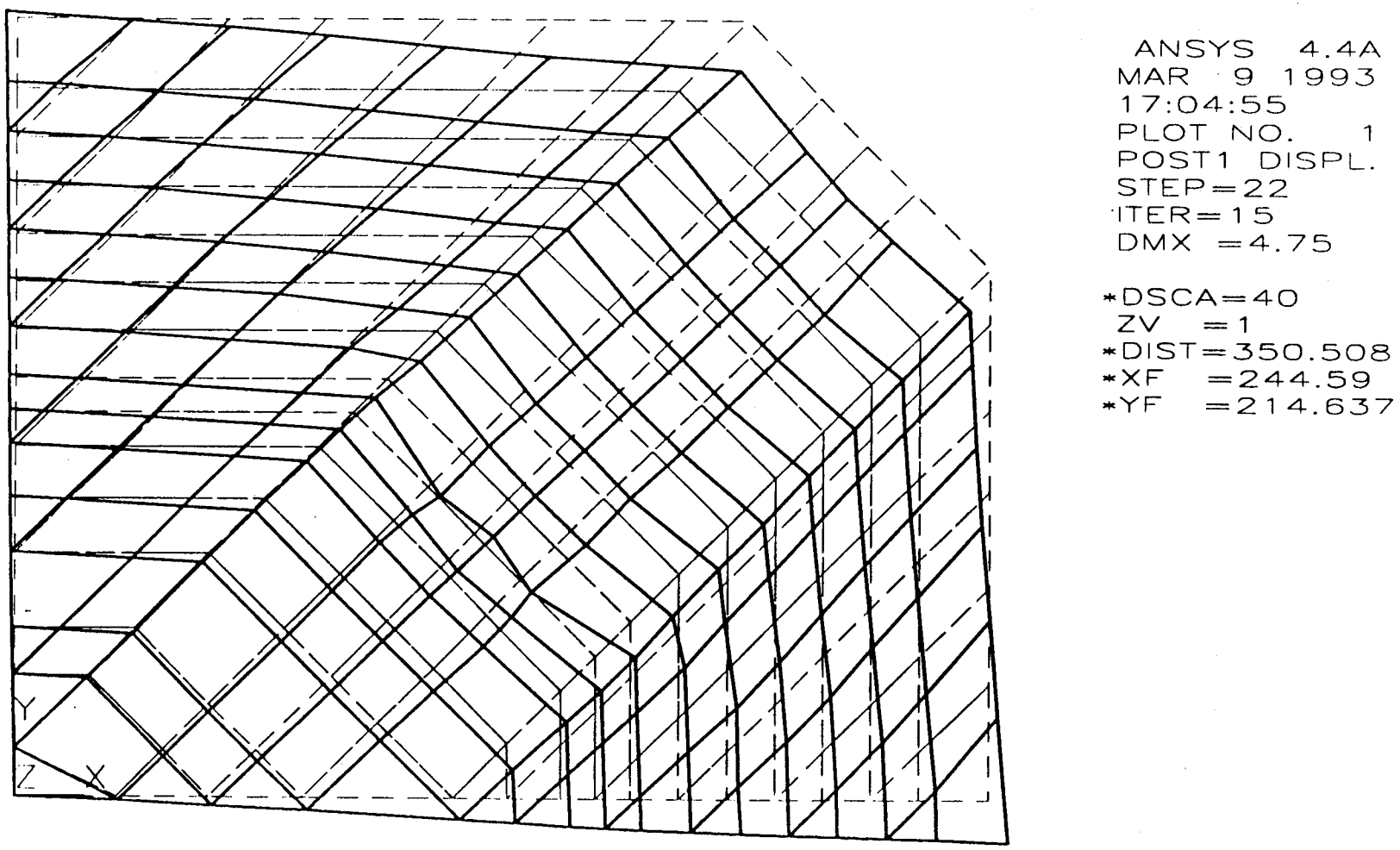


Fig. 2.36b In-Plane Deformation Mode for Specimen MP3A at P = 630 kN

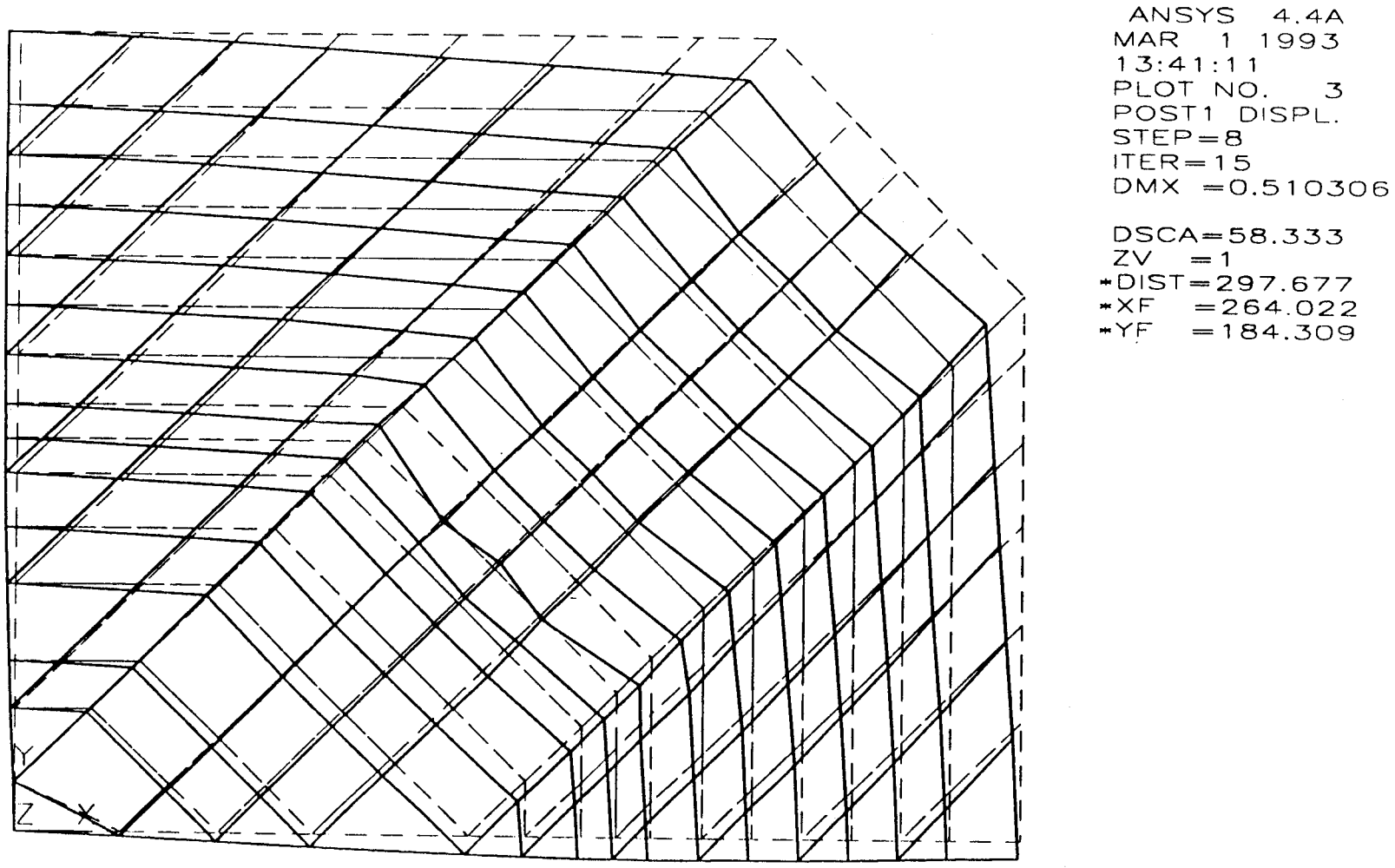


Fig. 2.36c In-Plane Deformation Mode for Specimen MP3B at P = 630 kN

Loading Eccentricity $c = \frac{13.3 + 9.5}{2}$

$= 11.4$ mm

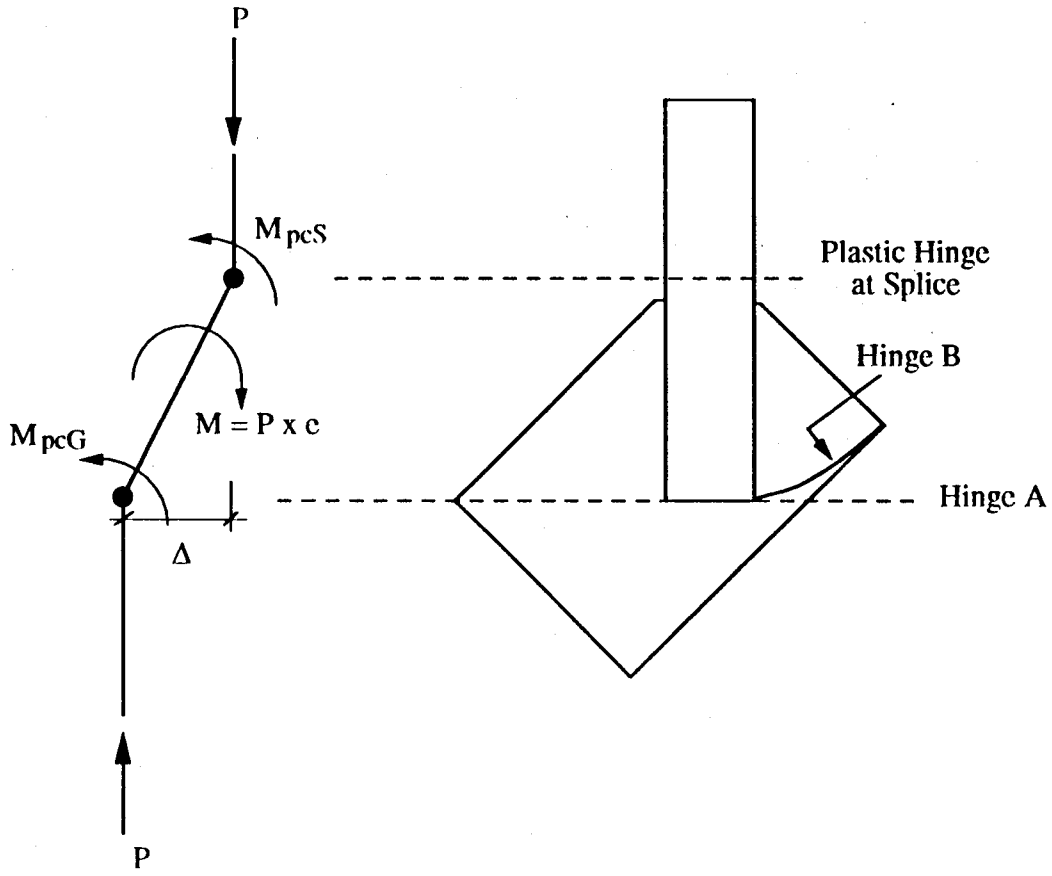


Fig. 2.37 Rigid-Plastic Collapse Mechanism for Specimens EP1 and EP2

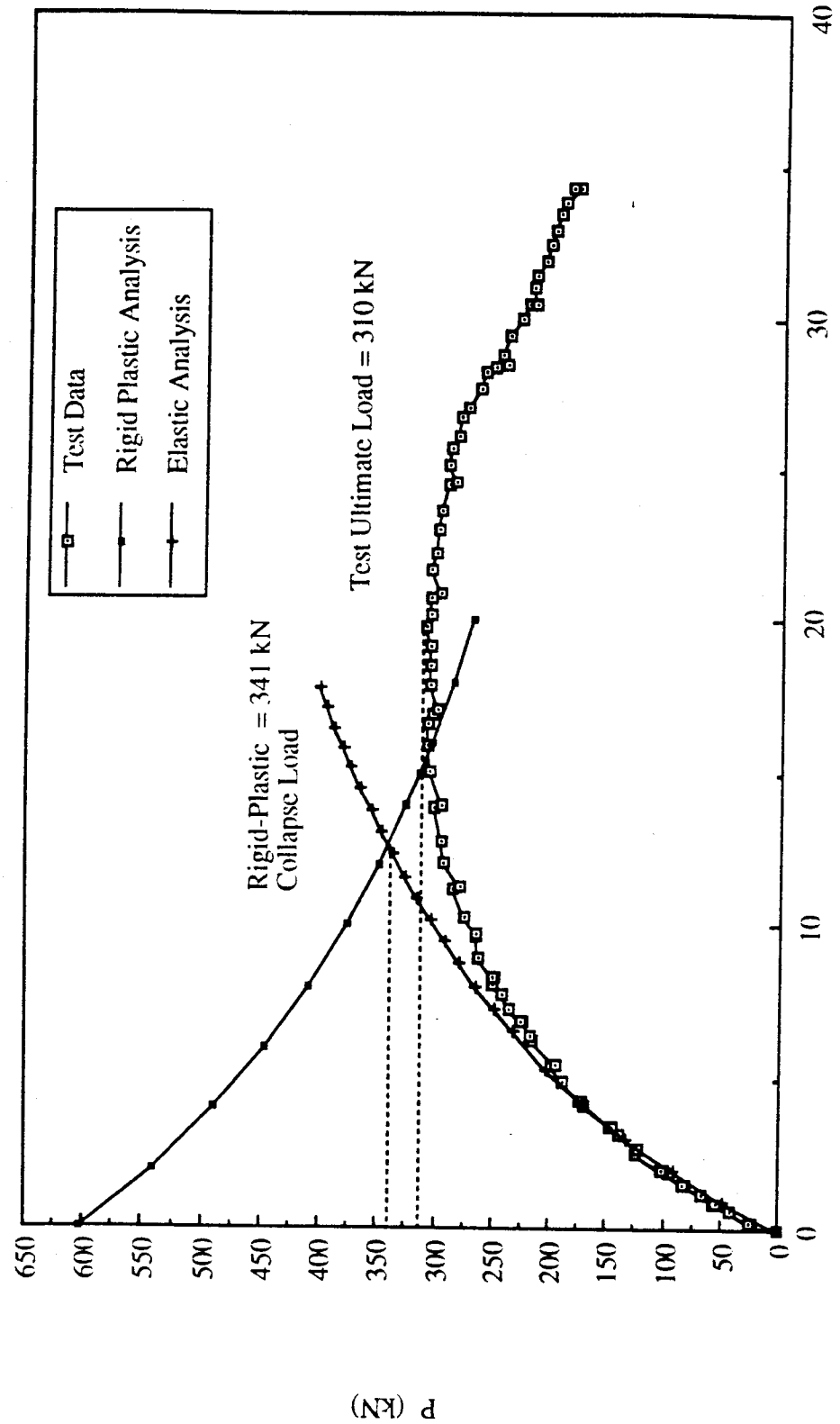


Fig. 2.38 Rigid-Plastic Unloading Line for Specimen EP1

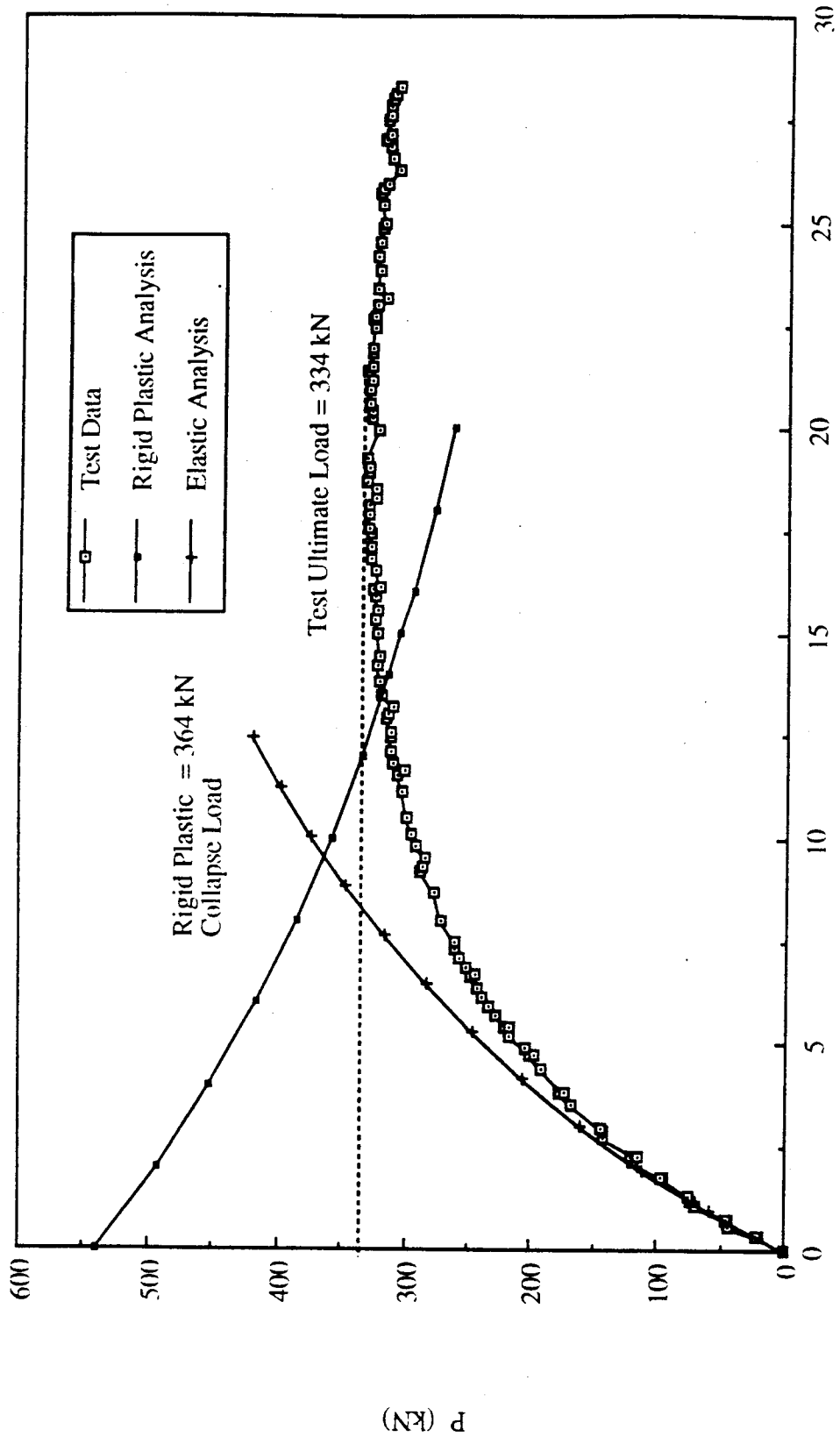


Fig. 2.39 Rigid Plastic Unloading Line for Specimen EP2

# 3. PROPOSED DESIGN GUIDELINES AND METHODS

## 3.1 General

A set of general design guidelines and methods are proposed in this chapter. The design guidelines are based on the parametric studies of the elastic buckling load of gusset plate connections (Cheng et al. 1994) which will be discussed in detail in the next section. The design method for gusset plate connections subject to compression is derived from the Thornton method (Thornton 1984), which has been examined in Yam and Cheng (1993). For the eccentrically loaded gusset plate connections, which were failed by significant yielding at the splice member, the strength of the connections is examined using the beam-column equation of a rectangular section.

## 3.2 Elastic Parametric Studies of Gusset Plate Connections

### 3.2.1 General

Hu and Cheng (1987) examined the compressive behavior and buckling strength of thin-walled gusset plate connections. The test setup for this experimental program is shown in Fig. 1.3. The test results of this investigation showed that elastic buckling of the gusset plate connection occurred in all the concentrically loaded specimens. The experimental elastic buckling loads of these specimens are shown in Table 3.1.

The analytical elastic buckling load of these test specimens obtained using the finite element program ANSYS was studied by Cheng et al.(1994). The typical specimen size and the finite element model are shown in Fig. 3.1. The analytical results from this study are shown in Table 3.1. It can be seen from this table that the analytical results and the test results of specimens C2 and C3 are in reasonable agreement. However, a large discrepancy exists for specimens C1 and C4. For specimen C1, the discrepancy was due to the yielding that occurred in the splice plate at the conjunction of gusset-to-splice during

testing. This yielding reduced the rotational restraint at the conjunction; hence, the buckling load of the specimens was decreased. However, in the analytical model, a rigid rotational restraint was assumed at the conjunction. For specimen C4, the test buckling load was significantly higher than the analytical buckling load. This was due to the post-buckling strength of specimen C4. The details of a large deflection analysis that was employed to investigate this post-buckling behavior can be found in Cheng et al. (1994).

Hu and Cheng (1987) concluded that the splice plate thickness and length and the rotational restraint at the conjunction of the gusset-to-splice have significant effects on the elastic buckling load of the gusset plate connections. In order to study the effects of these parameters, an elastic parametric study was conducted. The finite element program ANSYS and the finite element model shown in Fig. 3.1 were used in the parametric study. This study will provide the general guidelines for designing the concentrically loaded gusset plate connections.

### 3.2.2 Parametric Studies

#### 3.2.2.1 General

The parametric studies of the elastic buckling load of the gusset plate connections include the following parameters:

1) the thickness of the splice plate members;
2) the length of the splice plate members (SL; see Fig. 3.2) connected to the gusset plates;
3) the rotational restraint at the conjunction of the bracing member and the gusset plate.

Although this parametric study is limited to elastic analysis, the results can still illustrate the general influence of each parameter on the buckling load of the gusset plate connections.

### 3.2.2.2 Effects of Splice Plate Thickness

The effects of splice plate thickness on the elastic buckling strength of the gusset plate connections are shown in Fig. 3.3. As shown in the figure, the investigation was conducted with two gusset plate sizes, 850 x 550 mm and 850 x 700 mm, three gusset plate thicknesses, 3.11 mm, 6.7 mm, and 9.5 mm, and two splice member lengths (SL), 297 mm and 447 mm. The splice plate length of 297 mm corresponds to the length of four rows of bolts connected to the gusset plate, and the splice plate length of 447mm corresponds to six rows of bolts connected to the gusset plate, as shown in Fig. 3.4.

It can be observed from Fig. 3.3 that the 3.11mm thick gusset plates with a splice plate thickness of 7 mm achieve 80% or more of the buckling load of the same gusset plate with infinite splice plate thickness. At a splice plate thickness of 13mm, the 3.11mm thick gusset plate is able to reach more than 97% of the buckling load of the same gusset plate with infinite splice plate thickness. Therefore, it can be seen that when the splice plate thickness is increased, the buckling load of the gusset plate increases until a critical value of the splice plate thickness is reached, after which increases in the splice plate thickness do not produce a significant additional increase in the buckling load. This implies that this critical value of splice plate thickness provides a rigid support to the gusset plate. The critical value (Sc) is defined as the splice plate thickness at which a gusset plate specimen achieves 90% or more of the buckling load of the same specimen with infinite splice plate thickness. The critical values of the specimens shown in Fig. 3.3 are given in Table 3.2. It can be seen from the table that the critical splice plate thicknesses of the specimens range from about two to four times the corresponding gusset plate thickness. Therefore, it is believed that the elastic buckling load of a gusset plate connection with an infinite splice plate thickness can be achieved by providing a splice plate thickness of at least four times that of the gusset plate. It is also observed from Fig. 3.3 that, for the same gusset plate

size and the splice plate length, the buckling load of the gusset plates is proportional to the cube of the gusset plate thickness if infinitely thick splice plates are used.

### 3.2.2.3 Effects of Splice Plate Length

As can be seen from Fig. 3.3, for the same gusset plate size and thickness and splice plate thickness, the elastic buckling loads of the specimens increase with the increasing length of the splice member. The amount of the increase depends significantly on the splice plate thickness, as shown in the figure. To further investigate the effects of the splice plate length, the elastic buckling loads of the specimens with a splice plate thickness at least equal to the corresponding critical splice plate thickness are examined and are shown in Table 3.3a. As can be seen from this table, for the gusset plate size of 850 x 550, when the splice plate length is increased from 297 mm (4 rows of bolts) to 447 mm (6 rows of bolts), the elastic buckling loads are increased by approximately 2.4 times. It is also observed from this table that the same ratio of increase is recorded for all the gusset plate thicknesses examined. As mentioned above, since the elastic buckling loads of the specimens corresponding to each splice plate length increased proportionally to the cube of the gusset plate thickness if the critical splice plate thicknesses were used, the ratio of increase in the elastic buckling load due to an increase in the splice plate length was thus maintained with various gusset plate thicknesses. For the specimen with a plate size of 850 x 700 x 6.7 and the critical splice plate thickness of 20 mm, a 33% increase in the elastic buckling is observed when the splice plate length is increased from 447 mm (six rows of bolts) to 522 mm (seven rows of bolts), as shown in Table 3.3b. Hence, it can be seen that the length of the splice plate member has a significant effect on the elastic buckling load of the gusset plate connections.

The increase in the elastic buckling load due to an increase in the splice plate length can also be observed by examining Fig. 3.2. This figure shows a triangular area of the gusset plate

which is bounded by the beam and column boundary and a line (which will hereafter be referred to as the bending line) joining the extremities of the fixed edges. It is reasonable to assume that this triangular area provides out-of-plane and rotational supports to the connection if a significant part of the splice plate is extended beyond the bending line. Diagrams of the gusset plate specimens discussed above are shown in Fig. 3.4. This figure shows that, for the 850 x 500 mm specimens, increasing the number of rows of bolts from four to six moves the splice plate member from the outside of the triangular area to the inside of it with the first row of bolts extending beyond the bending line. The increase in buckling load due to this increase in splice plate length is 2.4 times, as mentioned above. Hence, it can be seen that in order to increase the buckling load of the gusset plate connections, the splice member should be extended beyond the bending line as close to the beam and column boundary as possible.

#### 3.2.2.4 Effects of Rotational Restraint at Conjunction of Bracing Member and Gusset Plate

The effects of rotational restraint at the conjunction of the bracing member and the gusset plate are shown in Table 3.4. This table shows the elastic buckling load of a gusset plate connection with a plate size of 850 x 550 and a splice plate thickness of 13 mm. As can be seen from the table, providing infinite rotational restraint at the conjunction of the bracing member and the gusset plate significantly increases the elastic buckling load of the gusset plates. The ratios of the buckling loads of the gusset plates with infinite restraint to the buckling loads of the gusset plates without restraint range from 2.6 to 3.1, as shown in the table.

To further examine the effects of the rotational restraint on the elastic buckling load, a rotational spring is applied to the gusset plate at the conjunction; the analytical results are shown in Fig. 3.5. As can be seen from this figure, the elastic buckling load of the

specimens increases with increasing rotational spring stiffness. However, the rate of increase diminishes significantly when the rotational spring stiffness reaches a critical value of about 400 kN·m/rad for both specimens. At this value of rotational spring stiffness, the buckling loads of the specimens have already reached more than 90% of the buckling load of the same specimens with infinite rotational restraint. To compare the flexural stiffness of a bracing member to the critical value of rotational spring stiffness, a W250x67 section with a length of 5650 mm is chosen to be the diagonal bracing member (a 4 m x 4 m frame is assumed). The diagonal bracing member is assumed to be subject to equal end moments; therefore, the flexural stiffness of the member (neglecting the axial force effects) is 2EI/L, where E is the modulus of elasticity (200 000 MPa), I is the moment of inertia of the section ($I_y$ = 22.2 x $10^6$ $mm^4$) and L is the span length of the diagonal member. For this section, the flexural stiffness based on 2EI/L is 1600 kN·m/rad. Hence, it can be seen that the chosen section, which is a reasonable size for a diagonal bracing member, provides sufficient rotational restraint to the gusset plate specimens examined in this section.

#### 3.2.2.5 General Design Guidelines

A set of general design guidelines is proposed in this section. It should be noted that these are based on the elastic parametric studies cited above. Further analytical studies which take into account the inelastic behavior of the compact gusset plate connections would be required in order to refine the proposed design guidelines. The general design guidelines for designing concentrically loaded gusset plate connections subject to compression are:

1) To increase the buckling strength of the gusset plate connections, the use of splice members which have a high out-of-plane bending rigidity is recommended, e.g., a tee-section or a channel section. Based on the specimens examined in the parametric

studies, a splice plate member which has a thickness of four times the gusset plate thickness is recommended.

2) The splice member should always be extended beyond the bending line and as close to the beam and column boundary as possible.

3) The use of bracing members with high out-of-plane flexural rigidity is recommended. Based on the elastic parametric studies of the specimens, a flexural stiffness of 600 kN·m/rad is recommended for the diagonal bracing members. The reduction of the flexural stiffness of the bracing members due to the axial forces in the members should be considered in the design.

## 3.3 Modified Thornton Method

### 3.3.1 General

The experimental results, the analytical plastic bifurcation buckling loads, the Whitmore loads, and the Thornton loads of the specimens are shown in Table 3.5. As can be seen from the table, the Thornton load ($P_{t30}$) predictions are generally very conservative: the ratio of the test loads to the Thornton loads ($P/P_{t30}$) varies from 1.31 to 1.87. This method recommends evaluating the critical buckling stress level at the Whitmore effective width (a $30^{\circ}$ dispersion angle), as discussed in Chapter 1.

The tests results and the analyses showed that the yielding of the specimens usually extended beyond the Whitmore effective width, provided that the specimens were stiff enough to avoid early instability failure. This suggests that a load redistribution has occurred in the test specimens. In order to account for this load redistribution behavior in designing gusset plate connections subject to compression, it is proposed that a $45^{\circ}$ dispersion angle be used to evaluate the effective width, instead of $30^{\circ}$, as shown in Fig. 3.6. The modified Thornton load is then calculated based on the extended effective width

and the appropriate column curves. It should be noted that the unsupported length of the unit column strip was evaluated from the end of the splicing member to the beam and column boundary, since a relatively rigid splicing member was used in the testing program (see Fig. 3.6). However, the unsupported length of the unit column strip measured from the effective width section can also be used for a more conservative estimate of the inelastic buckling strength.

The calculated design loads by the Thornton method based on a 45° dispersion angle, labeled as $P_{t45}$, are shown in Table 3.5. Again, the effective length factor, k=0.65 was used to evaluate the Thornton loads. However, the use of this value is intended to reflect the plate action that exists in the critical region bounded by the beam and column and not to account for a fixed-fixed boundary condition for the column strip as suggested by Thornton (1984). It can be seen from the table that a significant improvement in predictions is obtained using the modified Thornton method, except for specimen SP1. This discrepancy is attributed to the fact that the SP type specimens did not experience a significant amount of yielding prior to reaching the ultimate loads. In fact, the ultimate loads of the SP type specimens are lower than the corresponding Whitmore loads; hence, the load redistribution concept is not applicable for the SP type specimens.

As shown in Table 3.5, the ratio of test loads to the modified Thornton loads varies from 0.96 to 1.19, excluding SP type specimens. However, the ratio of the test loads to the Thornton loads, based on a 30° dispersion angle, varies from 1.51 to 1.87. For the purpose of comparison, the test specimens from Gross (1990) were also analyzed by the modified Thornton method and the results are shown in Table 3.5. It should be noted that, according to Gross (1990), a value of 0.5 was used for the effective length factor to account for the ideal no rotation end conditions occurring during his tests. Although three tests were conducted in the program, in only two tests did the gusset plate fail in compression. Table 3.5 shows that the test to predicted ratios which are 1.50 and 1.65 for

the Thornton loads based on 30° dispersion angle, improve to 1.05 and 1.15 for the modified Thornton method. Hence, it can be seen that the modified Thornton method produces a better estimate of the compressive strength of the gusset plate specimens.

### 3.3.2 Proposed Design Method

It is important to note that the modified Thornton method is developed on the basis of load redistribution due to yielding occurring in the gusset plates prior to stability failure. To ensure that sufficient yielding occurs in the gusset plate, the elastic buckling load of the gusset plates must be significantly higher than the corresponding Whitmore load. As shown in Table 3.6, the ratio of analytical elastic buckling loads (based on finite element analyses) to the Whitmore loads ranges from 1.51 to 5.33 (excluding the SP type specimens). The lowest ratio, 1.51, corresponds to specimen GP3. The test results for specimen GP3 showed that moderate yielding occurred in the gusset plate prior to stability failure and the ultimate load of the specimen is comparatively higher than the corresponding Whitmore load. Therefore, it is reasonable to establish a limit for the applicability of the modified Thornton method: namely, that the ratio of the elastic buckling load to the Whitmore load has to be greater than about 1.5.

The evaluation of the elastic buckling loads of the gusset plate connections by the finite element method is not a practical design procedure. Therefore, it is proposed that the elastic buckling load of the gusset plate connections be estimated by the Thornton method (30° dispersion angle) along with the elastic buckling equation of a column, that is:

$$\sigma_{cr} = \frac{\pi^2 E}{\left(\frac{kL}{r}\right)^2} \qquad [3.1]$$

where $\sigma_{cr}$ is the critical stress of a column and r is the radius of gyration. The elastic buckling load estimated by this procedure will be termed the Thornton elastic buckling load ($P_{TE}$). The Thornton elastic buckling loads of the test specimens are shown in Table 3.6. It can be seen from this table that the Thornton elastic buckling loads are generally higher than the corresponding elastic buckling loads evaluated by the finite element method. For specimen GP3, the ratio of the Thornton elastic buckling load to the Whitmore load increases to 2.1 from 1.51 (which is the ratio of the analytical elastic buckling load to the Whitmore load). Based on the estimation of the Thornton elastic buckling loads, the design method for designing concentrically loaded gusset plate connections subject to compression is:

$$P_{cr} = P_{t45} \quad \text{if} \quad \frac{P_{TE}}{P_w} \geq 2.0 \qquad [3.2a]$$

$$P_{cr} = P_{t30} \quad \text{if} \quad \frac{P_{TE}}{P_w} < 2.0 \qquad [3.2b]$$

where $P_{cr}$ is the compressive strength of the gusset plates and all the other terms have been defined previously. It is assumed that the general design guidelines presented in Section 3.2.2.5 will also be followed when equation [3.2] is used. If the gusset plate shapes are significantly different from a rectangular shape, equation [3.2b] is recommended regardless of the ratio of the Thornton elastic buckling load to the Whitmore load and the length of the unit column strip as suggested by Thornton (1984) should be used. It should also be noted that the above design method is based on a limited number of test data and analytical study. Therefore, further experimental and analytical investigations are required to refine the design method.

The above design method has also been applied to the test results from Hu and Cheng (1987). The test results of this investigation are repeated in Table 3.7, along with the Whitmore loads ($P_w$), the Thornton elastic buckling loads ($P_{TE}$), the Thornton loads ($P_{t30}$)

and the analytical elastic buckling loads, assuming an infinite splice plate thickness for the test specimens. Since the ratios of $P_{TE}$ to $P_w$ for all the specimens are significantly less than 2.0, equation [3.2b] should be used to estimate the buckling strength of the specimens. The $P_{t30}$ predictions of the specimens are conservative for three of the four cases. The overestimation of the buckling load for specimen C1 is because the splice plate used in the test of specimen C1 was only 13.0 mm thick, and this is not sufficient to provide the required stiffness as recommended in the general design guidelines. To further investigate this result, the analytical buckling loads (evaluated using ANSYS) with an infinite splice plate thickness ($P_E$) are evaluated and shown in Table 3.7. The table shows that the analytical buckling load of specimen C1 is two times the corresponding test load; however, the $P_{t30}$ prediction of specimen C1 is conservative relative to the analytical buckling load. Hence, it can be concluded that if the recommended general design guidelines are followed, the proposed design method will provide a conservative estimate of the compressive strength of gusset plate connections.

## 3.4 Eccentrically Loaded Gusset Plate Connections

### 3.4.1 General

The physical tests showed that the failure mode for the eccentrically loaded specimens was yielding at the splice member and the gusset plate. However, it should be noted that the yielding at the splice member was recorded during the loading stage whereas the yielding at the gusset plate was only observed when the applied load was very close to the ultimate load. Rigid plastic collapse analyses were conducted on specimens EP1 and EP2. These analyses, together with the elastic curves based on the large deflection assumption (evaluated using ANSYS), provided good estimates of the ultimate loads of the specimens, as discussed in Chapter 2. However, this method may not be practical in everyday design since a finite element analysis is required to evaluate the elastic curve.

According to Hu and Cheng (1987), the strength of the eccentrically loaded specimens can be evaluated using the beam-column equation for a rectangular cross-section. The beam-column formula for a rectangular section, as presented in the previous chapter is:

$$\left(\frac{P}{P_y}\right)^2 + \left(\frac{M_{pc}}{M_p}\right) = 1.0 \qquad [3.3]$$

The ultimate strengths of the EP type specimens estimated by equation [3.3] are shown in Table 3.8. It should be noted that the beam-column equation only considers the cross-sectional strength of the splice member. It was also assumed that the total eccentric moment was resisted by the splice member at the conjunction of gusset-to-splice, which is a conservative approximation. The detail calculations are contained in the Appendix.

It can be seen from Table 3.8 that the beam-column equation produces conservative estimates of the strength of the specimens. The test to predicted ratios range from 1.16 to 2.54. (It should be noted that a linear beam-column equation which used the yield moment of the cross-section was employed to evaluate the strength of specimen EP3. In this case, the tee-section splicing member used is a Class 3 section according to the steel design specification (S16.1)). A reasonable prediction of the strength by the beam-column equation was obtained for specimen EP3. This is probably because the splice member for this specimen was relatively rigid and hence more moment was distributed to the splice member. Therefore, the assumption that the eccentric moment was resisted by the splice member was quite valid.

For specimens EP1 and EP2, which have relatively slender splice plates, if the assumption of the distribution of the eccentric moment is modified such that both the splice plate and the gusset plate share an equal amount of eccentric moment, the ultimate loads estimated by the beam-column equation are significantly improved. The beam-column ultimate loads of specimens EP1 and EP2 based on this modified assumption are shown in Table 3.8. It can be seen that the test to predicted ratios for specimens EP1 and EP2 are greatly improved,

decreasing from about 2.54 down to 1.42. It is believed that this modified assumption is still quite conservative since the bending rigidity of the gusset plate is usually larger than that of the splice plate member and hence more moment will be distributed to the gusset plate.

### 3.4.2 General Design Guidelines

Keeping in mind that the number of test data are limited, general design guidelines for designing the eccentrically loaded gusset plate connections can be set out as follows:

1) Eccentricity of load should be avoided in the gusset plate connections in order to prevent premature yielding failure of the splice member.

2) If the loading eccentricity cannot be avoided, splice members which have a high out-of-plane flexural rigidity (such as tee-sections and channel sections) are recommended. In this case, the beam-column equations for a rectangular cross-section can be used to evaluate the strength of the splice members. It should be assumed that the total eccentric moment is resisted by the splice members.

3) If a plate type splice member is used for the eccentrically loaded gusset plate connections, the beam-column equation for a rectangular cross-section can be used to evaluate the strength of the splice plate member. It may be assumed that half of the eccentric moment is resisted by the splice plate member.

Table 3.1 Buckling Loads of Test Specimens from Hu and Cheng (1987)

| Specimen | Plate Size (mm x mm x mm) | Free Case Buckling Load P (kN) | Finite Element Buckling Load $P_{ANSYS}$ (kN) | Whitmore Load $P_w$ (kN) |
|---|---|---|---|---|
| C1 | 850 x 550 x 6.7 | 441.7 | 604.0 | 1922 |
| C2 | 850 x 550 x 3.11 | 122.4 | 94.5 | 424 |
| C3 | 850 x700 x 6.7 | 380.1 | 332.0 | 1922 |
| C4 | 850 x 700 x 3.11 | 89.6 | 37.3 | 424 |

Table 3.2 Critical Splice Plate Thickness for 850 x 550 and 850 x 700 Specimens

| Specimen Size | Gusset Plate Thickness t (mm) | Splice Plate Length SL (mm) | Critical Splice Plate Thickness Sc (mm) | $\frac{Sc}{t}$ |
|---|---|---|---|---|
| | 3.11 | 297 | 7 | 2.25 |
| | 3.11 | 447 | 13 | 4.18 |
| 850 x 550 | 6.7 | 297 | 13 | 1.92 |
| | 6.7 | 447 | 26 | 3.88 |
| | 9.5 | 297 | 26 | 2.74 |
| | 9.5 | 447 | 35 | 3.68 |
| 850 x 700 | 6.7 | 447 | 20 | 2.99 |
| | 6.7 | 552 | 20 | 2.99 |

Table 3.3a Effects of Splice Plate Length on Buckling Loads for Specimens with a Plate Size of 850 x 550

| Gusset Plate Size and Splice Plate Thickness | P SL = 297 4 Rows of Bolts (kN) | P SL = 447 Six Rows of Bolts (kN) | $\frac{P_{(SL=447)}}{P_{(SL=297)}}$ |
|---|---|---|---|
| 850 x 550 x 9.5 splice plate thickness = 35 | 1038 | 2526 | 2.43 |
| 850 x 550 x 6.7 splice plate thickness = 26 | 378 | 920 | 2.43 |
| 850 x 550 x 3.11 splice plate thickness = 13 | 38.8 | 95.9 | 2.47 |

Table 3.3b Effects of Splice Plate Length on Buckling Loads for Specimens with a Plate Size of 850 x 700

| Gusset Plate Size and Splice Plate Thickness | P SL = 447 Six Rows of Bolts (kN) | P SL = 552 Seven Rows of Bolts (kN) | $\frac{P_{(SL=552)}}{P_{(SL=447)}}$ |
|---|---|---|---|
| 850 x 700 x 6.7 splice plate thickness = 20 | 353 | 471 | 1.33 |

Table 3.4 Effects of Rotational Restraint at the Conjunction of Bracing Member and Gusset Plate

| Splice Plate Length (SL) (mm) | t Gusset Plate Thickness (mm) | P With Infinite Rotational Restraint (kN) | P Without Rotational Restraint (kN) |
|---|---|---|---|
| 297 | 12.7 | 1213 | 346 |
| | 9.50 | 758 | 152 |
| | 6.70 | 344 | 55.0 |
| | 3.11 | 38.3 | 5.60 |
| 447 | 12.7 | 1275 | 499 |
| | 9.50 | 849 | 237 |
| | 6.70 | 573 | 90.7 |
| | 3.11 | 95.9 | 9.65 |
| 522 | 12.7 | 1383 | 619 |
| | 9.50 | 888 | 315 |
| | 6.70 | 591 | 128 |
| | 3.11 | 144 | 14.2 |

Gusset Plate Size = 850 x 550 mm  Splice Plate Thickness = 13.0 mm
E = 200 000 MPa

Table 3.5 Comparison of Test Loads with Analytical and Design Loads

| Specimen | Ultimate Load P (kN) | $P_{ANSYS}$ (kN) | Whitmore Load $P_w$ (kN) | Thornton Load $P_{t30}$ (kN) | Thornton Load $P_{t45}$ (kN) | $\frac{P}{P_{ANSYS}}$ | $\frac{P}{P_{t30}}$ | $\frac{P}{P_{t45}}$ |
|---|---|---|---|---|---|---|---|---|
| GP1 | 1956 | 2336 | 1216 | 1142 | 1792 | 0.84 | 1.71 | 1.09 |
| GP2 | 1356 | 1483 | 930 | 828 | 1300 | 0.91 | 1.64 | 1.04 |
| GP3 | 742 | 680 | 555 | 439 | 689 | 1.09 | 1.69 | 1.08 |
| SP1 | 1606 | 1940 | 1852 | 1228 | 1997 | 0.83 | 1.31 | 0.80 |
| SP2 | 1010 | 940 | 1416 | 640 | 1041 | 1.07 | 1.58 | 0.97 |
| AP1 | 1720 | 2260 | 1216 | 1119 | 1757 | 0.76 | 1.54 | 0.98 |
| AP2 | 1210 | 1460 | 930 | 801 | 1257 | 0.83 | 1.51 | 0.96 |
| AP3 | 728 | 690 | 555 | 404 | 634 | 1.06 | 1.80 | 1.15 |
| MP1 | 1933 | 2320 | 1216 | 1142 | 1792 | 0.83 | 1.69 | 1.08 |
| MP2 | 1316 | 1450 | 930 | 828 | 1300 | 0.91 | 1.59 | 1.01 |
| MP3 | 721 | 755 | 555 | 439 | 689 | 0.95 | 1.64 | 1.05 |
| MP3A | 819 | 765 | 555 | 439 | 689 | 1.07 | 1.87 | 1.19 |
| MP3B | 821 | 735 | 555 | 439 | 689 | 1.12 | 1.87 | 1.19 |
| Gross 1* | 516 | - | - | 345 | 491 | - | 1.50 | 1.05 |
| Gross 2* | 614 | - | - | 371 | 534 | - | 1.65 | 1.15 |

* Test specimens from Gross (1990)

Plate thickness = 6.35 mm

Table 3.6 Comparison of Elastic Buckling Loads with Whitmore Loads of Test Specimens

| Specimen | Ultimate Load P (kN) | Elastic Buckling Load (ANSYS) $P_E$ (kN) | Thornton Elastic Buckling Load $P_{TE}$ (kN) | Whitmore Load $P_w$ (kN) | $\frac{P_E}{P_W}$ | $\frac{P_{TE}}{P_W}$ |
|---|---|---|---|---|---|---|
| GP1 | 1956 | 5428 | 10568 | 1216 | 4.46 | 8.69 |
| GP2 | 1356 | 2638 | 4333 | 930 | 2.81 | 4.65 |
| GP3 | 742 | 836 | 1165 | 555 | 1.51 | 2.1 |
| SP1 | 1606 | 2169 | 2206 | 1852 | 1.17 | 1.19 |
| SP2 | 1010 | 940 | 905 | 1416 | 0.66 | 0.64 |
| AP1 | 1720 | 6476 | 7751 | 1216 | 5.33 | 6.37 |
| AP2 | 1210 | 3181 | 3178 | 930 | 3.42 | 3.42 |
| AP3 | 728 | 910 | 854 | 555 | 1.64 | 1.54 |
| MP1 | 1933 | 6075 | 10568 | 1216 | 5.00 | 8.69 |
| MP2 | 1316 | 3118 | 4333 | 930 | 3.35 | 4.65 |
| MP3 | 721 | 985 | 1165 | 555 | 1.77 | 2.1 |
| MP3A | 819 | 985 | 1165 | 555 | 1.77 | 2.1 |
| MP3B | 821 | 985 | 1165 | 555 | 1.77 | 2.1 |

Table 3.7 Design Loads for Test Specimens from Hu and Cheng (1987)

| Specimen Size (mm x mm x mm) | P (kN) | $P_E$ (ANSYS) with infinite splice plate thickness (kN) | $P_{TE}$ Thornton Elastic Buckling Load (kN) | $P_w$ Whitmore Load (kN) | $P_{t30}$ Thornton Load (kN) | $\frac{P_{TE}}{P_w}$ |
|---|---|---|---|---|---|---|
| C1: 850 x 500 x 6.7 | 441.7 | 982.0 | 928.0 | 1922 | 780 | 0.48 |
| C2 : 850 x 500 x 3.11 | 122.4 | 98.3 | 86.6 | 424 | 79.7 | 0.20 |
| C3 : 850 x 700 x 6.7 | 380.1 | 395.0 | 596.0 | 1922 | 275.0 | 0.31 |
| C4 : 850 x 700 x 3.11 | 89.6 | 37.3 | 27.6 | 424 | 27.6 | 0.07 |

Table 3.8 Design Loads for EP Type Specimens

| Specimen | Ultimate Load P (kN) | Beam-Column Load with Full Eccentric Moment at Splice $P_{BC}$ (kN) | Beam-Column Load with 50% Eccentric Moment at Splice $P_{MBC}$ (kN) | $\frac{P}{P_{BC}}$ | $\frac{P}{P_{MBC}}$ |
|---|---|---|---|---|---|
| EP1 | 310 | 122 | 221 | 2.54 | 1.40 |
| EP2 | 334 | 132 | 233 | 2.53 | 1.43 |
| EP3 | 890 | 770 | - | 1.16 | - |

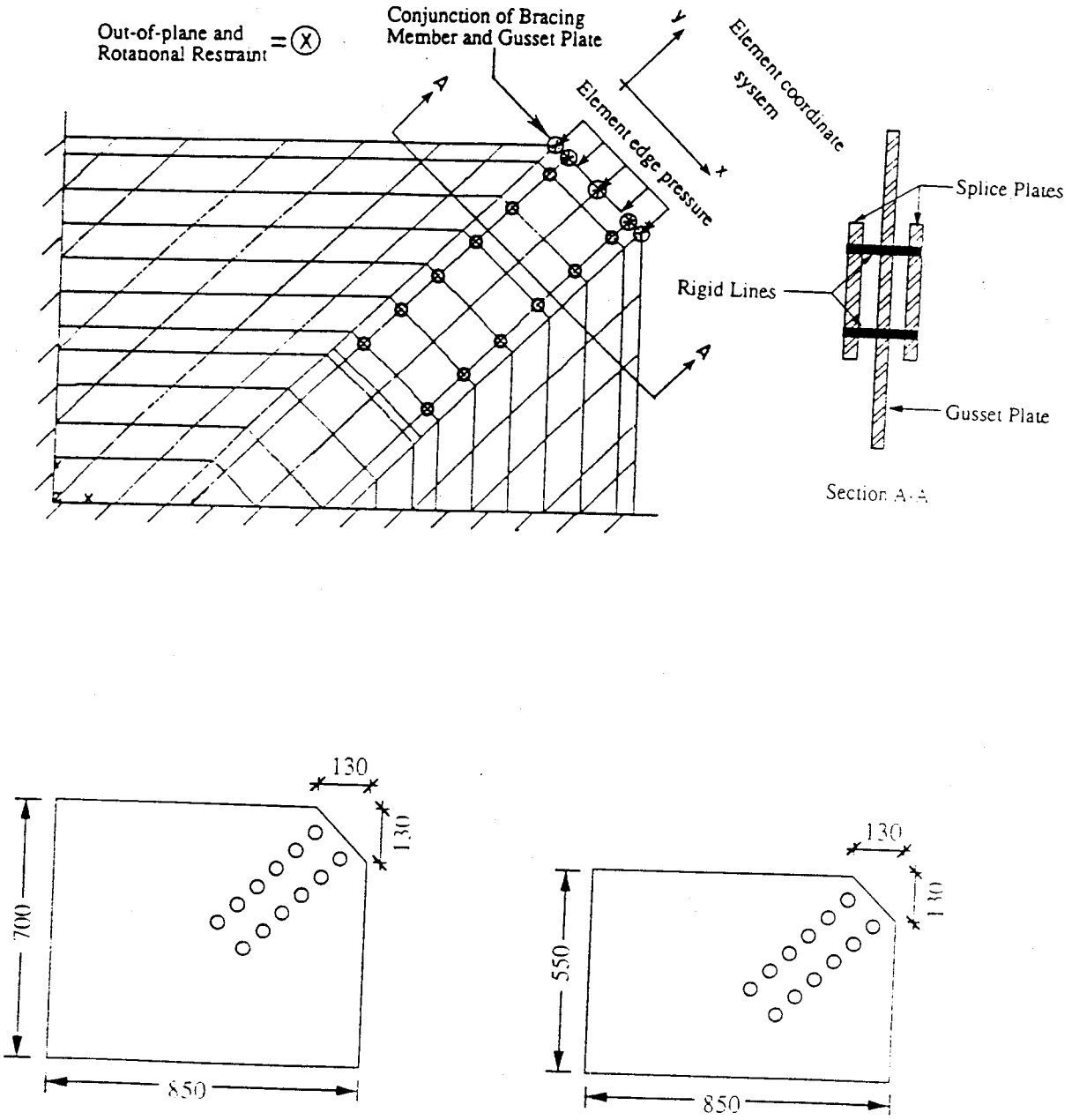


Fig. 3.1 Finite Element Model and Typical Specimens (Cheng et al. 1994)

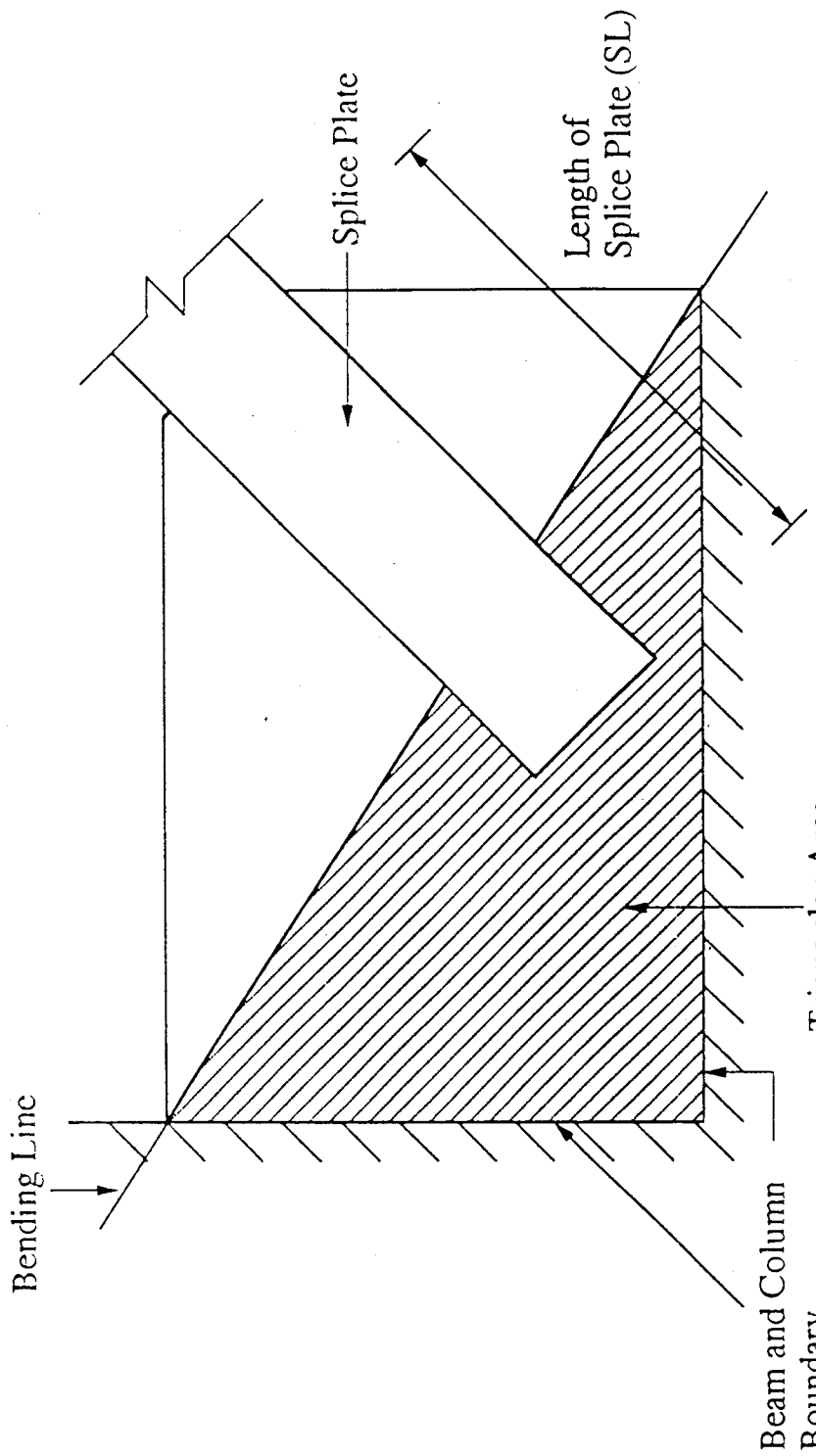


Fig. 3.2 Triangular Area of Gusset Plates

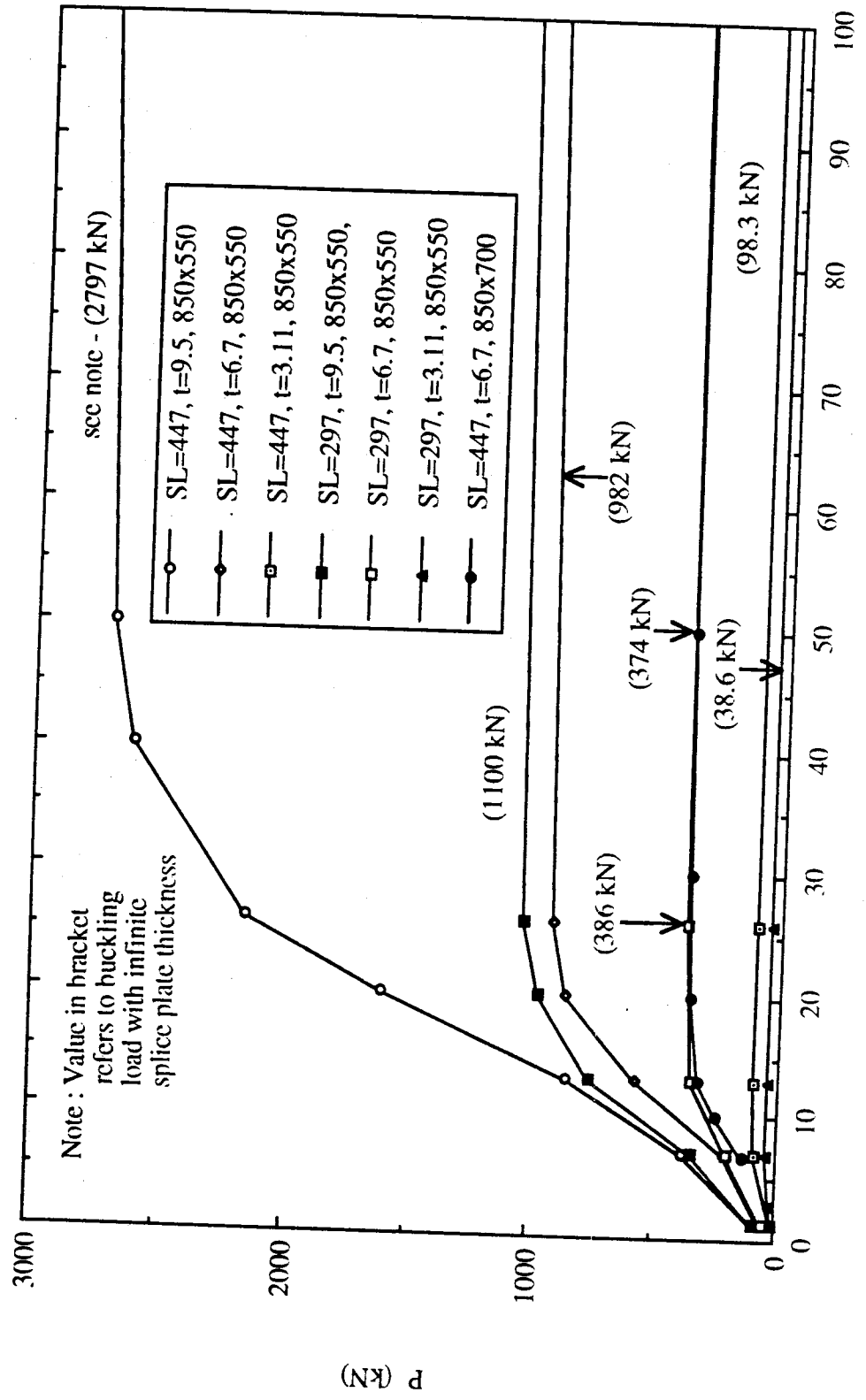


Fig. 3.3 Effects of Splice Plate Thickness on the Elastic Buckling Loads of Specimens

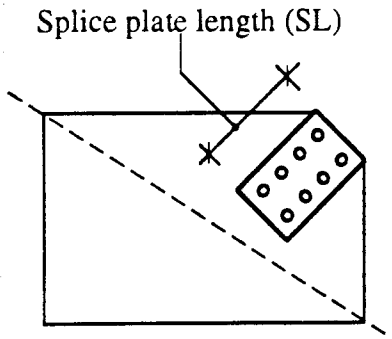


850 x 500
Splice plate length = 297 mm

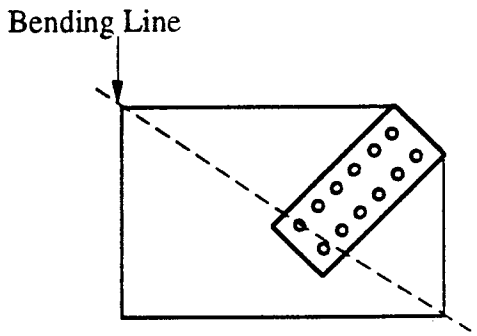


850 x 500
Splice plate length = 447 mm

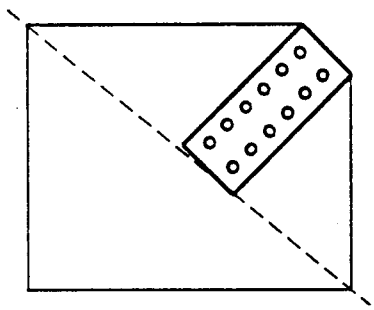

850 x 700
Splice plate length = 447 mm

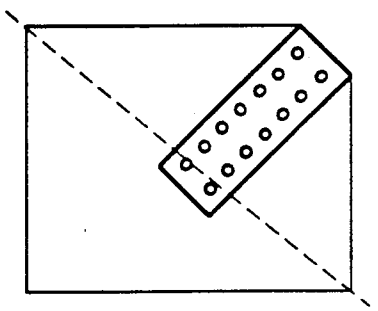

850 x 700
Splice plate length = 552 mm

Fig. 3.4 Various Splice Plate Lengths for the Specimens

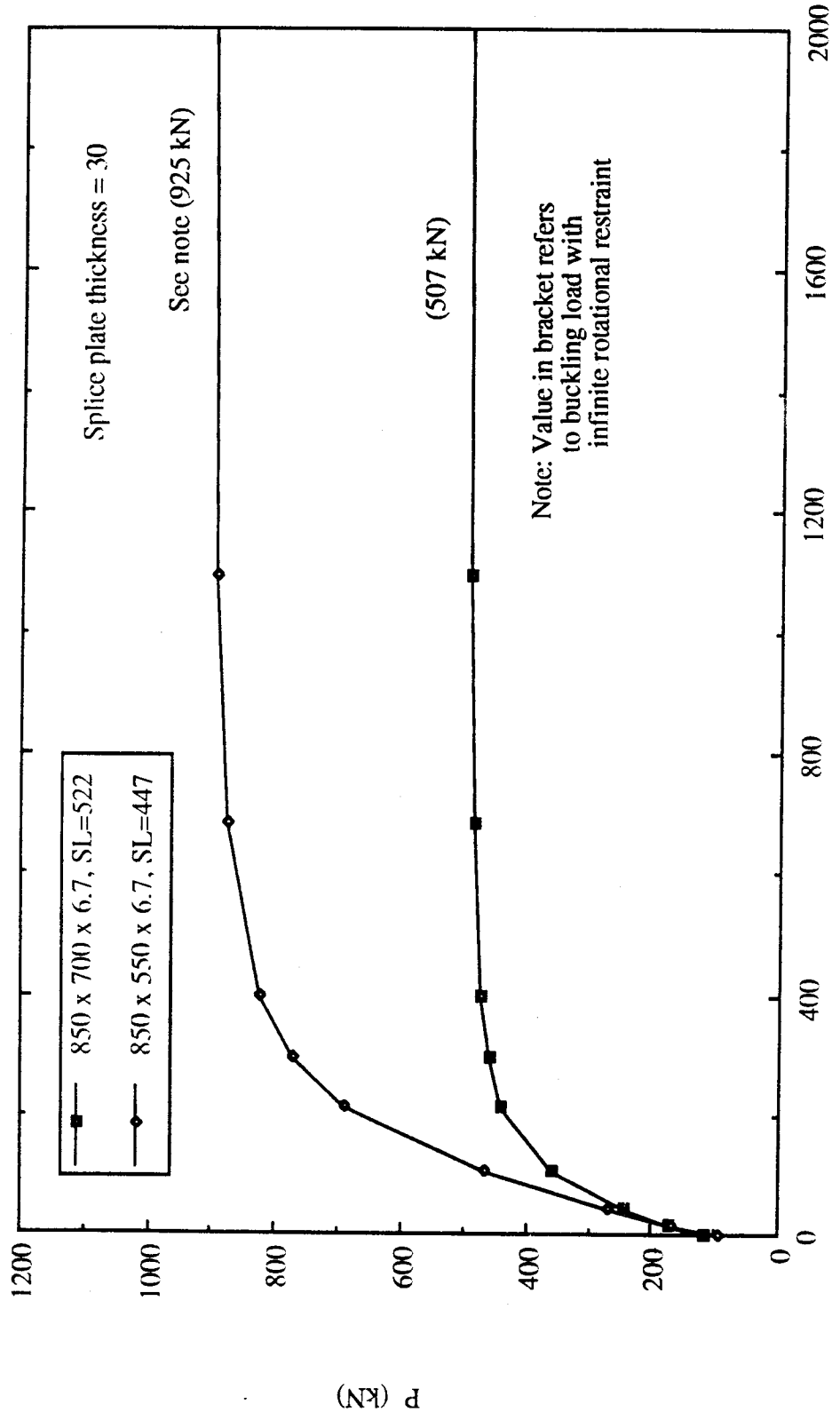


Fig. 3.5 Effects of Rotational Restraint on the Elastic Buckling Loads of Gusset Plate Specimens

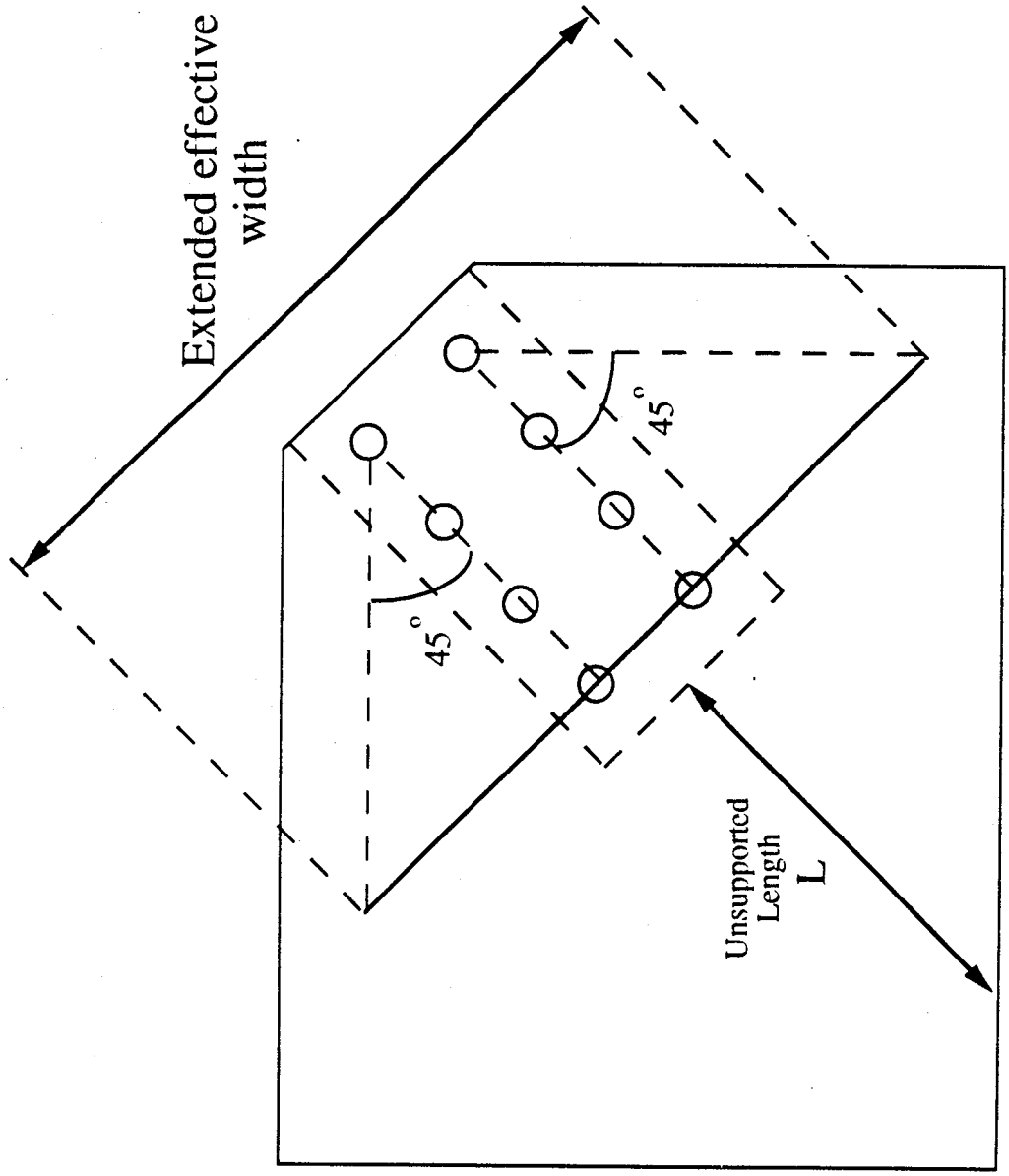


Figure 3.6 Modified Thornton Method

# 4. SUMMARY AND RECOMMENDATIONS

## 4.1 Summary

The finite element method was employed to analyze the test specimens. The finite element program ANSYS was used in these analyses. An elastic parametric study was conducted to examine the effects of splice plate thickness, splice plate length, and rotational restraint at the conjunction of the bracing member and the gusset plate upon the elastic buckling strength of the gusset plate connections.

The following is a summary of the research findings by the analysis.

1) Plastic bifurcation buckling analyses done using ANSYS give reasonable predictions of the ultimate loads of the test specimens. The test to predicted ratios range from 0.76 to 1.12.
2) The ultimate loads of the eccentrically loaded specimens evaluated by the load-deflection analysis using ANSYS are in good agreement with the test results. The test to predicted ratios range from 0.97 to 1.05.
3) The rigid plastic analysis, together with the elastic curve evaluated using ANSYS, provided a good estimate of the ultimate loads of the eccentrically loaded specimens which used a plate as the splice member.

## 4.2 Design Recommendations

### 4.2.1 Concentrically Loaded Gusset Plate Connections

It should be noted that the design recommendations are based on a limited number of test data and analytical studies. Therefore, further experimental and analytical investigations are required to refine these design recommendations. The method recommended for designing concentrically loaded gusset plate connections subject to compression is:

$$P_{cr} = P_{t45} \quad \text{if} \quad \frac{P_{TE}}{P_w} \geq 2.0$$

$$P_{cr} = P_{t30} \quad \text{if} \quad \frac{P_{TE}}{P_w} < 2.0$$

where $P_{cr}$ = the compressive strength of gusset plates

$P_{t45}$(modified Thornton load) = $\sigma_r$ x ( 2 $l_b$ tan 45° + s ) t

$\sigma_r$ = compressive stress of the unit column strip (Fig. 4.1) evaluated using the column curves in CAN/CSA-S16.1- M89 (Clause 13.3.1)

$P_{t30}$ (Thornton load) = $\sigma_r$ x ( 2 $l_b$ tan 30° + s ) t

$P_{TE}$ (Thornton elastic buckling load) = $\frac{\pi^2 E}{\left(\frac{kL}{r}\right)^2}$ x ( 2 $l_b$ tan 30° + s ) t

k = 0.65

$P_w$ (Whitmore load) = Fy x ( 2 $l_b$ tan 30° + s ) t

The dimensions $l_b$, s, L, and t are defined in Fig. 4.1. It is assumed that the general design guidelines presented in Section 10.2.2.5, which are not repeated here, are followed when employing the above design recommendations. If the gusset plate shapes are significantly different from a rectangular shape, the Thornton load ($P_{t30}$) is recommended, regardless of the ratio of the Thornton elastic buckling load to the Whitmore load, and the length of the column strip as suggested by Thornton (1984) should be used.

### 4.2.2 Eccentrically Loaded Gusset Plate Connections

Based on a limited number of test data and analyses, the following general design guidelines for designing eccentrically loaded gusset plate connections are recommended:

1) Loading eccentricity should be avoided in the gusset plate connections so as to prevent premature yielding failure at the splice member.

2) If loading eccentricity cannot be prevented, splice members that have a high out-of-plane flexural rigidity (such as tee-sections and channel sections) are recommended. The beam-column equations for a rectangular cross-section can be used to evaluate the strength of the splice members, assuming that the total eccentric moment is resisted by the splice members.

3) If a plate type splice member is used for the eccentrically loaded gusset plate connections, the beam-column equation for a rectangular cross-section can be used to evaluate the strength of the splice plate member, assuming that half of the eccentric moment is resisted by the splice plate member.

## 4.3 Recommendations for Future Research

In order to develop a set of complete guidelines for designing the compressive strength of the gusset plate connections, the following areas should be further investigated:

1) More tests should be conducted to investigate the effects of gusset plate shape, types of splicing members, and types of bracing members on the ultimate strength and compressive behavior of gusset plate connections.

2) Parametric studies on the inelastic compressive behavior of gusset plate connections by the finite element method should be performed and important design variables should be identified in order to develop complete rational design procedures.

3) More tests should be conducted to investigate the compressive behavior of eccentrically loaded gusset plate connections. Test variables such as the relative stiffness of the gusset plate and the splice member, stiffener requirements, and the types of splicing members should be further investigated.

4) Parametric studies of eccentrically loaded gusset plates should be conducted in order to develop rational design guidelines for this kind of connection.

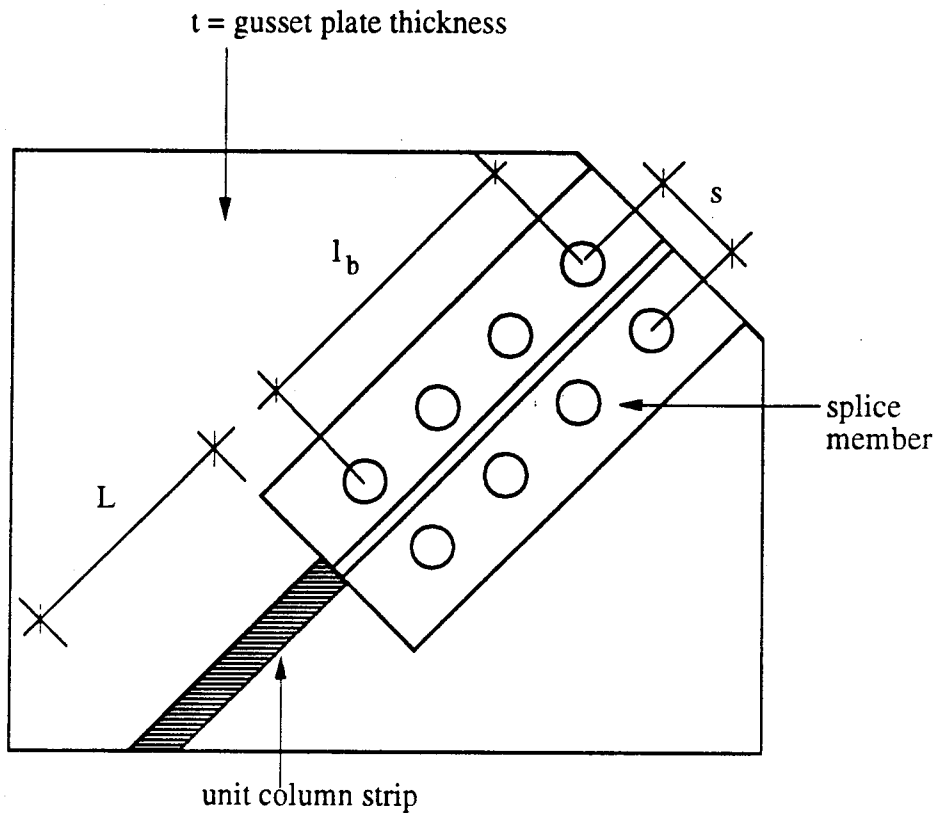


r = radius of gyration of unit column strip

$$= \frac{t}{\sqrt{12}}$$

k = effective length factor of unit column strip

= 0.65

Fig. 4.1 Dimensions Required in the Design Method

## REFERENCES

AISC, 1993. Load and Resistance Factor Design Specification for Structural Steel Buildings. American Institute of Steel Construction (AISC), Chicago, Illinois.

ANSYS User's Manual 4.4, 1989. Swanson Analysis System Inc.

Chang, S.C. and Chen, J.J., 1986. "Effectiveness of Linear Bifurcation Analysis for Predicting the Nonlinear Stability of Structures." Int. J. of Num. Meth. Engng., Vol. 23, No. 5, 831-846.

Cheng, J.J.R., Yam, M., and Hu, S.Z., 1994. "Elastic Buckling Strength of Gusset Plate Connections." Journal of Structural Engineering, ASCE, 120(2), 538-559.

Cook, R.D., Malkus D.S., and Plesha, M.E., 1989. Concepts and Application of Finite Element Analysis. 3rd edition, John Wiley & Sons.

CSA, 1992. CAN/CSA-G40.21-M92 - Structural Quality Steel. Canadian Standards Association (CSA), Rexdale, Ontario.

CSA, 1988. CAN/CSA-S6-88 - Design of Highway Bridges. Canadian Standards Association (CSA), Rexdale, Ontario.

CSA, 1989. CAN/CSA-S16.1-M89 - Limit States Design of Steel Structures. Canadian Standards Association (CSA), Rexdale, Ontario.

Gaylord, E.H., Gaylord, C.H., and Stallmeyer, J.E., 1992. Design of Steel Structures. 3rd edition, McGraw-Hill, New York.

Gross, J.L. 1990. "Experimental Study of Gusseted Connections." Engineering Journal, AISC, Vol. 27, No. 3, 89-97.

Horne, M.R. and Morris, L.J. 1981. Plastic Design of Low-rise Frames. Granada Publishing Limited - Technical Books Division, Great Britain.

Hu, S.Z., and Cheng, J.J.R. 1987. "Compressive Behavior of Gusset Plate Connections." Structural Engineering Report No.153, University of Alberta.

Kitipornchai, S., Al-Bermani, F.G.A. and Murray, N.R. 1993. "Eccentrically Connected Cleat Plates in Compression." Journal of Structural Engineering, ASCE, 119(3), 761-781.

Korol, R.M. and Sherbourne, A.N. 1972. "Strength Predictions of Plates in Uniaxial Compression." Proceedings of ASCE, ST9, 1965-1985.

Kulak, G.L., Fisher, J.W., and Struik, J.H.A. 1987. Guide to Design Criteria for Bolted and Riveted Joints. 2nd edition, Wiley-Interscience, New York, N.Y.

Murray, N.W. and Khoo, P.S. 1981. "Some Basic Mechanisms in the Local Buckling of Thin-Walled Steel Structures." Int. J. Mech. Sci. Vol. 23, No. 12, 703-713.

Rabinovitch, J.S. and Cheng, J.J. Roger. 1993. "Cyclic Behavior of Steel Gusset Plate Connections." Structural Engineering Report No. 191, University of Alberta.

Richard, R.M., Rabern, D.A., Hormby, D.E., and Williams, G.C. 1983. "Analytical Models for Steel Connections." Behavior of metal structures, Proceedings of the W.H. Munse Symposium, ASCE, edited by W.J. Hall and M.P. Gaus, 128-155.

Struik, J.H.A. 1972. "Applications of Finite Element Analysis to Non-Linear Plane Stress Problem." Ph.D. dissertation, Department of Civil Engineering, Lehigh University, Bethlehem, Pa.

Thornton, W.A. 1984. "Bracing Connections for Heavy Construction." Engineering Journal, AISC, 3rd Quarter, 139-148.

Whitmore, R.E. 1952. "Experimental Investigation of Stresses in Gusset Plates." Bulletin No.16, Engineering Experiment Station, University of Tennessee.

Williams, G.C. and Richard, R.M., 1986. "Steel Connection Design Based on Inelastic Finite Element Analysis." Report to the Department of Civil Engineering and Engineering Mechanics, the University of Arizona.

Yam, M.C.H. and Cheng, J.J.R. 1993. "Experimental Investigation of the Compressive Behavior of Gusset Plate Connections." Structural Engineering Report No.194, University of Alberta.

Yamamoto, K., Akiyama, N., and Okumura, T. 1988. "Buckling Strength of Gusseted Truss Joints." Journal of the Structural Division, ASCE, 114(3), 575-590.

# APPENDIX

**Example calculation: Specimen EP1**

Rigid-Plastic Unloading Line

Splice Plate:

$\sigma_y = 435$ MPa

$P_{yS} = 435 \times 148 \times 9.5 \times 10^{-3}$

$= 611$ kN

$M_{pS} = \sigma_y \left(\frac{bd^2}{4}\right)$

$= 435 \times \left(\frac{148 \times 9.5^2}{4}\right) \times 10^{-3}$

$= 1452$ kNmm

Gusset Plate :

$\sigma_y = 295$ MPa

$P_{yG} = 295 \times 565 \times 13.3 \times 10^{-3}$

$= 2217$ kN

$M_{pG} = \sigma_y \left(\frac{bd^2}{4}\right)$

$= 295 \times \left(\frac{565 \times 13.3^2}{4}\right) \times 10^{-3}$

$= 7371$ kNmm

$e = \frac{13.3 + 9.5}{2} = 11.4$ mm

From eqn. 9.4 :

$$P = \frac{-(e+\Delta) + \sqrt{(e+\Delta)^2 + 4\left(\frac{M_{pS}}{P_{yS}^2} + \frac{M_{pG}}{P_{yG}^2}\right)(M_{pS}+M_{pG})}}{2\left(\frac{M_{pS}}{P_{yS}^2} + \frac{M_{pG}}{P_{yG}^2}\right)} \qquad [9.4]$$

Therefore,

$$P = \frac{-(11.4+\Delta) + \sqrt{(11.4+\Delta)^2 + 4\left(\frac{1452}{611^2} + \frac{7371}{2107^2}\right)(1452+7371)}}{2\left(\frac{1452}{611^2} + \frac{7371}{2107^2}\right)}$$

$$P = \frac{-(11.4+\Delta) + \sqrt{(11.4+\Delta)^2 + 4\,(5.45 \times 10^{-3})(8458)}}{(2)(5.45 \times 10^{-3})}$$

| $\Delta$ | 0 | 2 | 4 | 6 | 8 | 10 | 12 | 14 | 15 | 16 | 18 | 20 |
|---|---|---|---|---|---|---|---|---|---|---|---|---|
| P | 581 | 521 | 471 | 429 | 393 | 362 | 335 | 312 | 302 | 292 | 274 | 258 |

Beam-Column Equation

$\sigma_y = 435$ MPa  e = 11.4 mm

$P_{yS} = 611$ kN

MpS = 1452 kNmm

$$\left(\frac{P}{P_{yS}}\right)^2 + \left(\frac{M_{pcS}}{MpS}\right) = 1.0$$

$$\left(\frac{P}{611}\right)^2 + \left(\frac{P \times 11.4}{1452}\right) = 1.0$$

$$P^2 + 2931P = 373321$$

$$\Rightarrow P = \left(\frac{-2931 +/- \sqrt{2931^2 - 4 \times (-373321)}}{2}\right)$$

P = <u>122 kN</u>

## Recent Structural Engineering Reports

Department of Civil Engineering

University of Alberta

181. *Numerical Analysis of Buried Pipelines* by Zhilong Zhou and David W. Murray, January 1993.

182. *Shear Connected Cavity Walls Under Vertical Loads* by A. Goyal, M.A. Hatzinikolas and J. Warwaruk, January 1993.

183. *Frame Methods for Analysis of Two-Way Slabs* by M. Mulenga and S.H. Simmonds, January 1993.

184. *Evaluation of Design Procedures for Torsion in Reinforced and Prestressed Concrete* by Mashour G. Ghoneim and J.G. MacGregor, February 1993.

185. *Distortional Buckling of Steel Beams* by Hesham S. Essa and D.J. Laurie Kennedy, April 1993.

186. *Effect of Size on Flexural Behaviour of High Strength Concrete Beams* by N. Alca and J.G. MacGregor, May 1993.

187. *Shear Lag in Bolted Single and Double Angle Tension Members* by Yue Wu and Geoffrey L. Kulak, June 1993.

188. *A Shear-Friction Truss Model for Reinforced Concrete Beams Subjected to Shear* by S.A. Chen and J.G. MacGregor, June 1993.

189. *An Investigation of Hoist-Induced Dynamic Loads* by Douglas A. Barrett and Terry M. Hrudey, July 1993.

190. *Analysis and Design of Fabricated Steel Structures for Fatigue: A Primer for Civil Engineers* by Geoffrey L. Kulak and Ian F.C. Smith, July 1993.

191. *Cyclic Behavior of Steel Gusset Plate Connections* by Jeffrey S. Rabinovitch and J.J. Roger Cheng, August 1993.

192. *Bending Strength of Longitudinally Stiffened Steel Cylinders* by Qishi Chen, Alla E. Elwi and Geoffrey L. Kulak, August 1993.

193. *Web Behaviour in Wood Composite Box Beams* by E. Thomas Lewicke, J.J. Roger Cheng and Lars Bach, August 1993.

194. *Experimental Investigation of the Compressive Behavior of Gusset Plate Connections* by Michael C.H. Yam and J.J. Roger Cheng, September 1993.

195. *Some Behavioural Aspects of Composite Trusses* by Berhanu Woldegiorgis and D.J. Laurie Kennedy, January 1994.

196. *Flexural Behavior of High Strength Concrete Columns* by Hisham H.H. Ibrahim and James G. MacGregor, March 1994.

197. *Prediction of Wrinkling Behavior of Girth-Welded Line Pipe* by L.T. Souza, A.E. Elwi, and D.W. Murray, April 1994.

198. *Assessment of Concrete Strength in Existing Structures* by F. Michael Bartlett and J.G. MacGregor, May 1994.

199. *The Flexural Creep Behavior of OSB Panels Under Various Climatic Conditions* by Naiwen Zhao, J.J. Roger Cheng, and Lars Bach, June 1994.

200. *High Performance Concrete Under High Sustained Compressive Stresses* by S. Iravani and J.G. MacGregor, June 1994.

201. *Strength and Installation Characteristics of Tension – Control Bolts* by Scott T. Undershute and Geoffrey L. Kulak, August 1994.

202. *Deformational Behavior of Line Pipe* by Mohareb, M., Elwi, A.E., Kulak, G.L., and Murray, D.W., September 1994.

203. *Behavior of Girth-Welded Line Pipe*, by Yoosef-Ghodsi, N., Kulak, G.L., and Murray, D.W., September 1994.

204. *Numerical Investigation of Eccentrically Loaded Tied High Strength Concrete Columns* by Jueren Xie, Alaa E. Elwi, and J.G. MacGregor, October 1994.

205. *Shear Strengthening of Concrete Girders Using Carbon Fibre Reinforced Plastic Sheets* by Efrosini H. Drimoussis and J.J. Roger Cheng, October 1994.

206. *Shrinkage and Flexural Tests of a Full-Scale Composite Truss* by Michael B. Maurer and D.J. Laurie Kennedy, December 1994.

207. *Analytical Investigation of the Compressive Behavior and Strength of Steel Gusset Plate Connections* by Michael C.H. Yam and J.J. Roger Cheng, December 1994.